AD-A033 554 DAVID W TAYLOR NAVAL SHIP RESEARCH AND DEVELOPMENT CE--ETC F/G 20/4
EXPERIMENTAL EVALUATION OF ANALYTICALLY SHAPED HELICOPTER ROTOR--ETC(U)
JUL 76 P S MONTANA

UNCLASSIFIED DTNSRDC/ASED-355 NL

1 OF 2
AD A033554

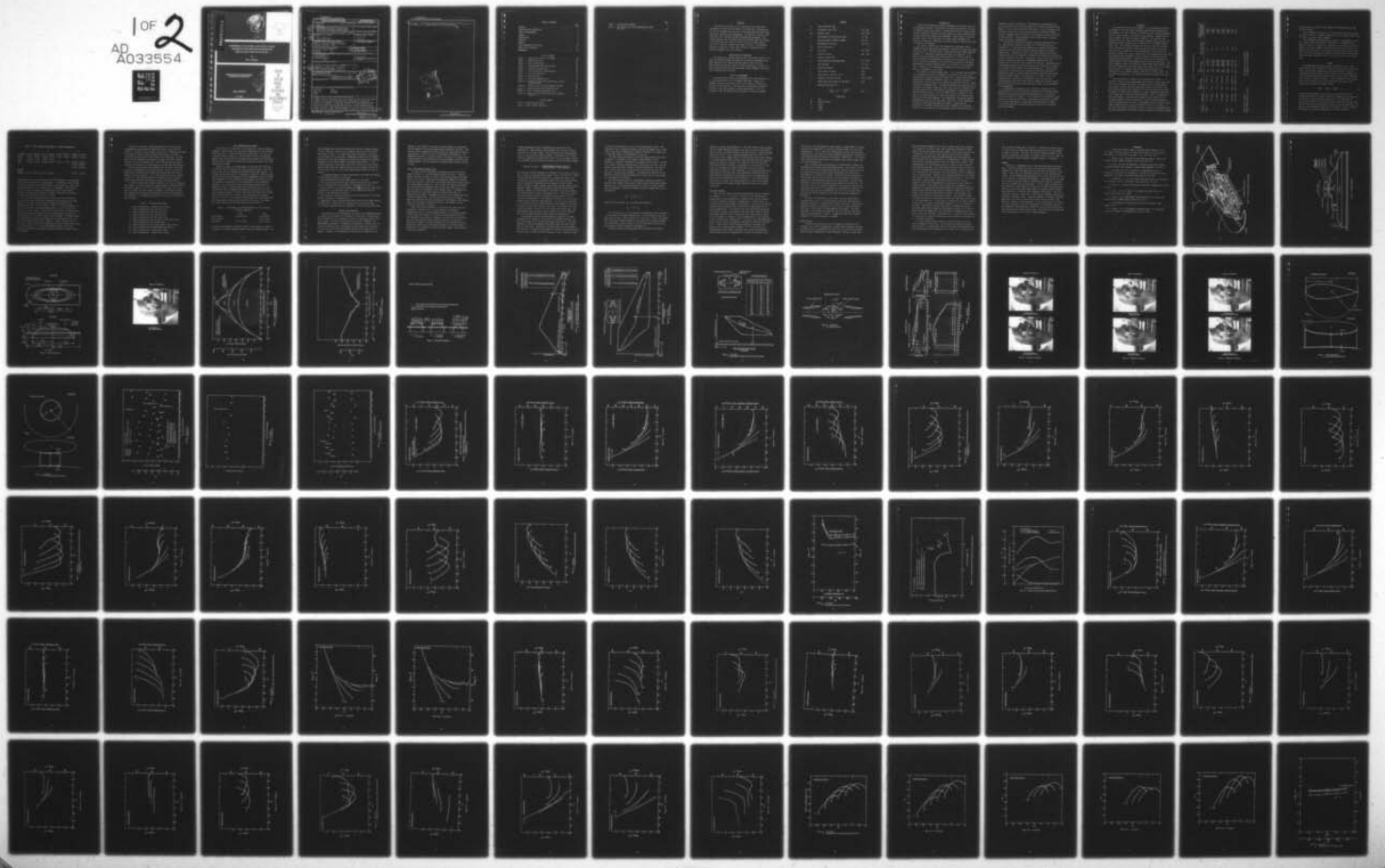

EXPERIMENTAL EVALUATION OF ANALYTICALLY SHAPED HELICOPTER ROTOR HUB-PYLON CONFIGURATIONS USING THE HUB PYLON EVALUATION RIG

by

Peter S. Montana

Report ASED-355

July 1976

DAVID
W.
TAYLOR
NAVAL
SHIP
RESEARCH
AND
DEVELOPMENT
CENTER

BETHESDA
MARYLAND
20084

UNCLASSIFIED

SECURITY CLASSIFICATION OF THIS PAGE (When Data Entered)

REPORT DOCUMENTATION PAGE

READ INSTRUCTIONS BEFORE COMPLETING FORM

1. REPORT NUMBER: ASED 355

2. GOVT ACCESSION NO.

3. RECIPIENT'S CATALOG NUMBER

4. TITLE (and Subtitle): EXPERIMENTAL EVALUATION OF ANALYTICALLY SHAPED HELICOPTER ROTOR HUB-PYLON CONFIGURATIONS USING THE HUB PYLON EVALUATION RIG

5. TYPE OF REPORT & PERIOD COVERED

6. PERFORMING ORG. REPORT NUMBER

7. AUTHOR(s): Peter S. Montana

8. CONTRACT OR GRANT NUMBER(s): F41.421.201
1-1619-105

9. PERFORMING ORGANIZATION NAME AND ADDRESS
David W. Taylor Naval Ship R&D Center
Aviation and Surface Effects Department
Bethesda, Maryland 20084

10. PROGRAM ELEMENT, PROJECT, TASK AREA & WORK UNIT NUMBERS

11. CONTROLLING OFFICE NAME AND ADDRESS
Naval Air Systems Command
AIR-320D
Washington, D.C. 20361

12. REPORT DATE: Jul 76

13. NUMBER OF PAGES: 105 pp

14. MONITORING AGENCY NAME & ADDRESS (if different from Controlling Office)

15. SECURITY CLASS. (of this report): UNCLASSIFIED

15a. DECLASSIFICATION/DOWNGRADING SCHEDULE

16. DISTRIBUTION STATEMENT (of this Report)

Approved for Public Release: Distribution Unlimited

DTNSRDC/ASED-355

17. DISTRIBUTION STATEMENT (of the abstract entered in Block 20, if different from Report)

F41421

WF41421201

DDC RECEIVED DEC 8 1976 C

18. SUPPLEMENTARY NOTES

19. KEY WORDS (Continue on reverse side if necessary and identify by block number)

Helicopter
Rotor Hub
Pylon
Shaft
Drag
Area Rule
Fairings

20. ABSTRACT (Continue on reverse side if necessary and identify by block number)

The hub-pylon evaluation rig, a new facility for wind tunnel experiments on large scale helicopter rotor hub-pylon configurations, was used to determine the variation of hub-pylon drag with shaft angle and height, and pylon angle parameters. In addition, a series of low drag "area rule" fairings and shaft fairings were evaluated. The results indicate that the proper selection of shaft angle with respect to the pylon and pylon angle of attack can yield a twenty percent reduction in drag for a given shaft angle → next page

DD FORM 1 JAN 73 1473 EDITION OF 1 NOV 65 IS OBSOLETE
S/N 0102-014-6601

UNCLASSIFIED

SECURITY CLASSIFICATION OF THIS PAGE (When Data Entered)

387695 LB

of attack. An additional reduction in drag of at least twenty percent is achievable with a properly designed "area rule" fairing.

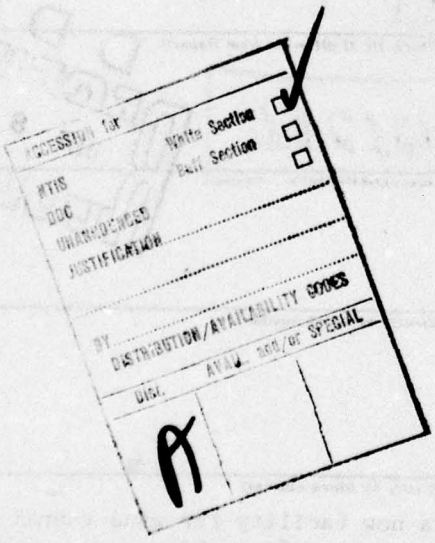

TABLE OF CONTENTS

LIST OF FIGURES

LIST OF TABLES

ABSTRACT

The hub-pylon evaluation rig, a new facility for wind tunnel experiments on large scale helicopter rotor hub-pylon configurations, was used to determine the variation of hub-pylon drag with shaft angle and height, and pylon angle parameters. In addition, a series of low drag "area rule" fairings and shaft fairings were evaluated. The results indicate that the proper selection of shaft angle with respect to the pylon and pylon angle of attack can yield a twenty percent reduction in drag for a given shaft angle of attack. An additional reduction in drag of at least twenty percent is achievable with a properly designed "area rule" fairing.

ADMINISTRATIVE INFORMATION

The experimental program reported herein was funded jointly by the Naval Air Systems Command (AIR-320) and the National Aeronautics and Space Administration (Langley Research Center) under task area WF41.421.201 and purchase request L-97786 respectively. The David W. Taylor Naval Ship Research and Development Center (DTNSRDC) work units were 1-1619-105 and 1-1619-108.

UNITS OF MEASUREMENT

All data recorded during this experiment were either measured in or converted directly to U.S. customary (US) units. Hence, U.S. customary units are the primary units in this report. Metric units are given either adjacent to the US units in parentheses or opposite US units in the case of graphs. Angular measurement is the only exception. The unit degrees is not converted to radians on graphs.

SYMBOLS

C_d	Drag coefficient, $\frac{D}{qs}$	
D	Aerodynamic drag force	lbs. (N)
D/q	Parasite area	ft.^{2} (m^2)
h	Gap between the hub and the pylon	ft. (m)
ℓ	Reynolds number reference length	ft. (m)
L	Aerodynamic lift force	lbs. (N)
L/D	Lift to drag ratio	
L/q	Lift area	ft.^{2} (m^2)
q	Dynamic pressure	psf. (Pa)
R	Reynolds number, $\frac{V\ell}{\nu}$	
S	Drag coefficient reference area	ft.^{2} (m^2)
t	Hub thickness	ft. (m)
V	Reference Velocity	fps (m/s)
α_p	Pylon angle of attack	deg.
α_s	Shaft angle of attack, $\alpha_p + \phi$	deg.
ν	Kinematic viscosity of air	ft.^{2}/s (m^2/s)
ϕ	Shaft angle with respect to the pylon	deg.
σ	Standard deviation of X, $\sqrt{\frac{1}{n-1}\left[X^2 - \frac{(X)^2}{n}\right]}$	[X]

Subscripts

H	Hub
HS	Hub plus shaft
P	Pylon
S	Shaft
T	Total

INTRODUCTION

Helicopter fuselage drag has been recognized as the major cause for the noncompetitiveness of helicopters with fixed wing aircraft in the low to moderate speed cruise mission. The American Helicopter Society (AHS) recently sponsored a study of rotorcraft drag by a panel of engineers and scientists from both industry and government. Their report[1] to the AHS National Forum in 1975 indicated that sizable gains throughout the spectrum of helicopter performance could be achieved by reducing the parasite drag of the fuselage.

The David W. Taylor Naval Ship Research and Development Center (DTNSRDC) has been addressing the problem of helicopter parasite drag since fiscal year 1973. The Navy effort, titled the Helicopter Drag Technology Program[2], is a continuing program funded under the cognizance of the Naval Air Systems Command with the participation of the U.S. Army Air Mobility Research and Development Laboratory (Eustis Directorate) in the area of interactive graphics[3] and of the National Aeronautics and Space Administration (Langley Research Center) in the area of rotor hub-pylon drag. A portion of the experimental evaluations of the latter joint effort is documented in this report.

The purposes of this experiment were: (1) to validate the performance of the hub-pylon evaluation rig (HPER), a new facility for wind tunnel testing large scale rotor hub-pylon models; (2) to provide basic hub-pylon configuration parameter information; and (3) to determine the merit of subsonic area rule fairings in the complex hub-pylon flow field as a means of reducing aerodynamic drag. The HPER was designed and constructed as an alternative to expensive large scale wind tunnel tests of helicopter full fuselage models for the investigation and reduction of drag associated with the hub-pylon region. Use of the HPER, makes it possible to test large scale hub-pylon models in small wind tunnels, thus reducing scale effects and costs simultaneously. Its capabilities include the separate measurement of forces on the hub, shaft, and pylon, and the independent variation of shaft and pylon angles of attack. A more detailed description of the HPER is given below under APPARATUS and a detailed rational for the separation of the hub-pylon region from the rest of the

fuselage is given in reference 4. The parameters investigated were: pylon angle of attack, varied from minus ten to plus five degrees; shaft angle of attack, varied from minus twenty-five to plus ten degrees; hub-pylon gap, varied one to three hub thicknesses; and Reynolds number, varied as dynamic pressure from ten to fifty pounds per square foot (479. to 2393. pascals). These parameters cover a broad range of possible flight and vehicle configurations.

The area rule concept was originally developed experimentally by R. T. Whitcomb for transonic aircraft (for a brief discussion see reference 5). It has since been extended on a theoretical basis into supersonic flow and in actual practice without analysis into high subsonic flow. (Reference 2 gives a very brief empirical discussion relating body radius distribution to diffuser flow separation criteria as a kind of subsonic area rule.) In practice, the area rule states that the drag of a body may be held near a minimum by avoiding sharp discontinuities in the body's area (radius) distribution. Transonically and supersonically, smooth area distribution pay off by reducing the number and strength of shock waves, hence reducing wave drag. Subsonically, smoothing the area distribution smoothes the pressure distribution eliminating regions of sharply adverse pressure gradients which would normally trigger boundary layer separation. Of course, even a configuration with a smooth area distribution may still have local discontinuities which will cause shocks or separation, but the overall area distribution and good design can prevent these local disturbances from propagating.

The HPER model configuration was designed for simplicity from a geometric point of view for modeling in potential flow analyses, while maintaining configuration parameters representative of a variety of actual or proposed helicopters. In this respect, the application of the area rule concept was restricted to the design of fairings to be added to the basic configuration to smooth the area distribution. These fairings take the shape of simple bumps and vanes and are described below under MODELS.

APPARATUS

The hub-pylon evaluation rig (HPER) is a new experimental facility at DTNSRDC for the wind tunnel testing of large scale helicopter hub-pylon models. As seen in Figure 1, the HPER is a very complex mechanism. Its five exterior parts, the splitter plate assembly, fuselage, pylon, shaft assembly, and hub, are shown in Figure 2. The splitter plate assembly serves to channel the wind tunnel boundary layer away from the model and provides a housing for the lower part of the HPER's support frame work. The fuselage represents the adjacent portion of the helicopter fuselage and serves to establish the flow field for the pylon. The pylon is the lowest part of the configuration on which loads are measured. Except for a seal to prevent air from leaking between the pylon and fuselage and disturbing the flow, the pylon is isolated from the fuselage and shaft assembly. (The pylon is part of the configuration being evaluated, while the fuselage is part of the test apparatus.) The shaft assembly consists of two parts, an inner shaft which supports the hub and is connected to the shaft angle drive system, and an outer shaft. The outer shaft is isolated from the pylon and hub models and is supported by a one component balance attached to the inner shaft. The hub model is supported by a six component balance attached to the inner shaft.

The functioning of the HPER is also represented in Figure 2. To reiterate, there are three independent force balances, pylon, shaft, and hub, and two remotely controlled, independent angle drive mechanisms, pylon angle of attack and shaft angle with respect to the pylon. The pylon balance measures five components of forces and moments (side force excluded); the shaft balance measures one force component perpendicular to the shaft axis; and the hub balance measures a full six components of forces and moments. The pylon and fuselage can be remotely driven through an angle of attack of minus ten to plus five degrees measured from the horizontal and the shaft can be remotely driven through an angle range of minus fifteen to plus five degrees relative to the pylon. As the pylon and fuselage are driven in angle of attack, the fuselage passes through an opening in the splitter plate and maintains a constant minimum

Table 1 - Calibration Accuracy

Balance	Component	Max Applied Load lbs.	Max Applied Load (N)	Min Applied Load lbs.	Min Applied Load (N)	Max. Deviation as % Max. Load	Standard Deviation of Measured Load / Applied Load
Pylon	(-) Axial	-50.	(-222.40)	-1.	(-4.45)	1.7	0.034
				-10.	(-44.48)		0.008
	(+) Axial	+50.	(+222.40)	+1.	(+ 4.45)	0.6	0.044
				+10.	(+44.48)		0.005
	(-) Normal	-320.	(-1423.36)	-20.	(-88.96)	2.0	0.019
				-60.	(-226.88)		0.006
	(+) Normal	+320.	(+1423.36)	+20.	(+88.96)	3.7	0.010
				+60.	(+226.88)		0.006
Shaft	(+) Axial	+35.	(+155.68)	+0.5	(+2.22)	1.76	0.044
				+5.0	(+22.24)		0.030
Hub	(±) Axial	±125.	(±556.00)	+25.	(+111.20)	0.27	0.004
	(±) Normal	±750.	(±3336.00)	±150.	(±667.20)	0.05	0.003

Pylon Angle of Attack	0.02 degree (0.4 milliradian)
Shaft Angle Relative to Pylon	0.02 degree (0.4 milliradian)

clearance gap as a result of the shapes of the fuselage surface and splitter opening.

The calibration accuracies of the force balances and angle drives are given in Table 1. Further descriptions of the fuselage, pylon, hub, and shaft, are given below in MODELS.

The experimental evaluation was conducted in the DTNSRDC 8- by 10-Foot Subsonic North Wind Tunnel[6]. The output of the HPER balances, angles of attack, and tunnel flow information were digitally recorded on magnetic tape with a Beckman high speed data acquisition system. The HPER was bolted directly to the floor of the wind tunnel test section, and all balance, and angle drive power and position cables were routed inside the model through the floor of the test section to the control room.

MODELS

The HPER models evaluated were of the following types: basic configuration, basic configuration with various area rule fairings and vanes, and the basic configuration with shaft fairings. The basic configuration which consists of the non-metric parts of the HPER, the splitter plate assembly and fuselage, and the metric parts, the pylon, shaft and hub, is shown in Figure 3. Of the components, the fuselage, pylon, shaft, and hub can all be mathematically described by the equation of a general ellipsoidal surface.

$$\left(\frac{x}{a}\right)^2 + \left(\frac{y}{b}\right)^2 + \left(\frac{z-h}{c}\right)^2 = 1 \qquad (1)$$

In addition the opening in the splitter plate through which the fuselage passes when the angle of attack is changed is also elliptical. The origin of the axes system to which all of the components are related, is located on the floor of the wind tunnel test section with the positive z-axis vertical and the x-axis in the wind direction. The models, unless otherwise noted, have left-right and fore-aft symmetry. The values of constants in equation (1) are given in Table 2.

Table 2 - Model Geometric Constants In Inches (Centimeters)

	a		b		c		h	
Fuselage	78.324	(198.94)	27.414	(69.63)	78.324	(198.94)	-30.000	(-76.20)
Pylon	51.050	(129.67)	17.868	(45.38)	7.190	(18.26)	28.810	(73.18)
Shaft	3.000	(7.62)	3.000	(7.62)			-	-
Hub	15.000	(38.10)	15.000	(38.10)	3.750	(9.53)	47.250	(120.02)
							54.750	(139.07)
							62.250	(158.12)
Splitter Plate Opening	60.125	(152.72)	21.125	(53.66)	-	-	20.340	(51.66)

The constants were selected to match the surface tangents of the fuselage and pylon along their line of intersection. In addition, the pylon angle of attack mechanism pivots the model about an axis parallel to the y-axis through the point (x, y, z) equal (0., 0., h-fuselage). This ensures that the clearance between the fuselage and splitter plate remains constant as pylon angle of attack is changed. The shaft pivot point is located just beneath the surface of the pylon.

The area rule fairings and vanes are more difficult to describe. There were two area distributions considered in developing the fairings and vanes: the body area distribution (BAD) and stream tube area distribution (STAD). Both are shown in Figure 4. The BAD includes all of the cross sectional area (taken perpendicular to the free stream flow direction) of the fuselage, pylon, shaft, and hub above the splitter plate with the pylon and shaft angles set at zero degrees and the hub at the lowest height (the only height used with any fairings). The STAD was used in consideration of nozzle and diffuser type flow beneath the hub. The stream tube used was that shown in Figure 5. Simple straight lines or curves were drawn to smooth the discontinuities in the distributions caused by the hub and shaft. It is this additional area added to the distributions (dashed lines in Figure 4) which was molded into bump or vane type fairings.

There were three types of bump fairings used, all of which were implemented by distributing the additional area as a half body (or bodies) of revolution on the surface of the pylon. The BAD was utilized to generate two types of bump fairings, single bumps on the pylon centerline and twin bumps on either side of the centerline. The skew axis of the twin bumps was an attempt to account for lateral distribution of the cross sectional area. The third type bump fairing was derived from the STAD in the same manner as the BAD twin bump fairing.

The vane type fairings were developed from the STAD. Aside from structural considerations, the design criteria for the vanes was the maintenance of constant local stream tube areas between the vanes or between the vanes and shaft. All of the fairings and vanes are shown in Figure 6. (The bump fairings do not include any cross sectional area to smooth the area distributions between the hub and shaft.)

Two shaft fairings were tested in addition to the six inch diameter outer shaft: an airfoil shape and a larger diameter cylinder (Figure 7). The airfoil shape was a 29.5 inch (0.7493 m) chord, NACA 0028 section and the cylinder was twelve inches in diameter. Both shaft fairings were evaluated at the shortest shaft length on the basic configuration. For simplicity, the configuration numbers in Table 3, will be used to label the data.

Table 3 - Configuration Numbers

1. Basic Configuration - shortest shaft length
2. Basic Configuration plus four STAD bumps
3. Basic Configuration plus four BAD bumps
4. Basic Configuration plus four hub vanes
5. Basic Configuration plus four shaft vanes
6. Basic Configuration plus four hub and four shaft vanes
7. Basic Configuration plus two BAD bumps
10. Basic Configuration plus large diameter shaft fairing
11. Basic Configuration plus NACA 0028 shaft fairing
12. Basic Configuration - medium shaft length
13. Basic Configuration - longest shaft length

DATA CORRECTION AND ACCURACY

Corrections to the data were, for the most part, kept as simple as possible. Initially the only correction planned was for solid blockage (see Reference 7). Since the HPER and the models were very large and unusual in shape in respect to the wind tunnel and more conventional models, other corrections (e.g. buoyancy) were omitted until theoretical analyses can be conducted to develop new methods of accounting for these effects for the HPER.

During the course of the experiment, it was noted that there were significant shifts in the wind off zero data points taken at the end of wind on data runs for information recorded from the pylon balance. An analysis revealed the cause to be temperature gradients inside the model. Even though free stream temperature and one temperature inside the model were recorded, it was not possible to make rigorous corrections to the pylon balance data because of the non-uniformity of the temperature gradients. The correction for zero shift which was applied was to apportion the shift linearly among the data points of each run. The rational was that the temperature change was a function of the rate at which energy was added to the wind stream which was essentially constant while the wind tunnel was running. Since time was not a recorded variable, the pylon force change was divided among the data points which were approximately equally spaced during each data run. The average zero shift magnitude for lift and drag are given in Table 4.

Table 4 - The Average Zero Shift Magnitudes for Lift and Drag In Pounds (Newtons)

	Lift	Drag
Pylon Balance	13.46 (59.87)	4.16 (18.50)
Shaft Balance	- -	0.38 (1.69)
Hub Balance	0.11 (0.49)	0.03 (0.13)

Each data point reported on herein consists of the average of a series of about ten individual readings taken at one half second intervals. For

most configurations, three data points were taken at a dynamic pressure of fifty pounds per square foot with angles of attack of the pylon and shaft equal to zero. It is these data points which give an indication of the accuracy of the test data. Computing the means and the standard deviations (σ) of these repeated data points and correcting the standard deviations for the actual number of readings yields Figure 8. (The standard deviation of three data points can be shown to be about twenty percent higher than that computed from all of the readings included in the three data points or about thirty-seven percent higher for two data points.)

By examining Figure 8, several observations can be made with respect to the precision (scatter) of the data.

1. Data recorded by the hub and shaft balances is very good
2. Drag data recorded from the pylon balance generally has an adequate level of precision with the exception of configurations 10 and 11.
3. The precision of lift data recorded from the pylon balance varies from configuration to configuration with a 3σ value approaching thirteen percent of the mean value in one case.
4. The scatter of lift/drag ratios is less than the scatter of lift data with the exception of configuration 11.
5. Comparison of data including pylon balance output can be made between configurations if differences are outside of the 3σ precision band.
6. No special considerations are necessary to use the hub and shaft data.

RESULTS AND DISCUSSION

The purposes of this experiment as set forth in the INTRODUCTION were: to validate the performance of the HPER; to provide basic hub-pylon parameter information; and to determine the merit of hub-pylon subsonic area rule fairings. The first purpose was discussed under APPARATUS, and CORRECTIONS and ACCURACY. To summarize, the HPER is a valuable tool and reliable conclusions can be drawn from the data, where load differences (as they were in this test) are greater than the error bands shown in Figure 8. However, the performance of the HPER can be improved in two

respects: the accuracy of the shaft and pylon balances as calibrated; and the behavior of the pylon balance during temperature variation. The accuracy could be improved for both balances by curvefitting the balance sensitivities. This will be done for subsequent investigations. The temperature behavior of the pylon balance is believed to be caused by non uniform expansion and contraction of structural members between the load sensing elements. Further analysis is required before corrective action is taken.

BASIC CONFIGURATION PARAMETER DATA

The basic hub-pylon parameters investigated were pylon and shaft angles of attack at a constant dynamic pressure of 50 psf. (2393 Pa), dynamic pressure at angles of attack of zero, and hub height (configurations 1, 12, and 13). These data are presented in Figure 9 as parasite area, D/q, and lift to drag ratio, L/D, versus shaft angle of attack, and D/q versus dynamic pressure, q. Total D/q and L/D values are presented and, in addition, the component values of D/q, hub, shaft, pylon, and hub plus shaft, are presented for the constant q data. (Throughout the data presentation, data point symbols have been omitted where no ambiguity exists between configurations, because of the implied precision conveyed by symbol size.) The data points were spaced as follows: angles of attack were varied in increments of five degrees (.0873 radians) about zero; and dynamic pressure was varied in increments of 10 psf (478.8 Pa) starting at 10 (478.8).

Some of the trends observable in the data for all three basic configurations in Figure 9 are: (1) the existence of minimums in parasite area, D/q, at constant dynamic pressure, q, for constant values of shaft angle with respect to the pylon for total D/q and pylon D/q, and, similarly, the existance of maximums for total lift to drag ratios, L/D; (2) the relatively constant values of shaft D/q for each configuration as angles of attack were varied; (3) the decrease in hub D/q and hub plus shaft D/q as shaft angle decreases; and (4) the relative magnitudes of the component D/q values (hub D/q largest, then shaft D/q, and pylon D/q smallest).

Comparisons among the basic configurations yield several other observations. Shaft parasite area increases with, but not in direct proportion to the shaft length. This illustrates the nozzle-diffuser effect of the hub and the pylon on shaft. An estimate of the "super-velocity" caused by the constriction of the flow, can be made by using the streamtube area distribution of Figure 4 and the following formula:

$$\text{Velocity Increase} = \frac{(\text{Area Change})\ (\text{Entrance Velocity})}{(\text{Entrance Area}) - (\text{Area Change})}$$

The resultant velocity increases (as decimals of the entrance velocity) are, in order to increasing shaft length: 0.69, 0.40, and 0.28. (Shaft area was excluded from the calculation.) Computing the shaft drag coefficients, C_d, and re-referencing them to the local velocities (the sum of the velocity increments and the entrance velocity) yields Figure 10 where the shaft cylinder drag coefficients are plotted versus Reynolds' number. Comparisons are made to drag coefficient versus Reynolds' number data from reference 9 and data for the larger twelve inch diameter shaft fairing of configuration 10. Using the increased velocities reduced the drag coefficients to values close to those expected from Reference 9. The remaining differences for the six inch diameter shaft fairing of configurations 1, 12, and 13 are attributed to a small shaft angle of attack pitch drive cover exposed to the flow at the base of the shaft fairing. This cover is attached to the shaft fairing; and hence, forces on it are included in the shaft drag. The large diameter shaft fairing covers the pitch drive cover completely and its drag coefficient more closely agrees with Reference 9.

Pylon parasite area has the same range of values for all three configurations in Figure 9. This result is reasonable because of the low profile shape of the pylon and its small frontal area. Thus flow separation on the pylon caused by the hub and shaft has only a small effect on pylon drag. The bulk of the pylon drag can be attributed to skin friction. At negative pylon angles of attack the pressure forces on the pylon tend to reduce the pylon drag and, in fact, result in a small

net thrust from the pylon in some of the configurations tested. Configuration 1 has the smallest parasite area and the highest lift to drag ratio of the three configurations in Figure 9 because of the added drag of the longer shafts of configurations 12 and 13.

The drag trends associated with the hub height variation are shown in Figure 11. Although a wider range of shaft lengths would be desirable, a number of conclusions can be drawn from this data. The hub has a region of adverse interference as indicated by the peak in the hub parasite area curve near a height of two hub thicknesses. For heights, (h/t), greater than three the hub parasite area should decrease and approach a constant value (unknown). For heights less than one the hub parasite area may decrease and approach a non zero value at zero height, but its behavior is not known.

The shaft parasite area is a continuously increasing function of height for hub heights less than one, shaft parasite area should smoothly approach zero. For hub heights greater than three, the shaft parasite area will approach a linearly increasing function of height which can be expressed as:

$$\frac{D}{q} = C_1 \frac{h}{t} + C_2$$

where the first constant, C_1, can further be defined as

$$C_1 = \pi r^2 t \; C_d$$

The coefficient, C_d, is the cylinder two dimensional drag coefficient, r is the radius of the shaft fairing, and t is the thickness of the hub. Using the two points, ((h/t), (D/q)), (0, 0.33) and 4., 0.58), the straight line intercept as drawn in Figure 11 and a point on the assumed straight line respectively, yields a value of 0.51 for the drag coefficient, C_d, which agrees well with reference 9 and Figure 10.

The pylon parasite area decreases as (h/t) increases and should

approach a constant value (Figure 11). The total parasite area increases with hub height through the range of test data, but the trends noted for the hub, shaft, and pylon parasite areas indicate that a relative maximum exists near (h/t) = 3 and a relative minimum exists near (h/t) = 4.5. For values of (h/t) greater than 4.5, total parasite area should increase in the same manner as shaft parasite area since pylon and hub values are expected to approach constants. For values of (h/t) less than one, total parasite area is expected to decrease to a finite value at (h/t) equal zero although the trends in this region are not as clearly established as those for large hub heights. If this decreasing trend in total parasite area holds true, then considerable additional drag reduction should be possible at a hub height of zero by integrating the hub and pylon and contouring their intersection. The integrated hub-pylon would, of course, only have application to rigid rotor configurations because of the greater blade clearance necessary with softer rotor types.

AREA RULE FAIRINGS

There were six area rule fairing configurations tested, configuration numbers 2, 3, 4, 5, 6, and 7. Of the six, all configurations except number 5 were evaluated over a range of shaft and pylon angles of attack and dynamic pressures. Configuration 5 (shaft vanes) was evaluated only over the dynamic pressure range as a result of an earlier experiment which indicated that it would have a higher drag than the other configurations. The results of the area rule fairing evaluation are plotted in Figure 12 as parasite area verse shaft angle of attack and dynamic pressure, and lift-drag ratio verse shaft angle of attack in the same manner as Figure 9. Using configuration 1 as the baseline "clean" configuration, configuration 7, the single body area distribution bump fairings, yielded a substantial improvement in drag and lift-drag ratio. In more detail, the following observations were made from Figure 12 for constant dynamic pressure. (1) All of the area rule configurations except number 3 yielded lower parasite areas than the clean configuration with configuration 7 as much as 24 percent lower.

(2) All area rule configurations except number 6 yielded higher lift-drag ratios with configuration 7 as much as 19 percent higher than the clean configuration. (3) All area rule configurations had lower hub and lower shaft parasite areas than the clean configuration values with configuration 7 showing reductions 93 percent and 83 percent respectively. (4) All area rule configurations except number 2 had higher pylon parasite areas than the clean configuration.

The outstanding drag characteristics of configuration 7 support the integrated hub low drag concept mentioned earlier. The presence of large area rule bumps ahead of and behind the shaft evidently cause the flow to go around the hub-shaft region rather than between the hub and pylon. This effectively blocks out the shaft, closing its wake and reducing its interference with the flow on the hub. The aft bump also contributes directly by constraining the lower part of the hub wake. The very large reductions in hub and shaft parasite area confirm this postulation. The relatively smaller (20 percent) reduction in total parasite area and the pylon parasite area plot for configuration 7 show that the large hub and shaft drag reductions are substantially off set by the increased skin friction and pressure drag due to the area rule fairing's presence on the pylon.

In view of the difference in the size of the area bump between configurations 2 and 7, it is interesting to note that configuration 2 achieved a reduction in parasite area of about 12 percent. The decrease appeared primarily as a reduction in hub drag with a small additional reduction in pylon drag at extreme negative shaft angles. The small area bumps, derived from the stream tube area distribution, lend themselves to drag reduction in vehicle configurations where the existing clearance to rotating components is minimal.

SHAFT FAIRINGS

In addition to the basic six inch in diameter cylindrical shaft fairing of the "clean" configuration, a twelve inch in diameter cylindrical shaft fairing, configuration 10, and a 29.5 inch chord airfoil shape shaft fairing, configuration 11, were evaluated. Neither of these two

shaft fairings were adapted to the pylon to permit shaft angle variation with respect to the pylon; hence, test conditions included only pylon angle of attack and dynamic pressure changes. The results are presented in Figure 13. The plots of total parasite area at constant dynamic pressure indicate that these two configurations have even lower drag than the best area rule configuration. An examination of Figure 8 shows that these two configurations also have the largest data scatter of all configurations for total parasite area as a result of large scatter in pylon parasite area data. For this reason conclusions about the merit of these two configurations overall should not be drawn. However, Figure 8 also indicates that the precision of the hub and shaft data is comparable for all configurations. Therefore the following observations can be made with respect to the hub and shaft fairing data of Figure 13. The airfoil shape shaft fairing causes a substantial reduction in hub drag as compared to the clean configuration hub drag as pylon (shaft) angle of attack increases. This characteristic would make configuration 11 a candidate for a high speed helicopter equipped with auxiliary propulsion where slightly positive shaft angles of attack are expected in cruise flight, if the low pylon drag could be verified. The following brief analysis with respect to pylon drag is offered. The theoretical peak pressure coefficient for an ellipsoid of about the same shape as the pylon is -.127 (Reference 10). If this value is applied over the entire surface of the pylon, a pressure force/dynamic pressure of 2.45 is possible for the pylon. Rotating the pressure force minus ten degrees would give a theoretical pylon thrust (negative drag)/dynamic pressure of .43 which is about one half the magnitude of that obtained for configuration 10, but greater than that obtained for configuration 11. From this brief analysis it is possible to state that the parasite area recorded for configuration 11 is probably obtainable.

The shaft parasite areas increased at least 60 percent over the clean configuration shaft value. The increases were expected and most likely are due to increased skin friction drag (both configurations) and increased pressure drag (Configuration 10). Figure 15 is a comparison of

all the shaft fairings used in the test. It shows that from the point of view of just the shaft drag, that the simple short six inch diameter cylinder is the best. Note also the effect of Reynolds number and the apparent transition from laminar to turbulent flow on the two longer six inch cylindrical shaft fairings as dynamic pressure is increased.

GENERAL

There was a considerable body of data recorded during this experiment. Since the primary objective of the Helicopter Drag Technology Program is to reduce fuselage drag, only that data is presented in this report. These final two observations apply to all the configurations tested. (1) The minimum drag and maximum lift to drag ratio do not occur at the same set of configuration parameters. This implies that the usual set of trade offs must be made in establishing the hub-pylon configuration for "optimum" vehicle performance. (2) For a given configuration, the selection of shaft angle with respect to the pylon and pylon angle of attack to achieve the desired shaft angle of attack can yield hub-pylon drag reductions or lift/drag ratio increases of 20 percent. Thus for a helicopter required to operate at a wide variety of flight conditions for significant lengths of time, it would be desirable to provide a variable angle main rotor shaft if the weight penalty can be justified. More important, perhaps, is the application of this observation to the design of a basic airframe to meet the requirement of the different services. The tailoring of the shaft angle (fixed) for each services mission could mean the difference between constructing a helicopter which performs most of the missions well or only some of them adequately.

REFERENCES

1. "Rotorcraft Parasite Drag", a Special Report Presented to the 31st Annual National Forum of the American Helicopter Society by the Ad Hoc Committee on Rotorcraft Drag, Wash., D.C., 14-15 May 1975.

2. Montana, P.S., "Helicopter Drag Technology Program - Fiscal 1973 Progress Report" DTNSRDC Technical Note AL-310, Sep 1973.

3. Kelly, B.M. and M.B. Marquardt, "Interactive Helicopter Design: A Geometry Package User's Manual," DTNSRDC Report CMD-28-74, Sep 1974.

4. Williams, R.M. and P.S. Montana, "A Comprehensive Plan for Helicopter Drag Reduction," Presented at the American Helicopter Society Symposium on Helicopter Aerodynamic Efficiency, 6-7 Mar 1975.

5. Goodmanson, L.T. and L.B. Gratzer, "Recent Advances in Aerodynamics for Transport Aircraft," Aeronautics and Astronautics, Dec 1973.

6. Kidd, M.A., "Subsonic Wind Tunnel Facilities," DTNSRDC Report 3782, Jan 1972.

7. Pope, A. and J.J. Harper, "Low Speed Wind Tunnel Testing," John Wiley and Sons, Inc., 1966.

8. Montana, P.S., "Experimental Investigation of Three Rotor Hub Fairing Shapes," DTNSRDC Report ASED 333, May 1975.

9. Schlichting, H., "Boundary Layer Theory," McGraw-Hill Book Company, 1968.

10. Shapiro, A.H., "The Dynamic and Thermodynamics of Compressible Fluid Flow, Volume I," The Ronald Press Company, 1953.

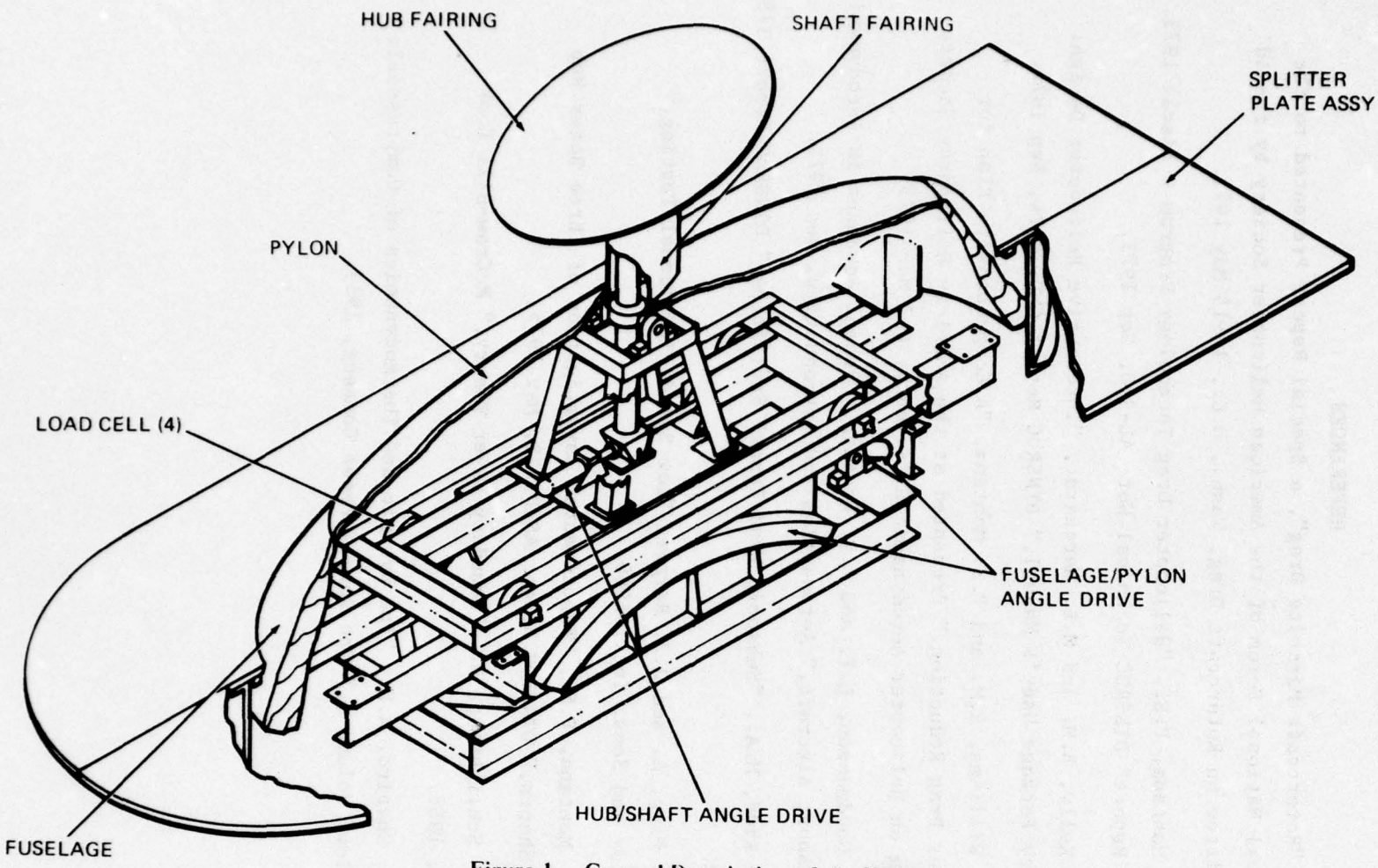

Figure 1 – General Description of the HPER

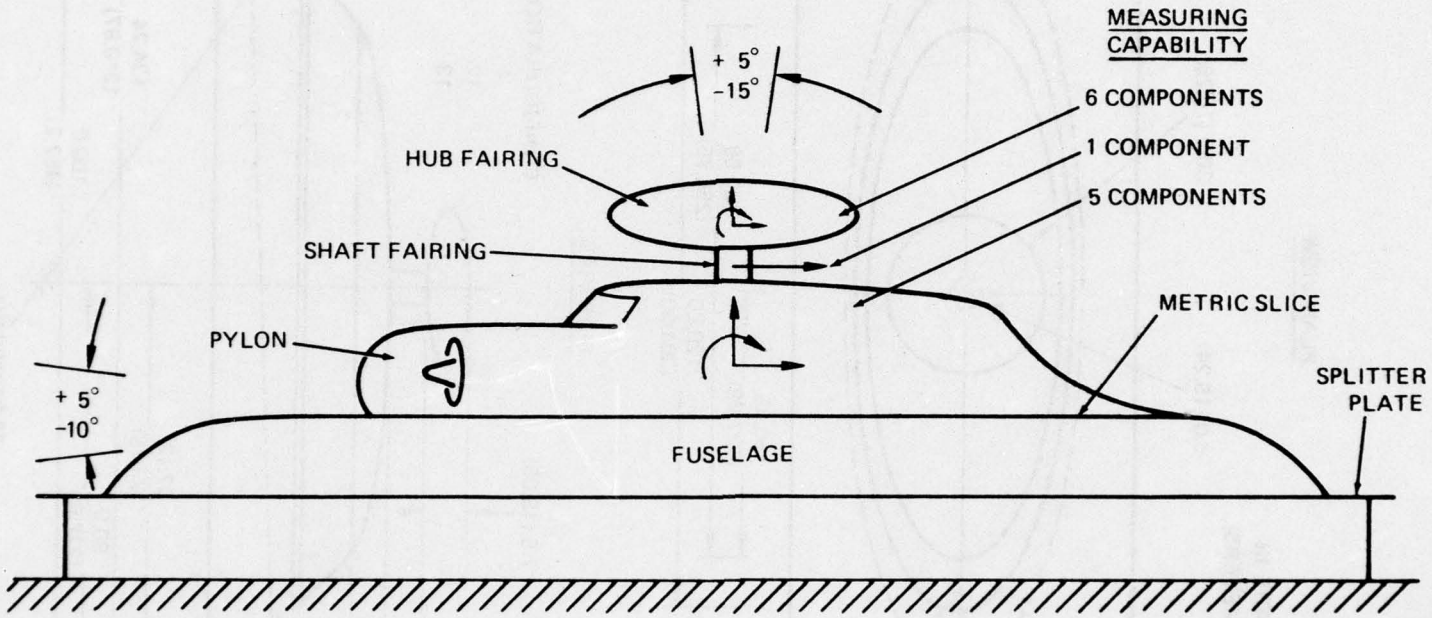

Figure 2 – HPER Capabilities

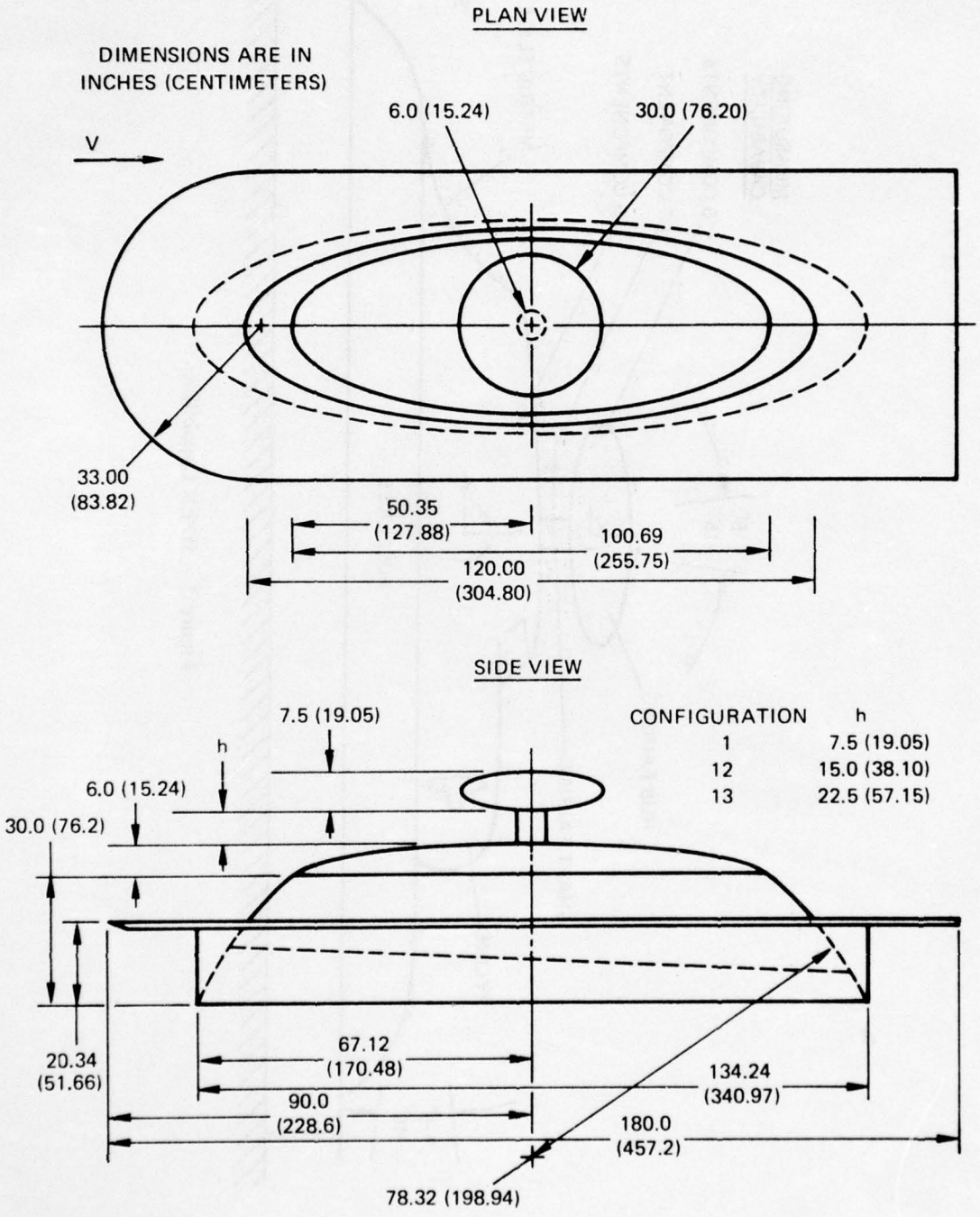

Figure 3 – Basic Configuration

Figure 3 (Continued)

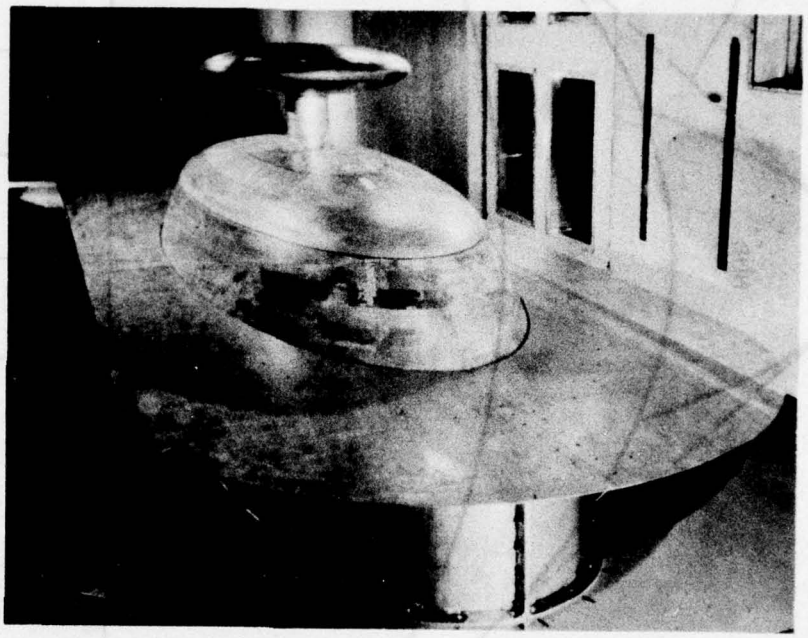

CONFIGURATION 1 –
BASIC CONFIGURATION

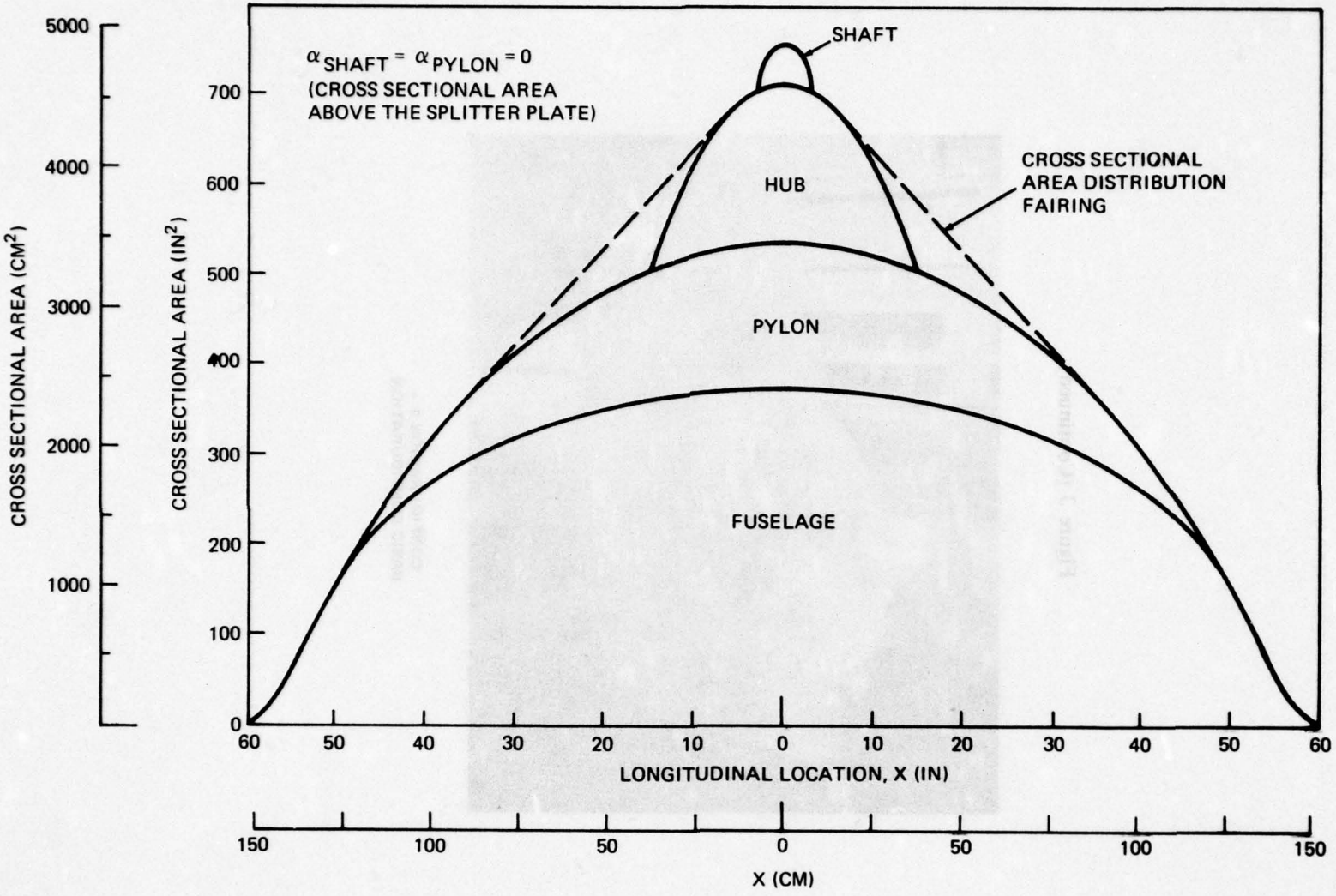

Figure 4 – Configuration Area Distributions
(a) Cross Sectional Area Distribution

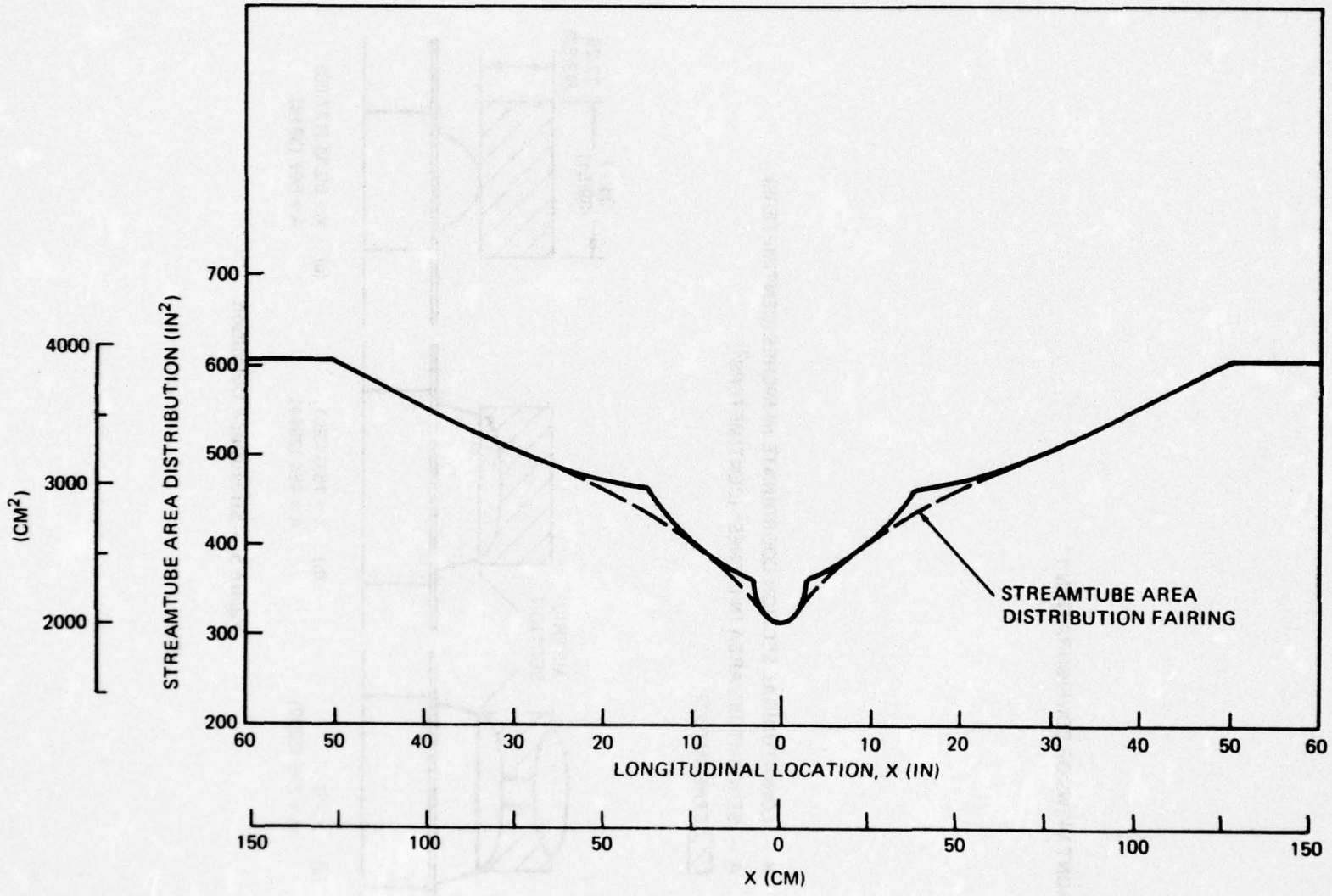

Figure 4 – (Concluded)
(b) Streamtube Area Distribution

FRONT VIEWS OF CONFIGURATION 1

X – LONGITUDINAL SECTION COORDINATE IN INCHES (CENTIMETERS)

A – STREAMTUBE AREA IN INCHES^2 (CENTIMETERS^2)

STREAMTUBE

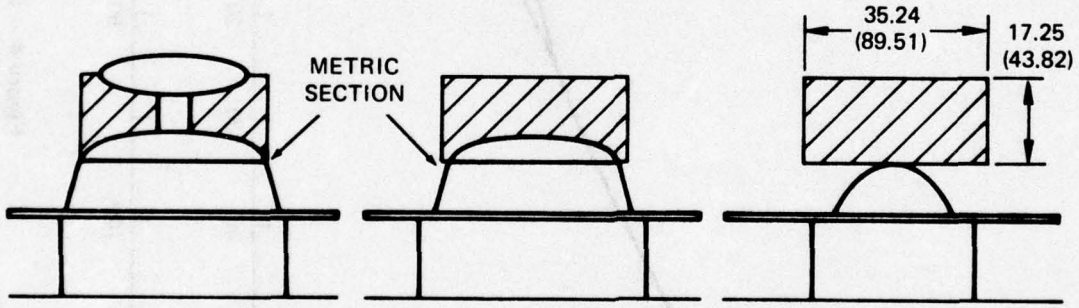

(a) X = 0
A = 315 (2032)

(b) X = 15.0 (38.1)
A = 464 (2994)

(c) X = 50.35 (127.88)
A = 607 (3916)

Figure 5 – Streamtube Definition

DIMENSIONS IN INCHES.

FAIRING COORDINATES

DISTANCE FROM TRANSVERSE ℄ "Y"	STATION RADIUS "X"
7.0"	0.00"
7.25	0.74
7.50	1.09
8.0	1.59
9.0	2.39
10.0	3.11
12.0	4.61
14.0	6.16
14.75	6.72
15.0	6.80
15.5	6.80
16.0	6.65
18.0	6.08
20.0	5.46
22.0	4.83
24.0	4.18
26.0	3.52
28.0	2.87
30.0	2.21
32.0	1.56
33.0	1.19
33.5	0.89
33.75	0.66
34.0	0.00

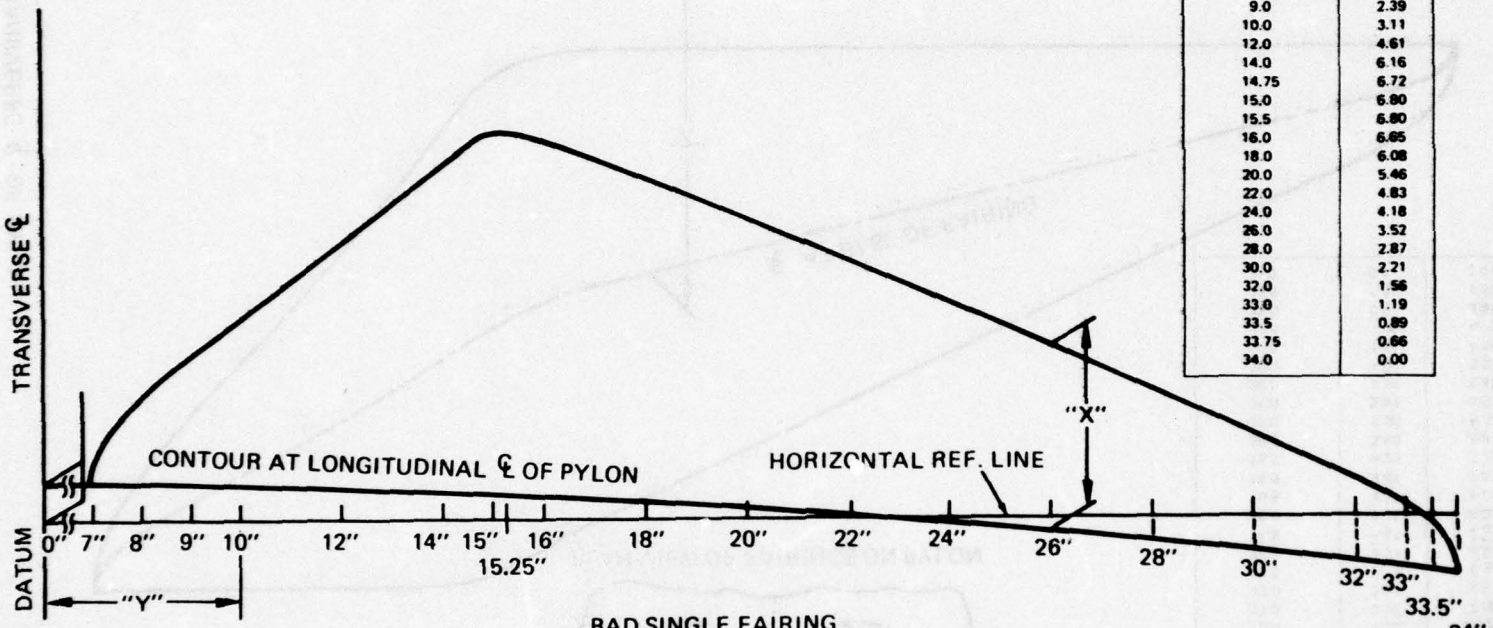

BAD SINGLE FAIRING
PROFILE VIEW
LOCATED ON LONGITUDINAL ℄ OF PYLON

Figure 6 – Area Distribution Fairing Models
(a) Body Area Distribution (BAD) Single Bump Fairings

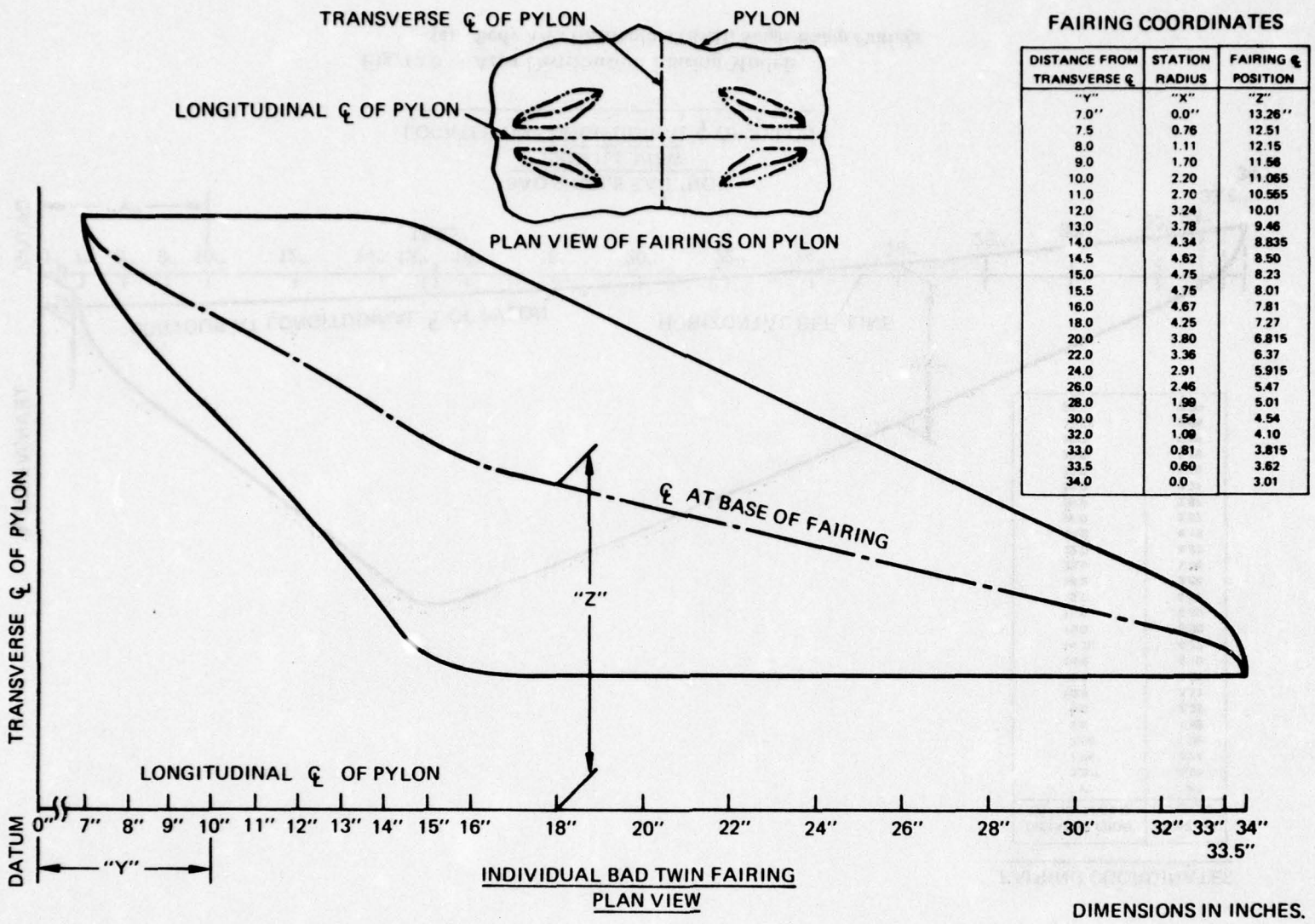

FAIRING COORDINATES

DISTANCE FROM TRANSVERSE ℄	STATION RADIUS	FAIRING ℄ POSITION
"Y"	"X"	"Z"
7.0"	0.0"	13.26"
7.5	0.76	12.51
8.0	1.11	12.15
9.0	1.70	11.56
10.0	2.20	11.065
11.0	2.70	10.565
12.0	3.24	10.01
13.0	3.78	9.46
14.0	4.34	8.835
14.5	4.62	8.50
15.0	4.75	8.23
15.5	4.75	8.01
16.0	4.67	7.81
18.0	4.25	7.27
20.0	3.80	6.815
22.0	3.36	6.37
24.0	2.91	5.915
26.0	2.46	5.47
28.0	1.99	5.01
30.0	1.54	4.54
32.0	1.09	4.10
33.0	0.81	3.815
33.5	0.60	3.62
34.0	0.0	3.01

Figure 6 – (Continued)
(b) Twin Bump Fairings

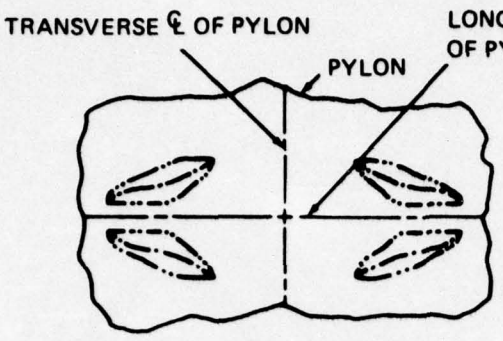

PLAN VIEW OF FAIRINGS ON PYLON

DIMENSIONS IN INCHES.

FAIRING COORDINATES

DISTANCE FROM TRANSVERSE ℄	STATION RADIUS	FAIRING ℄ POSITION
"Y"	"X"	"Z"
9.5"	0.0"	8.69"
10.0	0.28	8.41
11.0	0.84	7.86
12.0	1.37	7.31
13.0	1.89	6.80
14.0	2.36	6.32
14.5	2.58	6.10
15.0	2.68	5.90
15.5	2.61	5.71
16.0	2.53	5.55
17.0	2.26	5.25
18.0	2.00	4.99
19.0	1.76	4.75
20.0	1.53	4.52
21.0	1.32	4.31
22.0	1.11	4.10
23.0	0.89	3.87
24.0	0.61	3.61
24.5	0.36	3.365
24.75	0.20	3.205
25.00	0.00	3.03

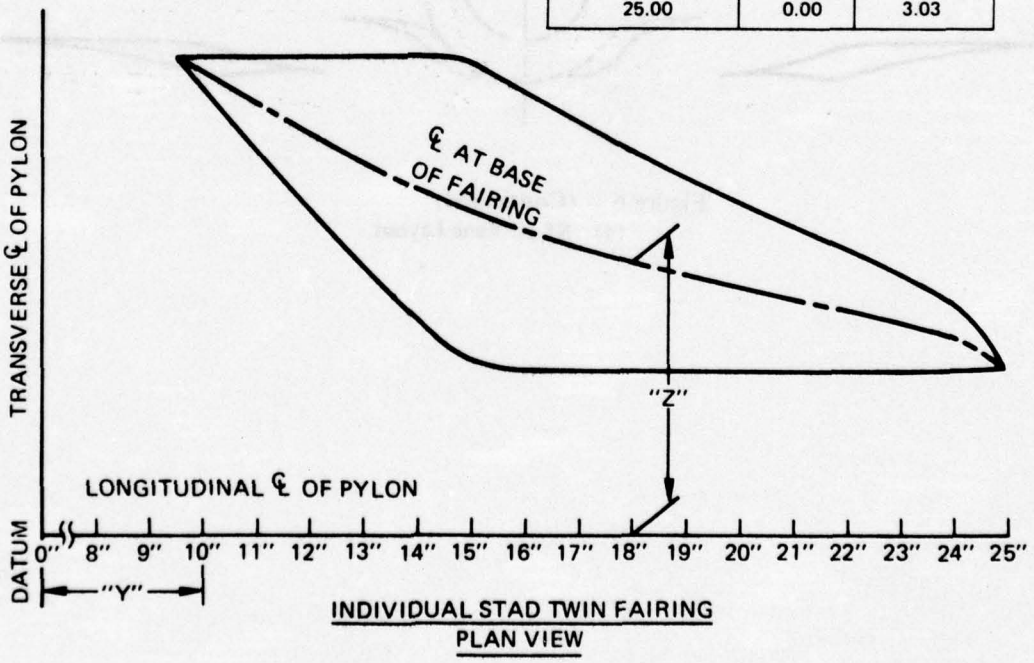

INDIVIDUAL STAD TWIN FAIRING
PLAN VIEW

Figure 6 – (Continued)
(c) Streamtube Area Distribution (STAD) Twin Bump Fairings

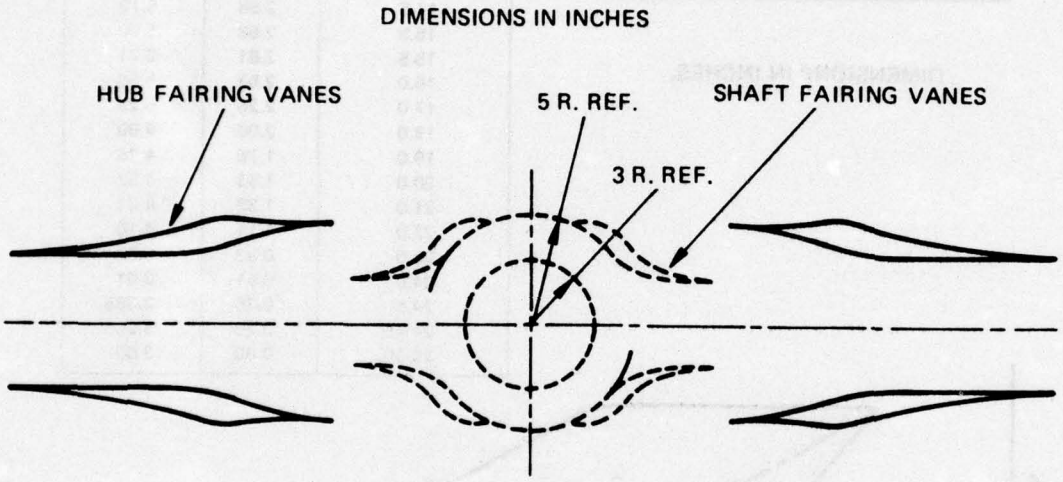

Figure 6 – (Continued)
(d) STAD Vane Layout

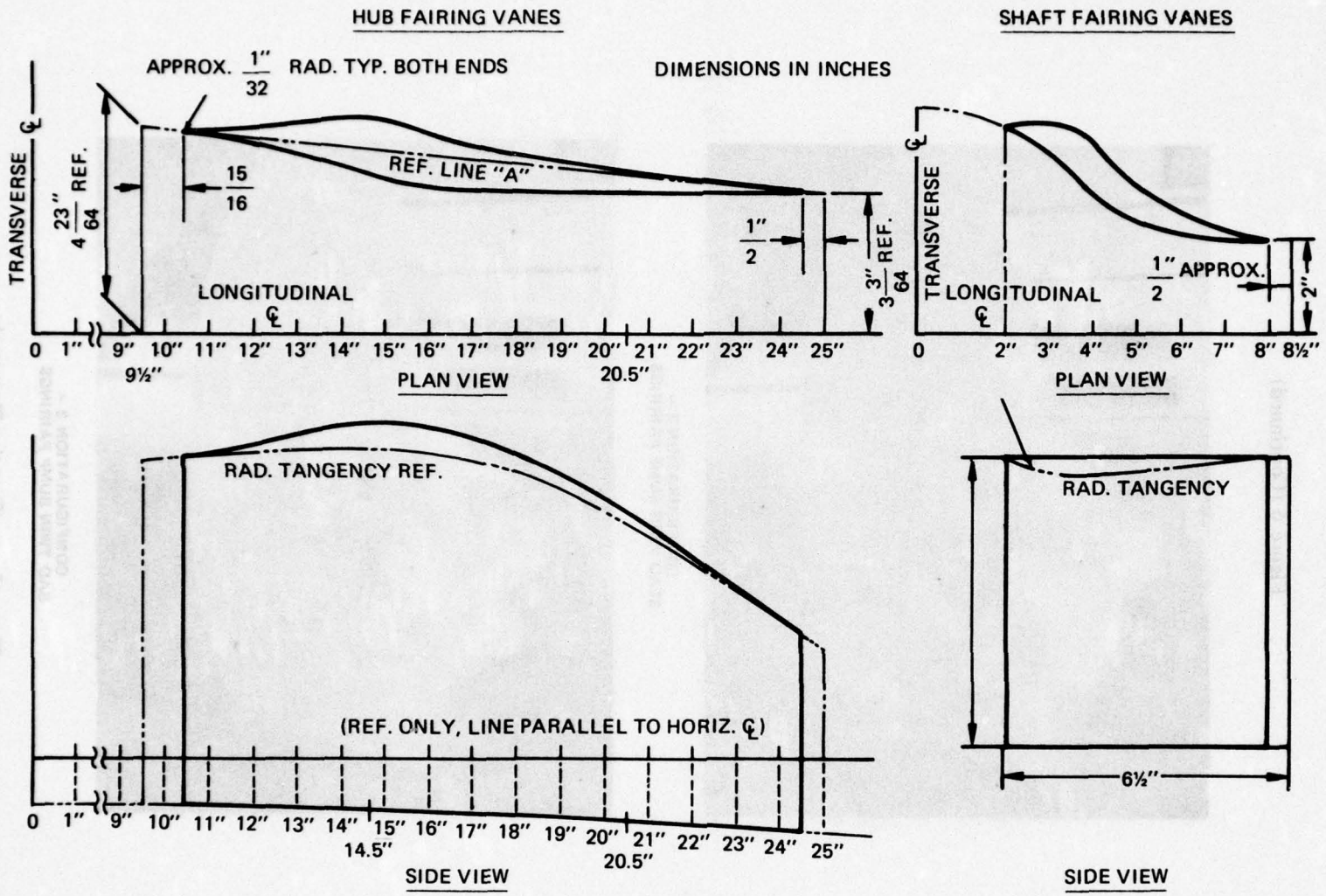

Figure 6 – (Concluded)
(e) STAD Vane Dimensions

Figure 6 (Continued)

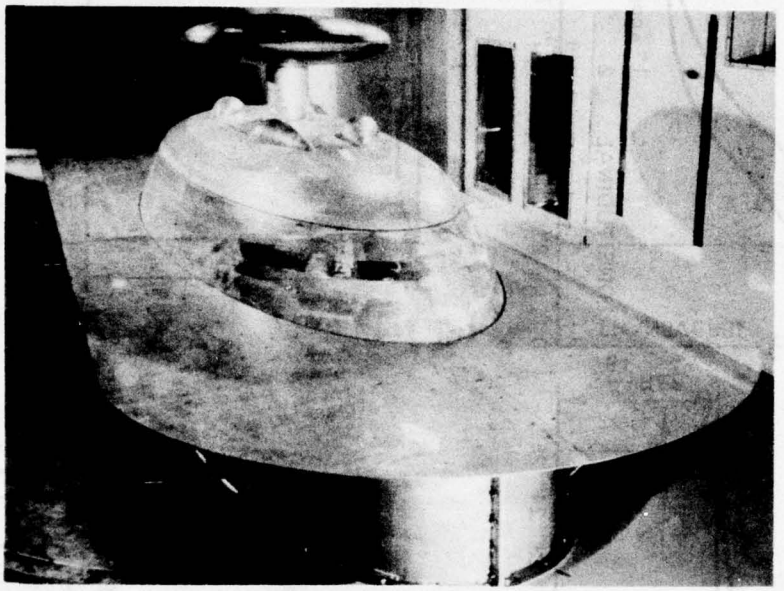

CONFIGURATION 2 –
STAD TWIN BUMP FAIRINGS

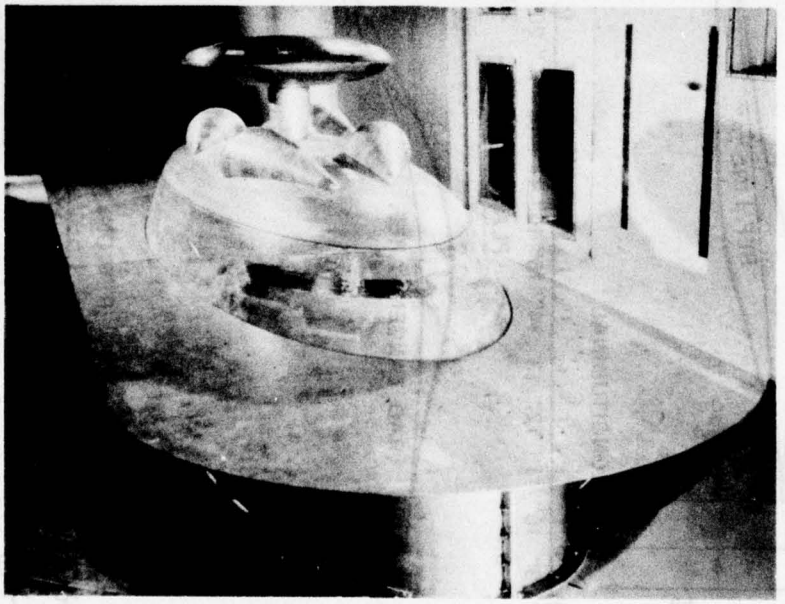

CONFIGURATION 3 –
BAD TWIN BUMP FAIRINGS

Figure 6f – Configuration Photographs

Figure 6 (Continued)

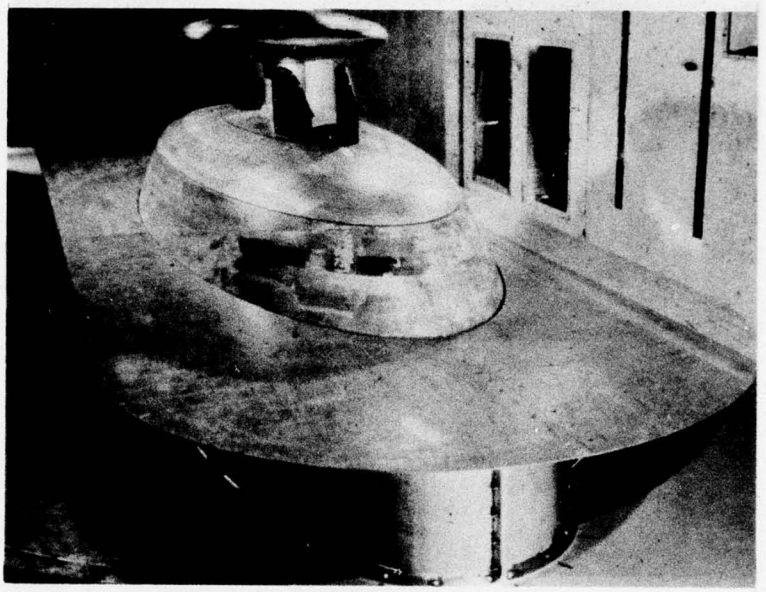

CONFIGURATION 4 –
STAD HUB VANES

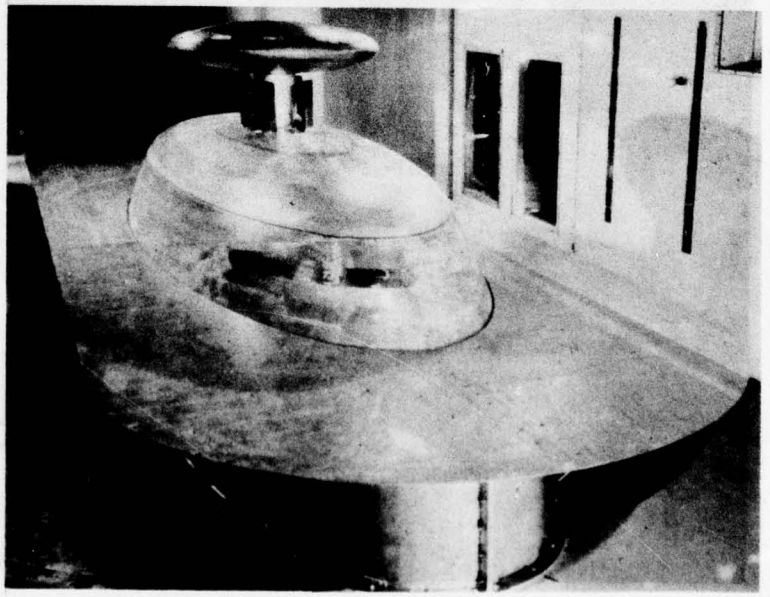

CONFIGURATION 5 –
STAD SHAFT VANES

Figure 6f – Configuration Photographs

Figure 6 (Continued)

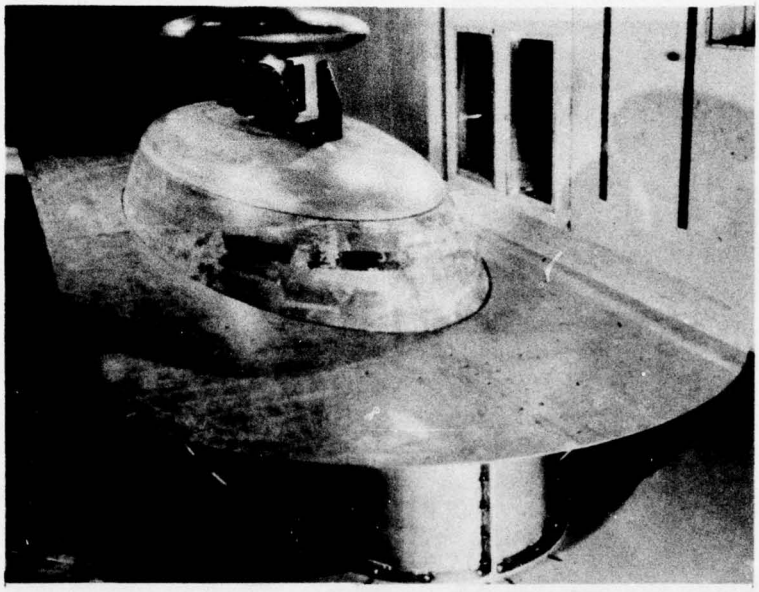

CONFIGURATION 6 –
STAD HUB AND SHAFT VANES

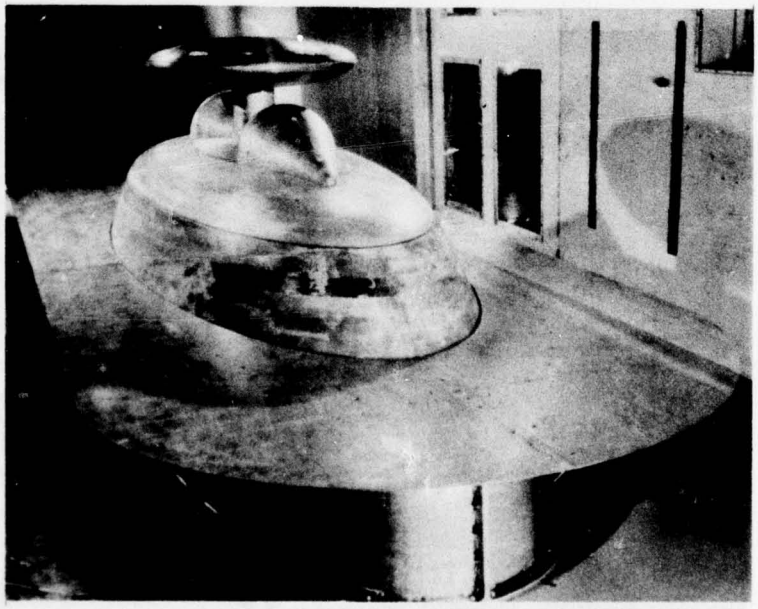

CONFIGURATION 7 –
BAD SINGLE BUMP FAIRINGS

Figure 6f – Configuration Photographs

GPO 909-474

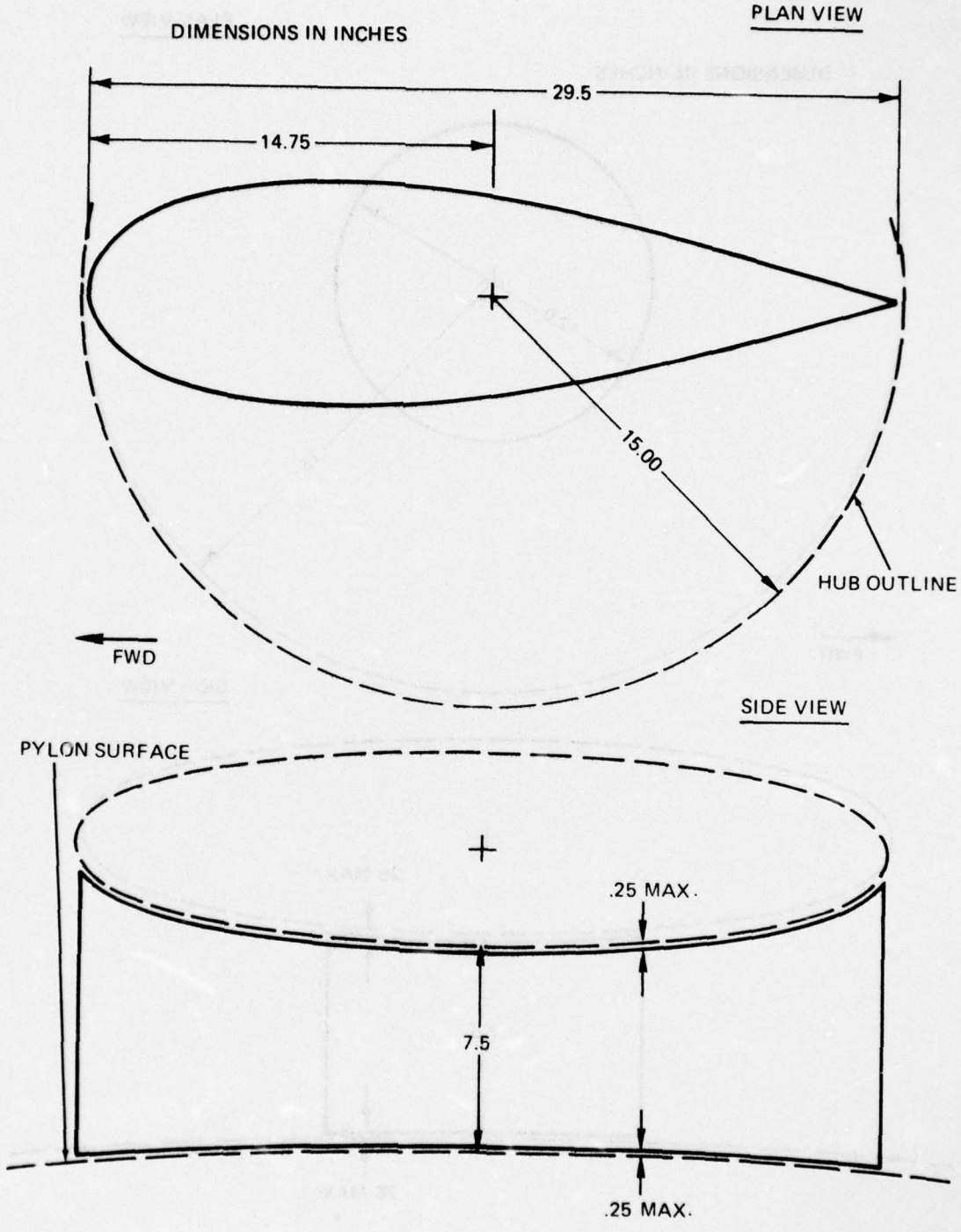

Figure 7 – Shaft Fairing Models
(a) NACA 0028 Airfoil Shaft Fairing

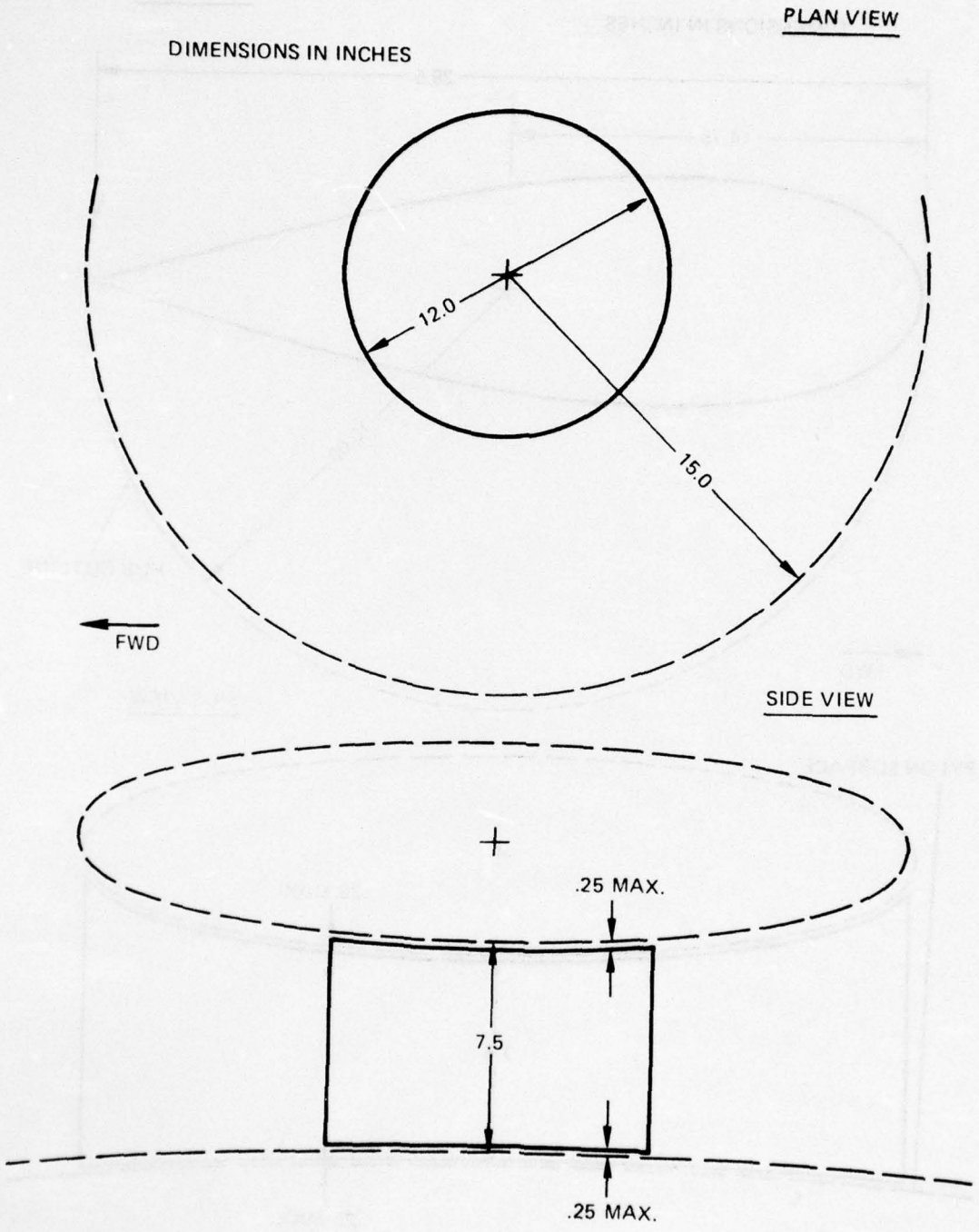

Figure 7 – (Concluded)
(b) 12 Inch Diameter Cylinder Shaft Fairing

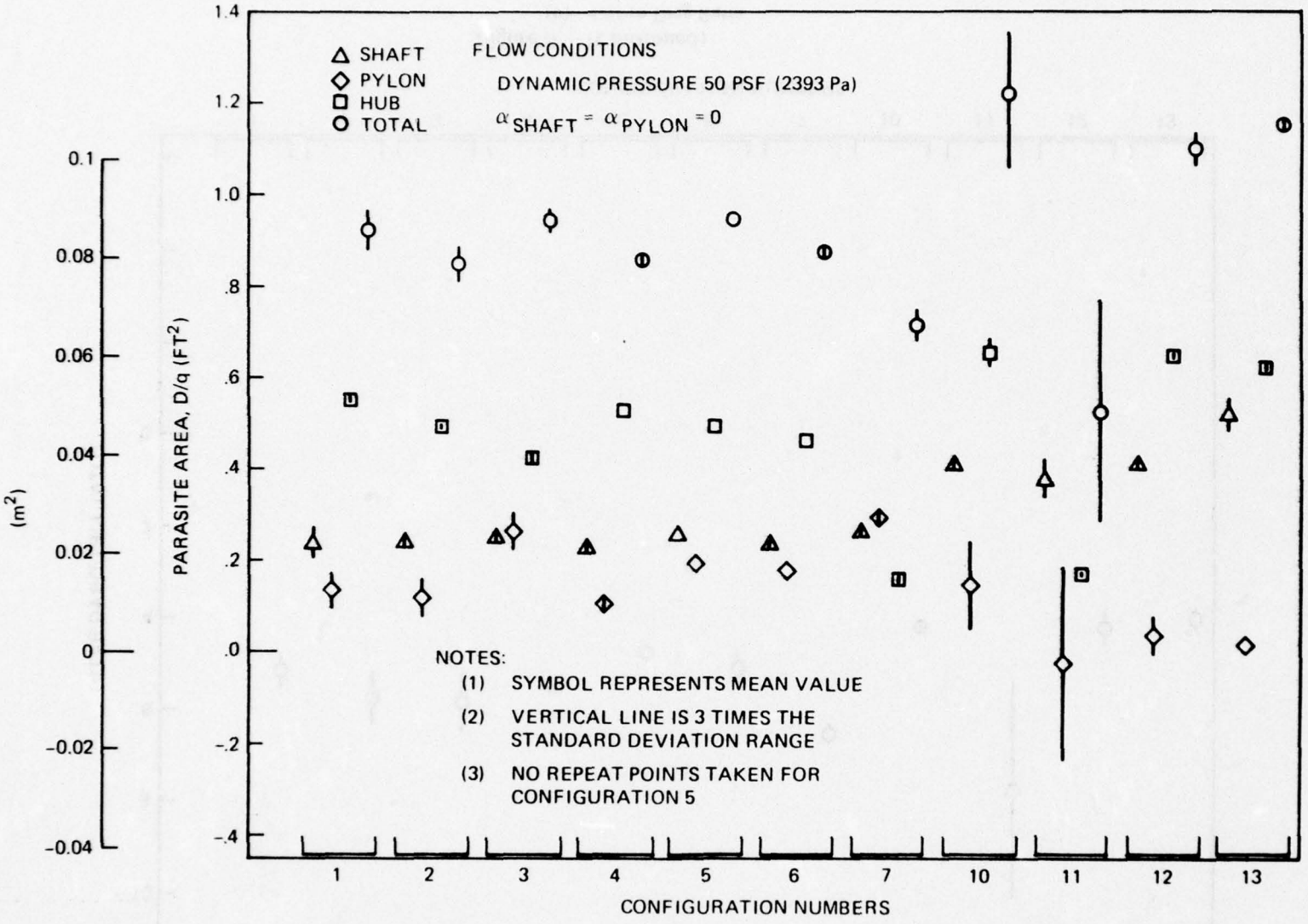

Figure 8 — Data Precision
(a) Parasite Area

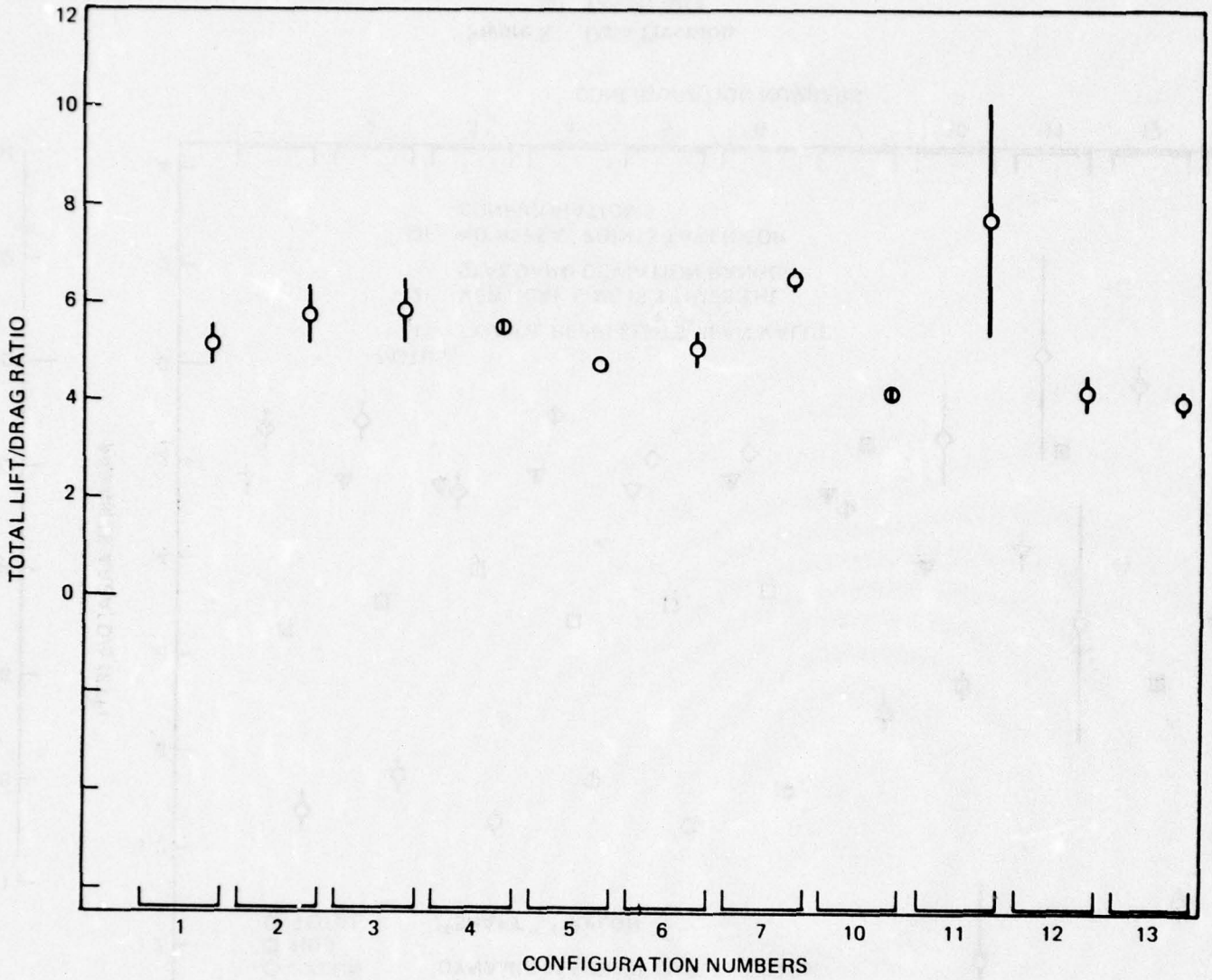

Figure 8 – (Continued)
(b) Lift to Drag Ratio

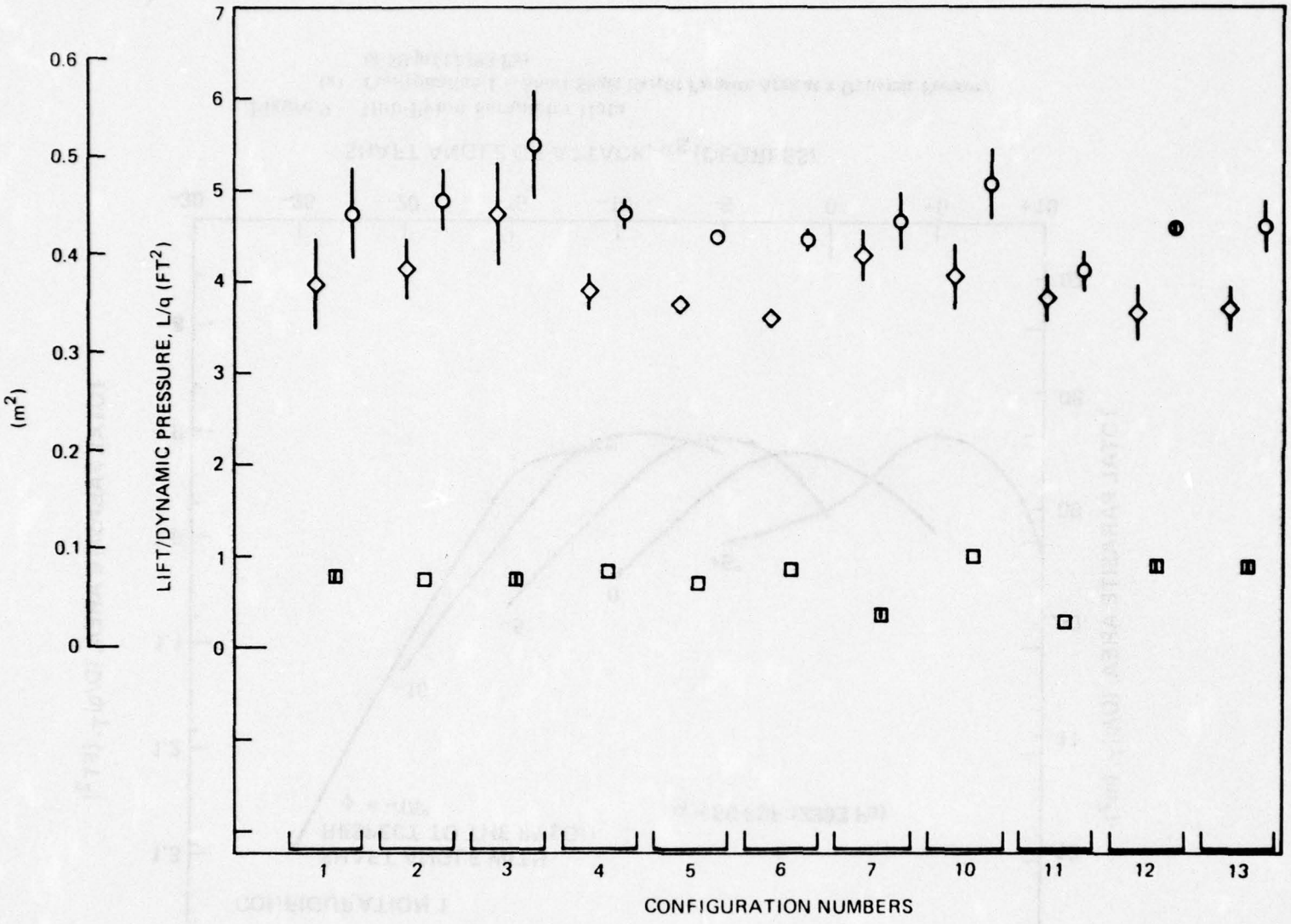

Figure 8 – (Concluded)
(c) Lift Divided by Dynamic Pressure

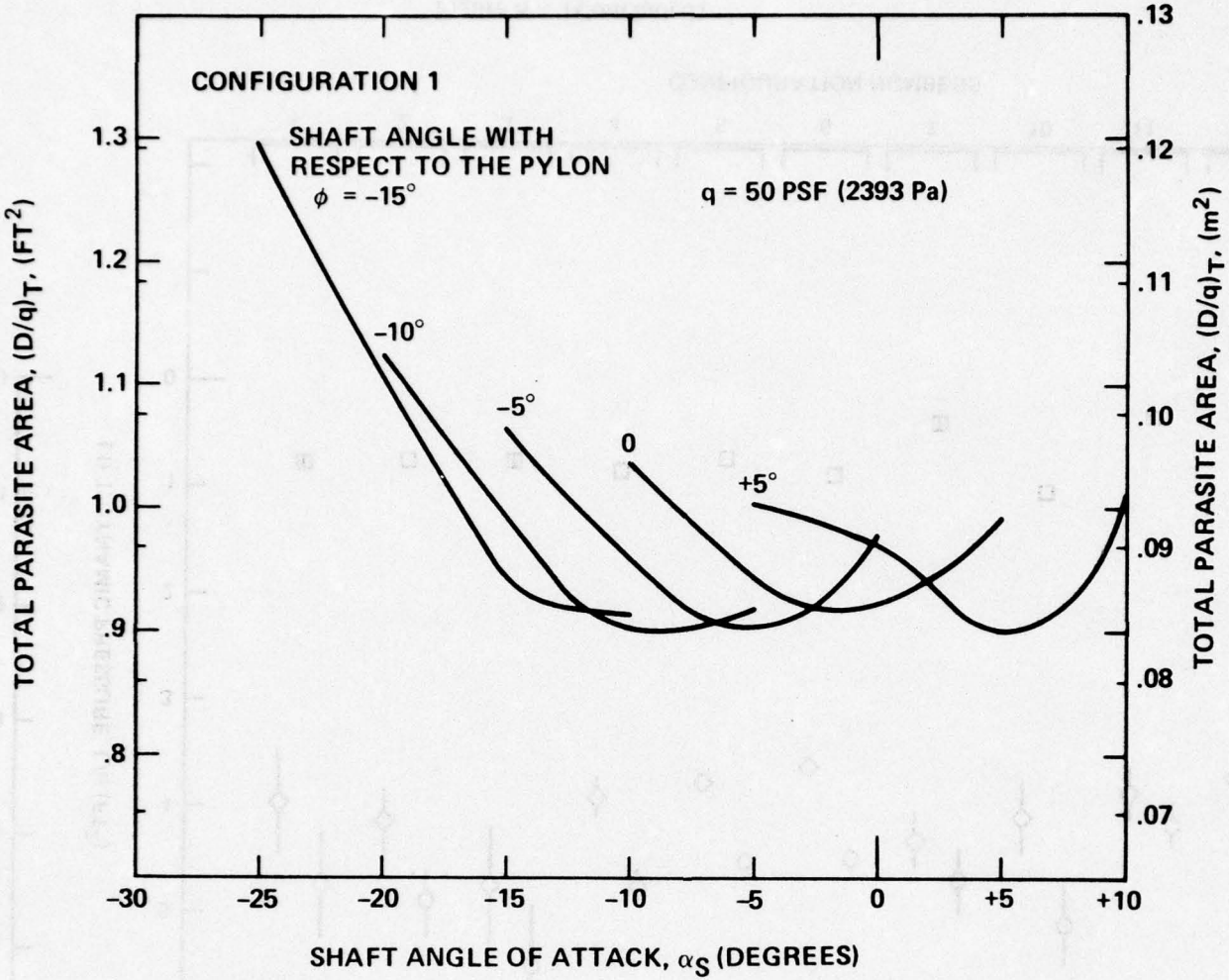

Figure 9 – Hub-Pylon Parameter Data

(a) Configuration 1 – Short Shaft Height Parasite Area at a Dynamic Pressure of 50 psf (2393 Pa)

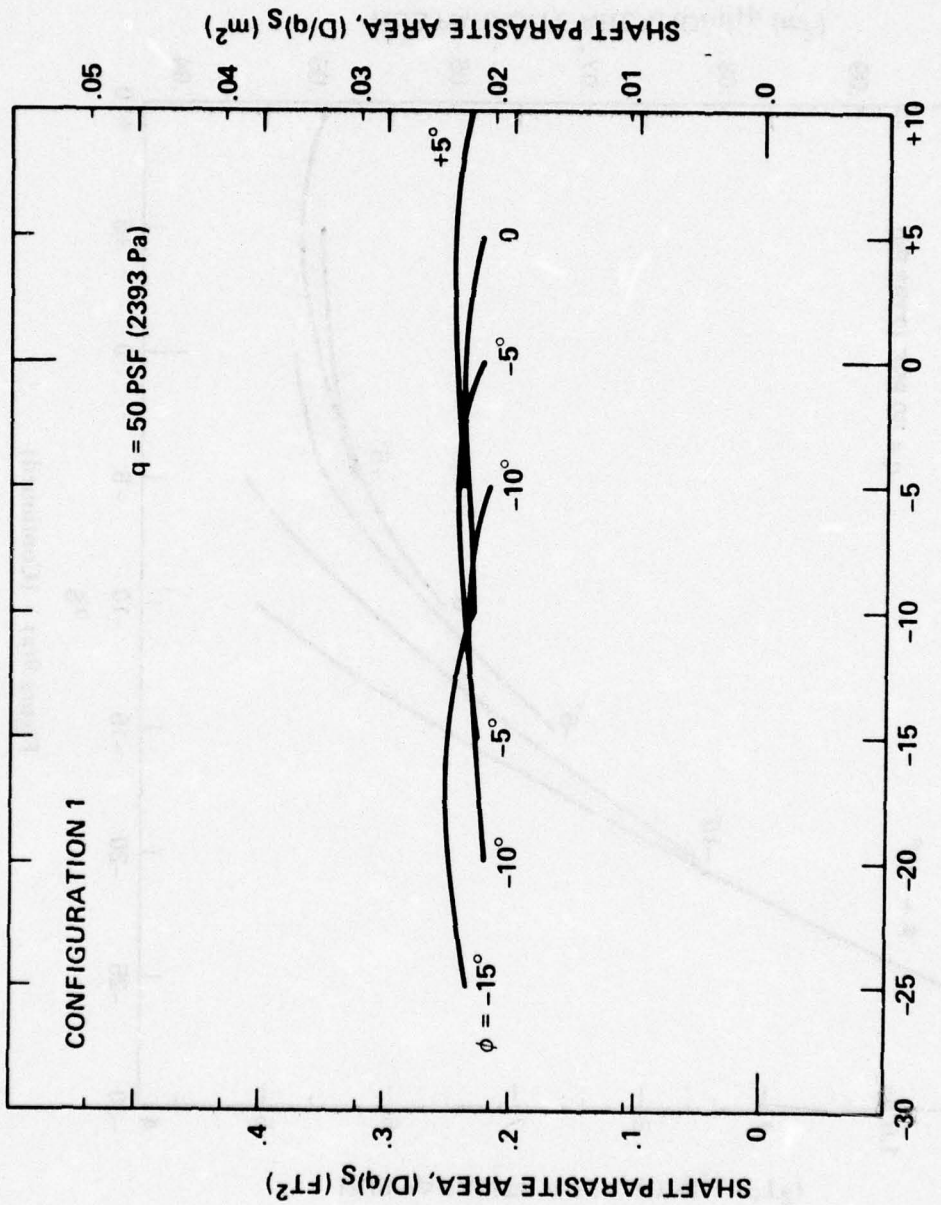

Figure 9(a) – (Continued)

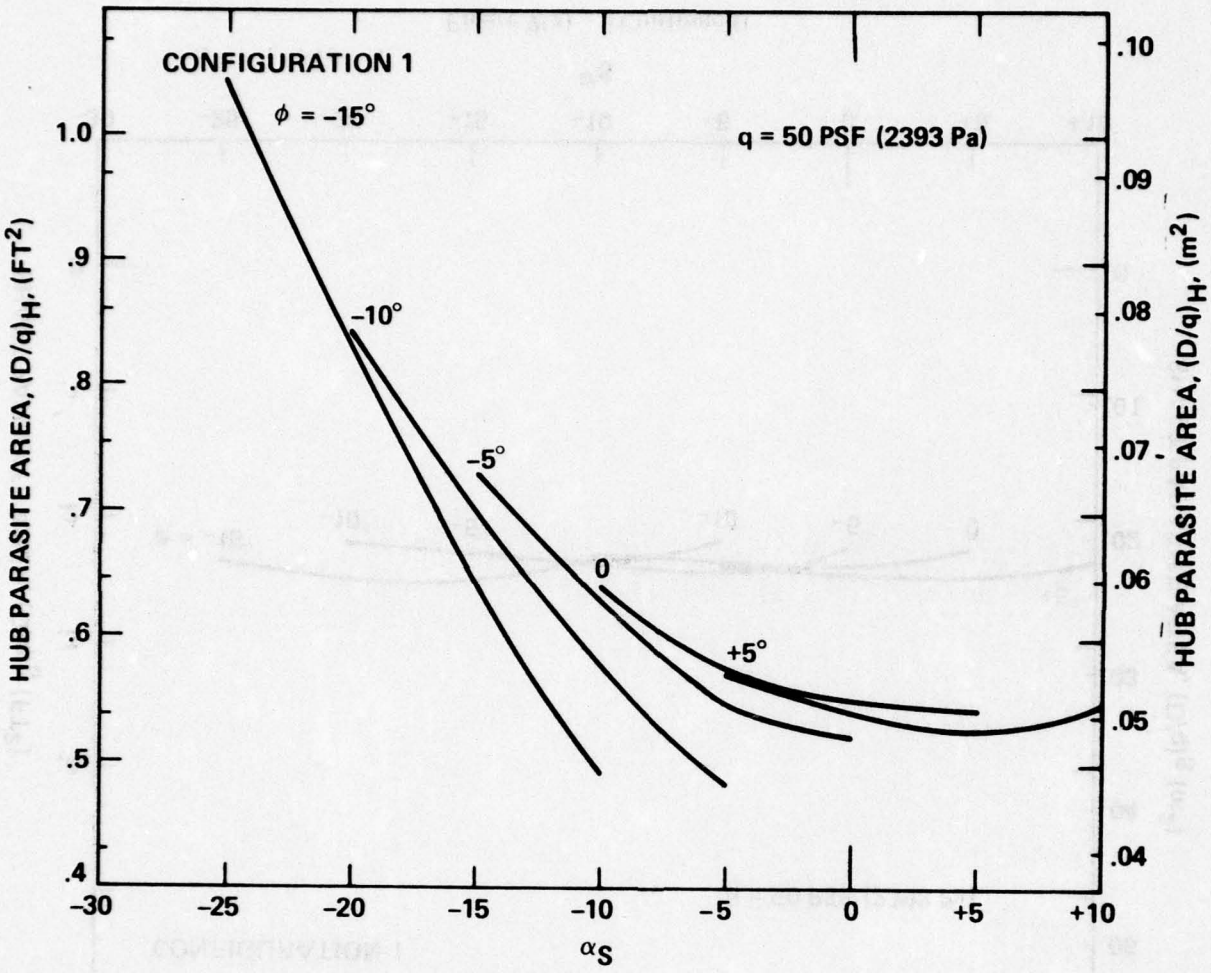

Figure 9(a) – (Continued)

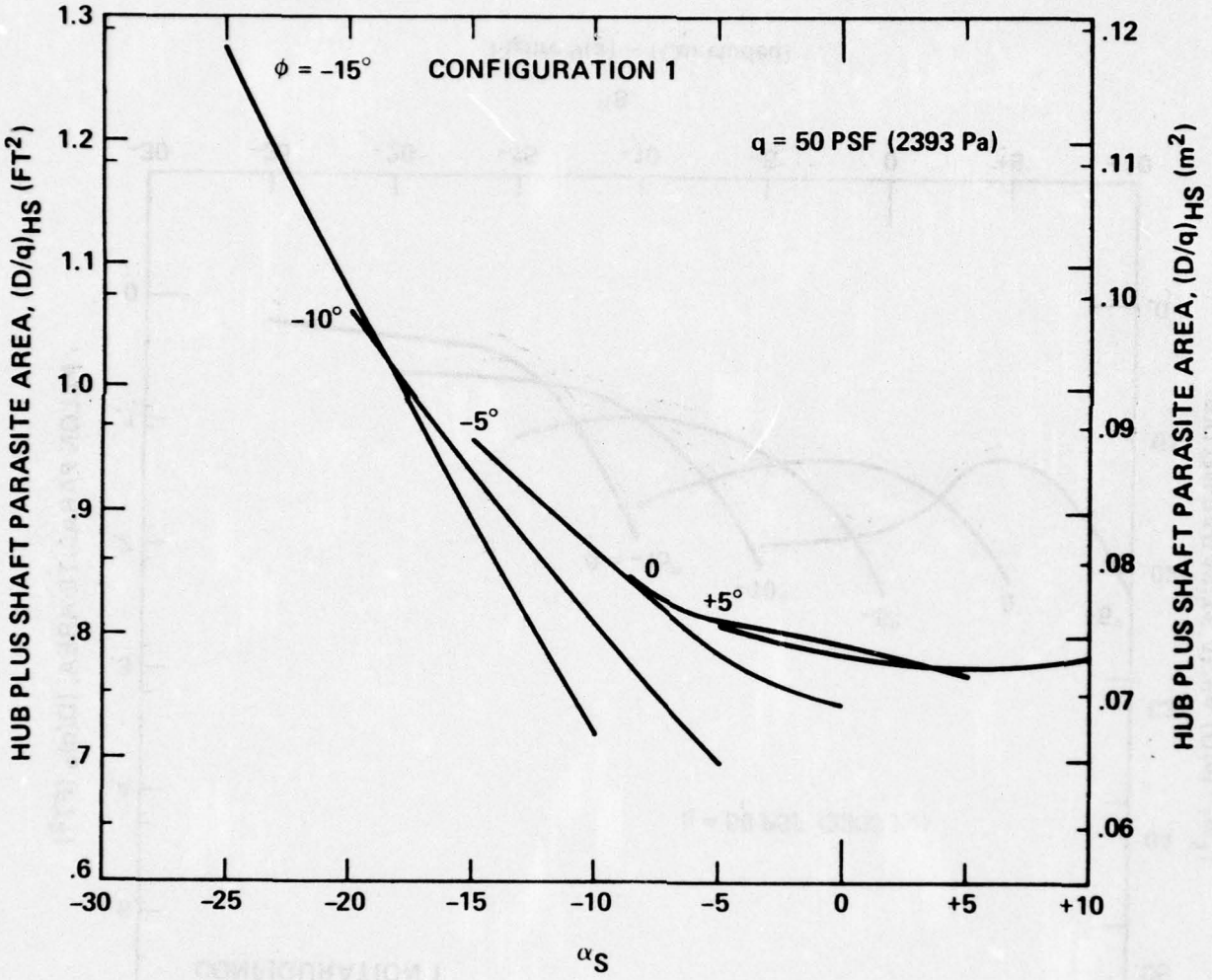

Figure 9(a) — (Continued)

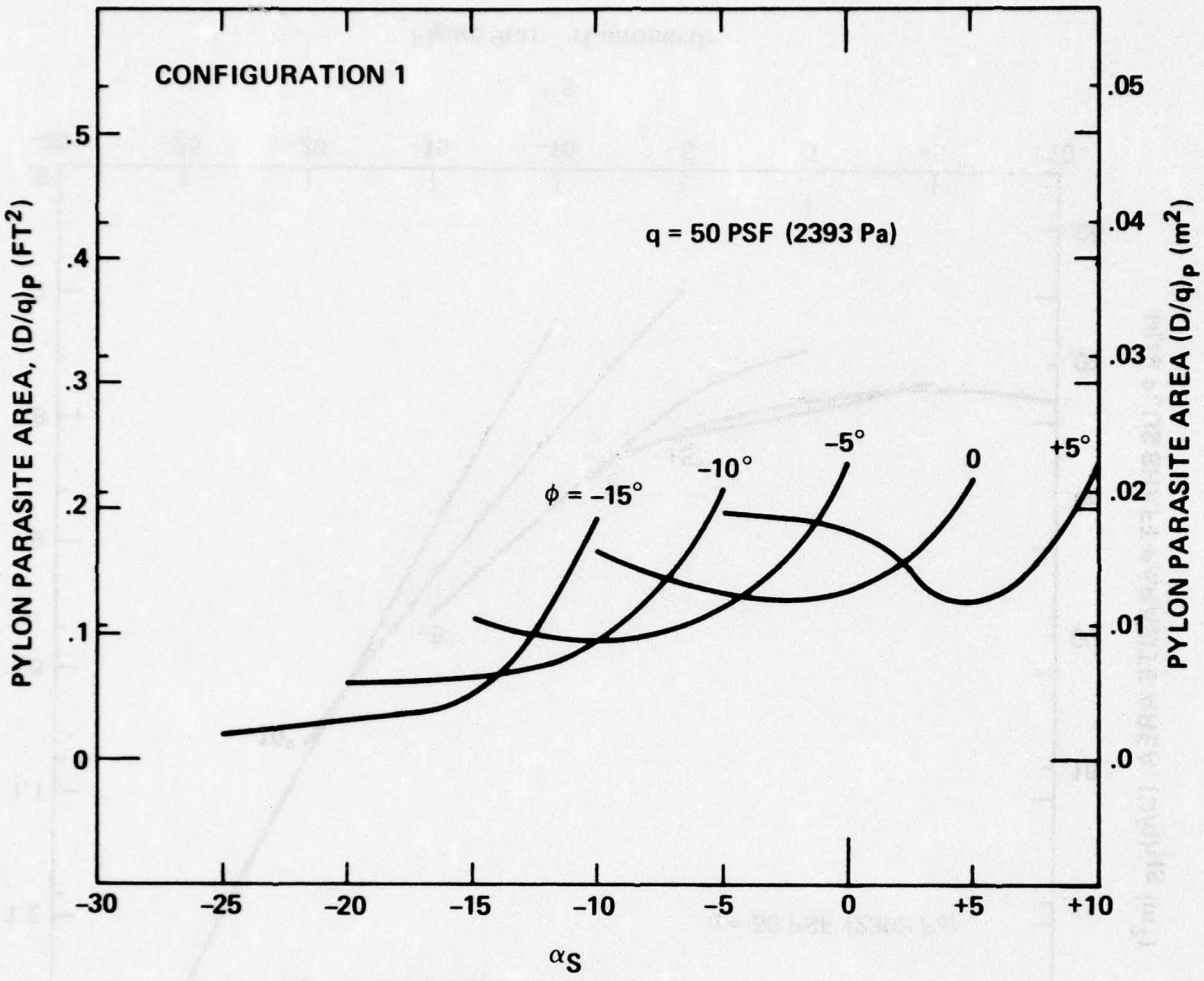

Figure 9(a) – (Concluded)

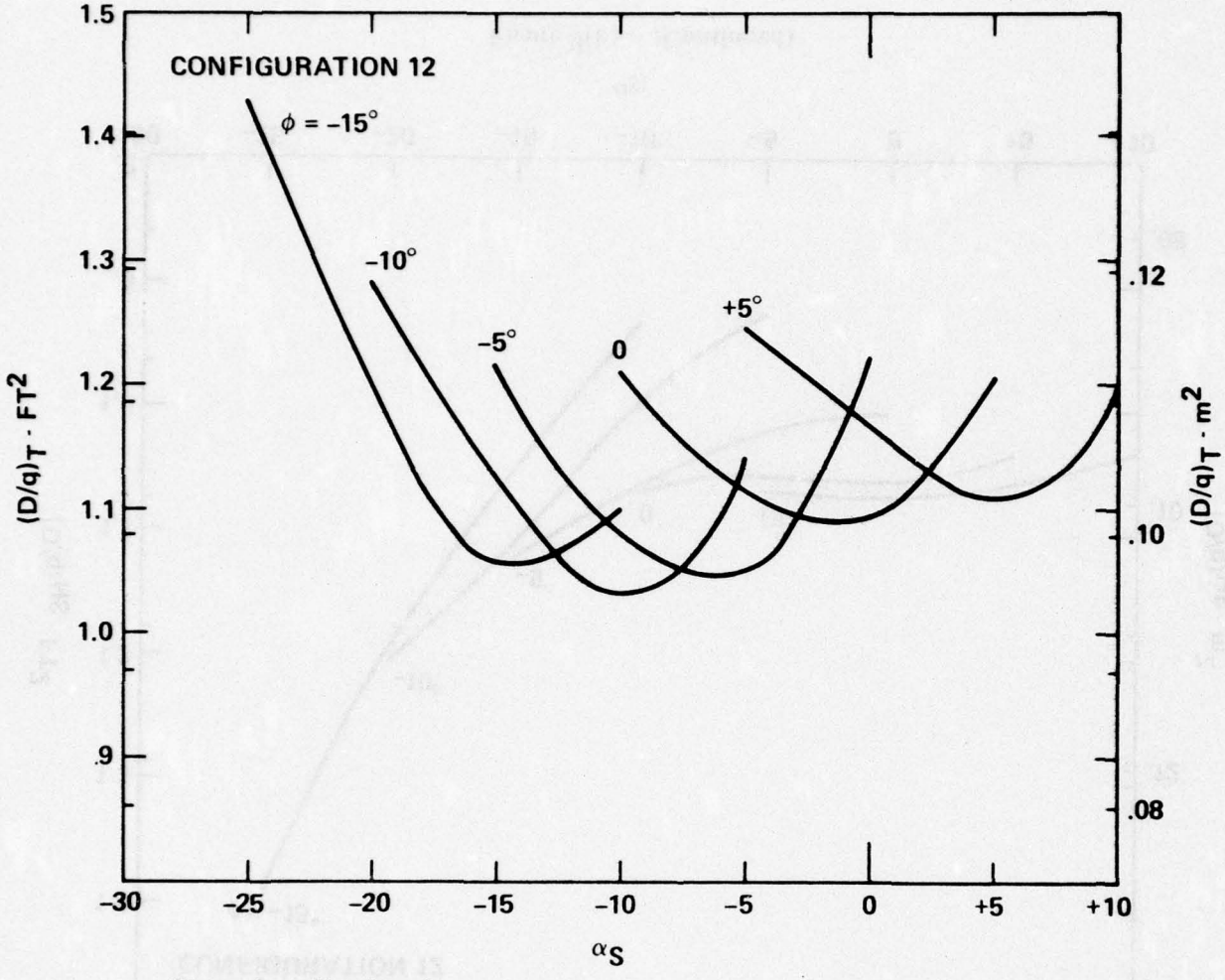

Figure 9 - (Continued)

(b) Configuration 12 – Medium Shaft Height Parasite Area at a Dynamic Pressure of 50 psf (2393 Pa)

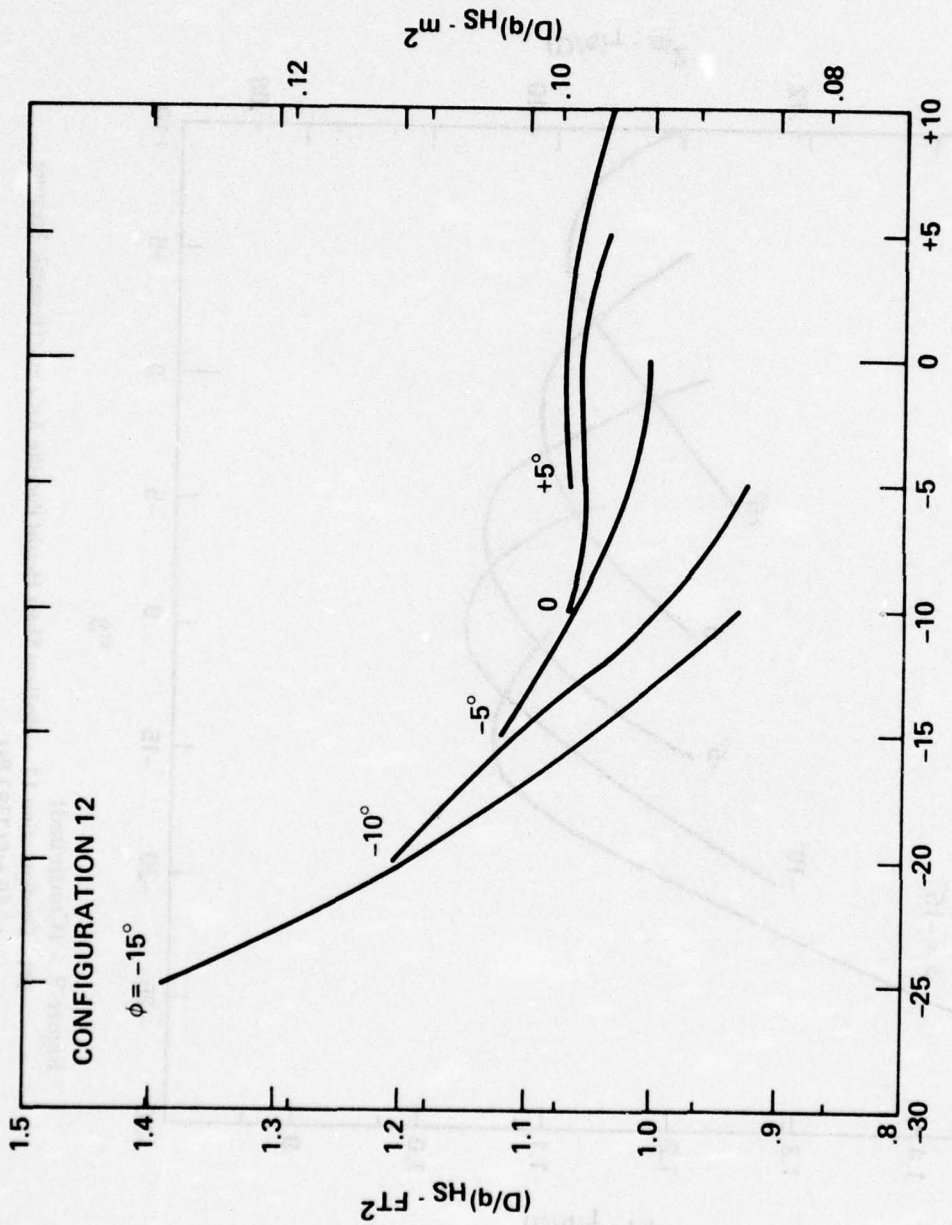

Figure 9(b) – (Continued)

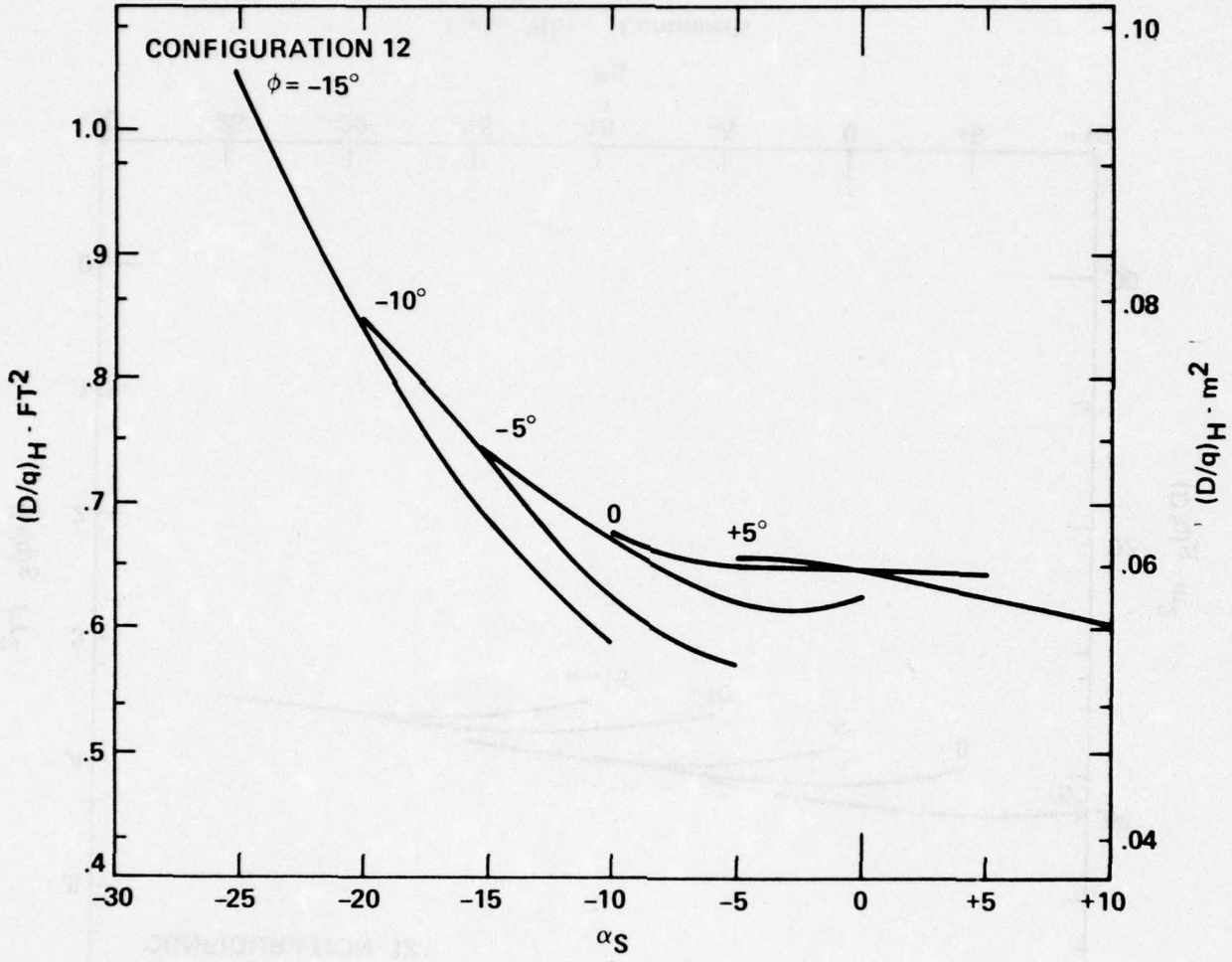

Figure 9(b) (Continued)

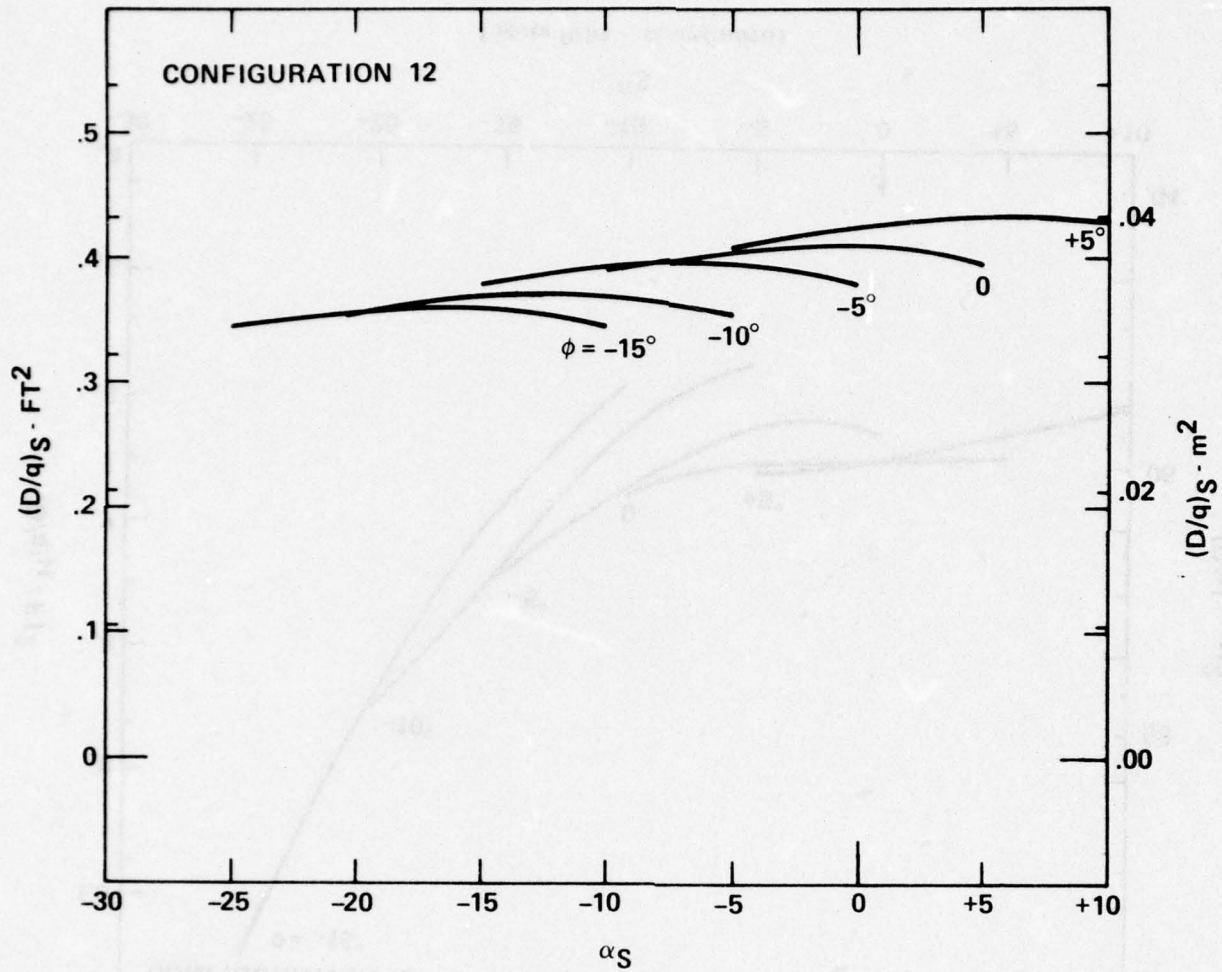

Figure 9(b) – (Continued)

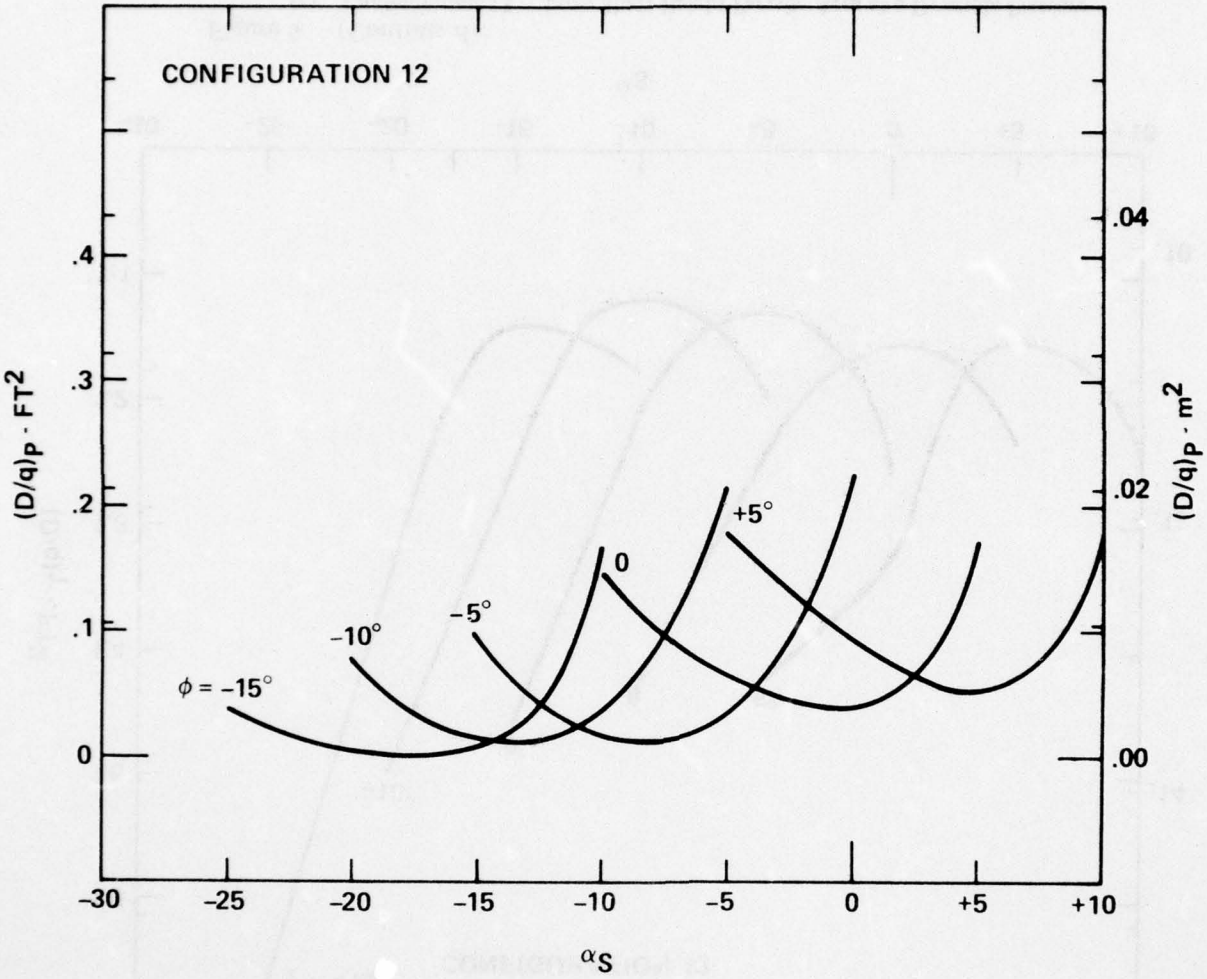

Figure 9(b) – (Continued)

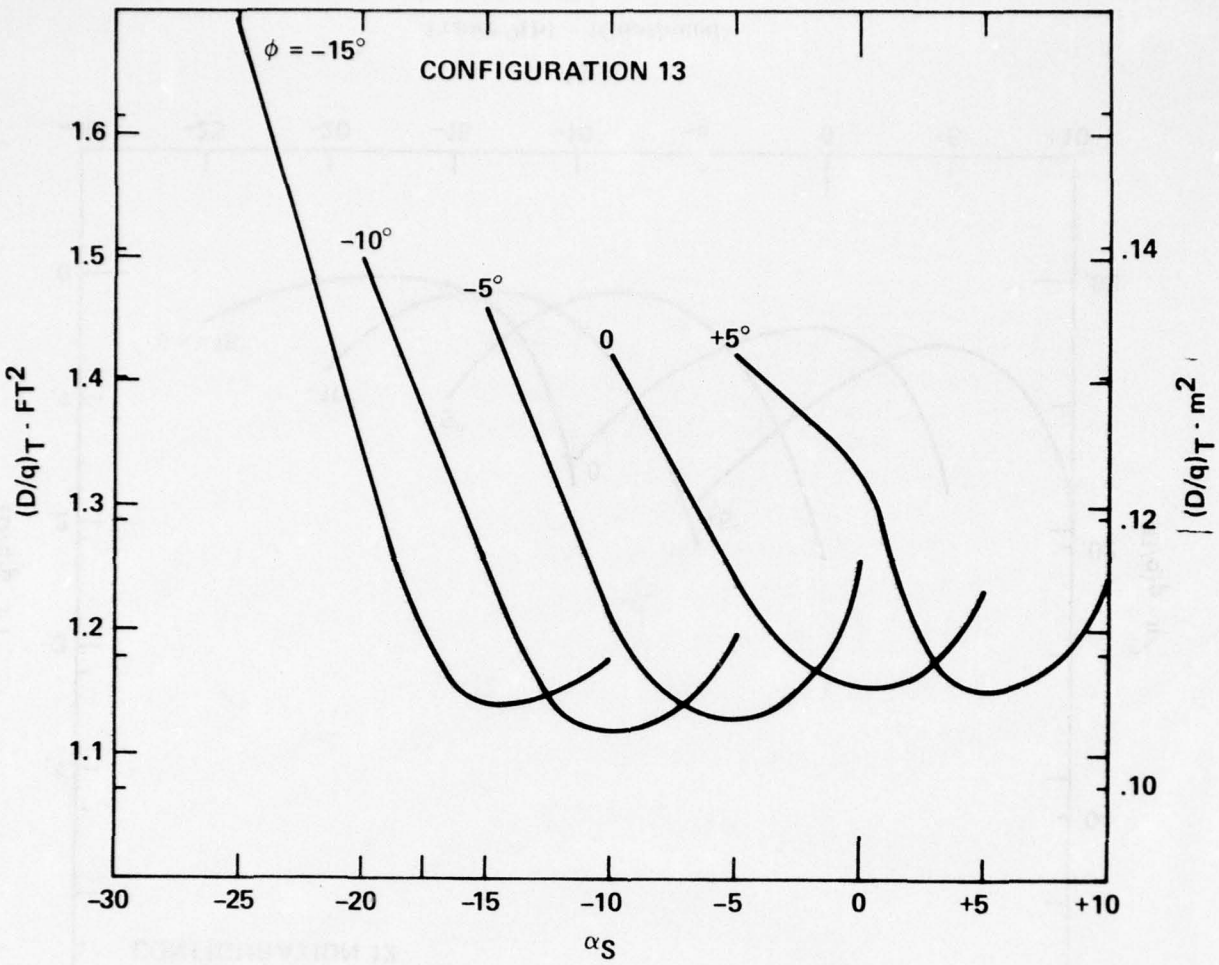

Figure 9 – (Continued)

(c) Configuration 13 – Long Shaft Height Parasite Area at a Dynamic Pressure of 50 psf (2393 Pa)

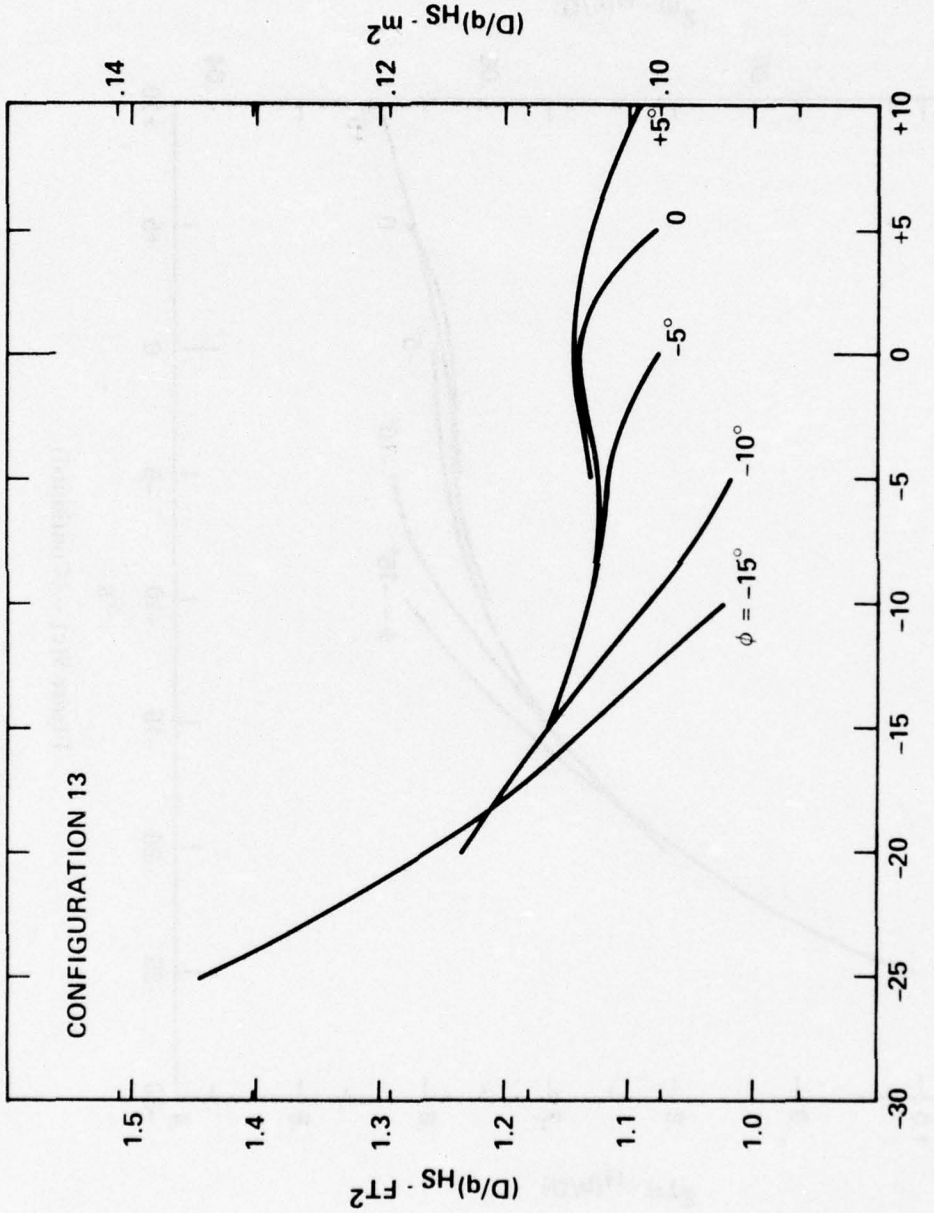

Figure 9(c) – (Continued)

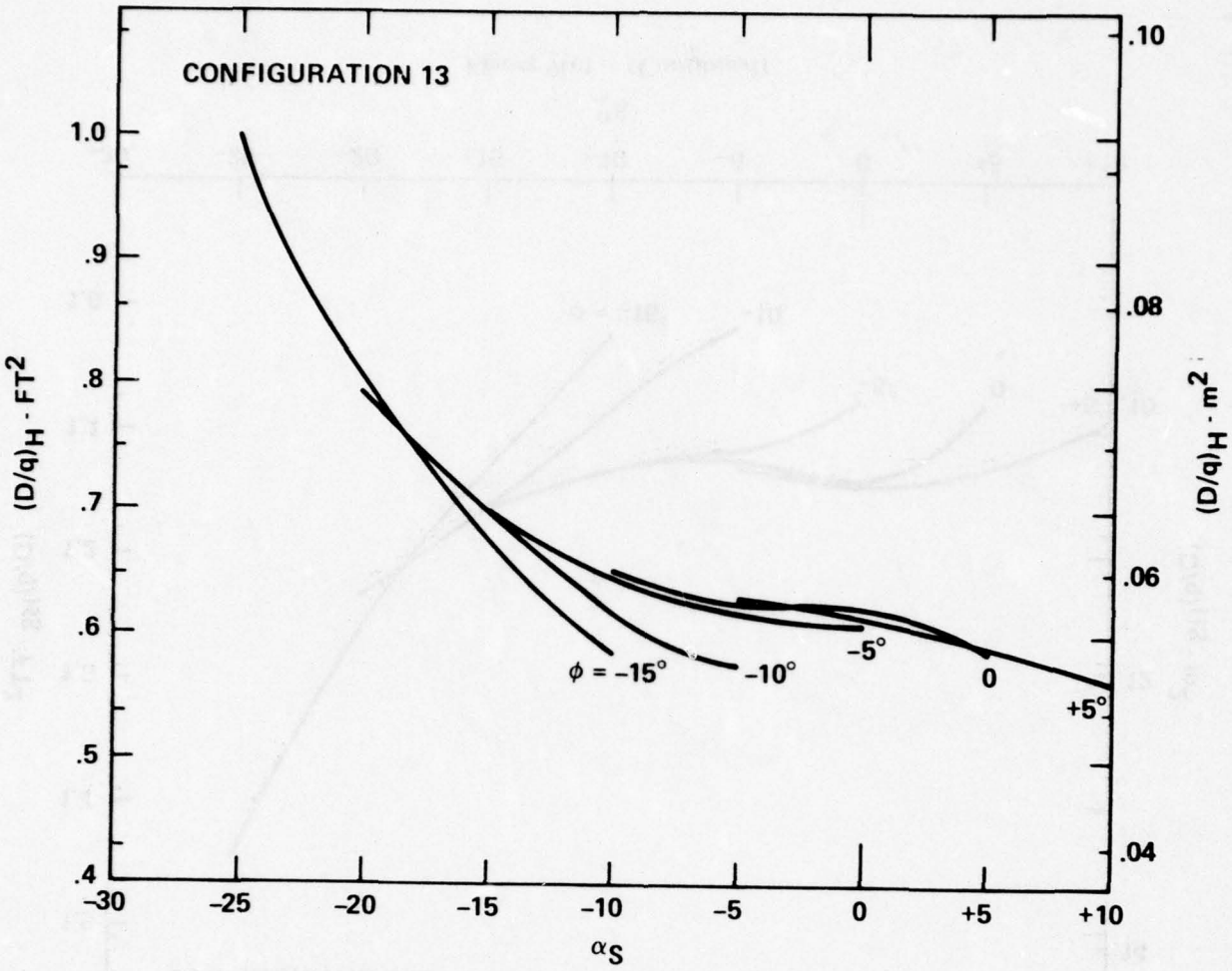

Figure 9(c) – (Continued)

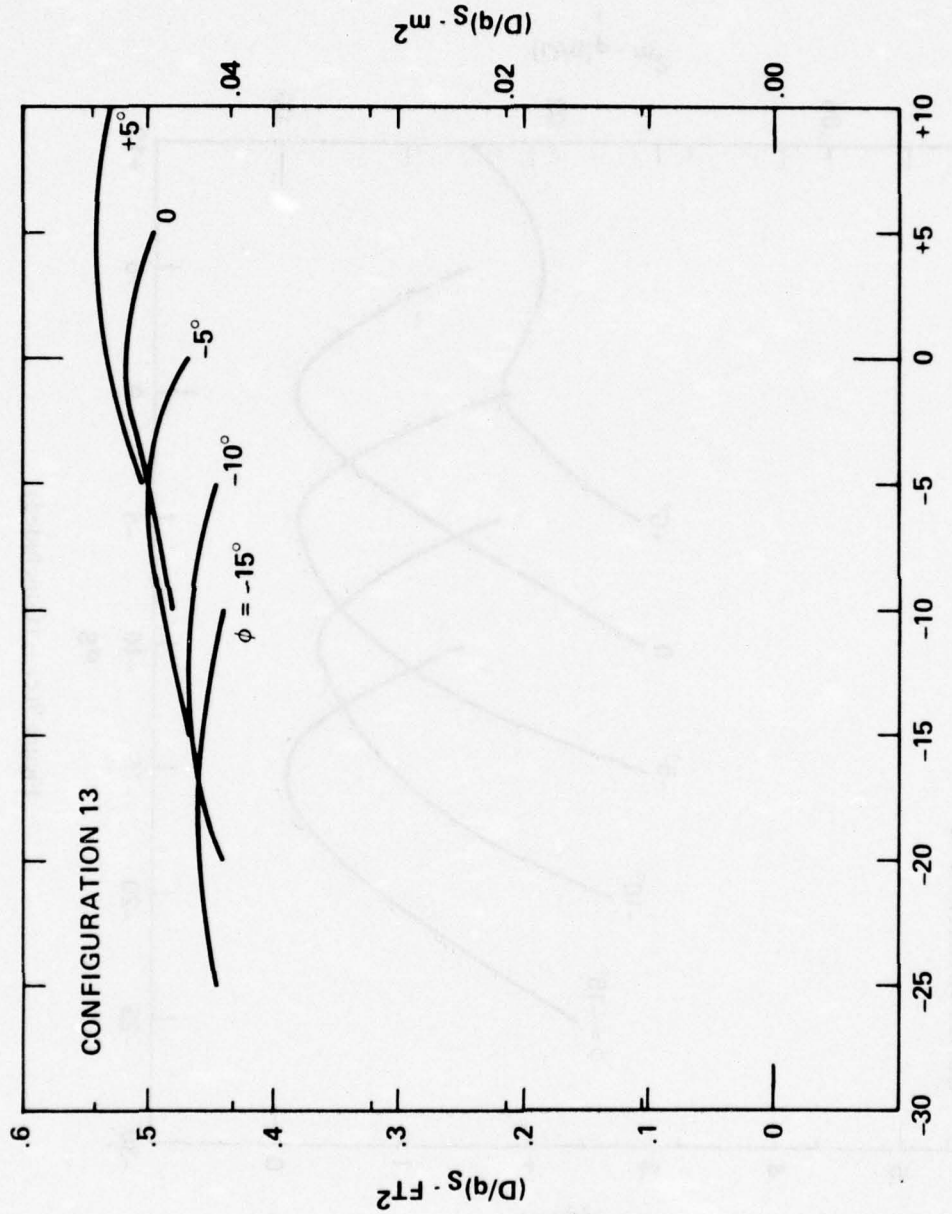

Figure 9(c) (Continued)

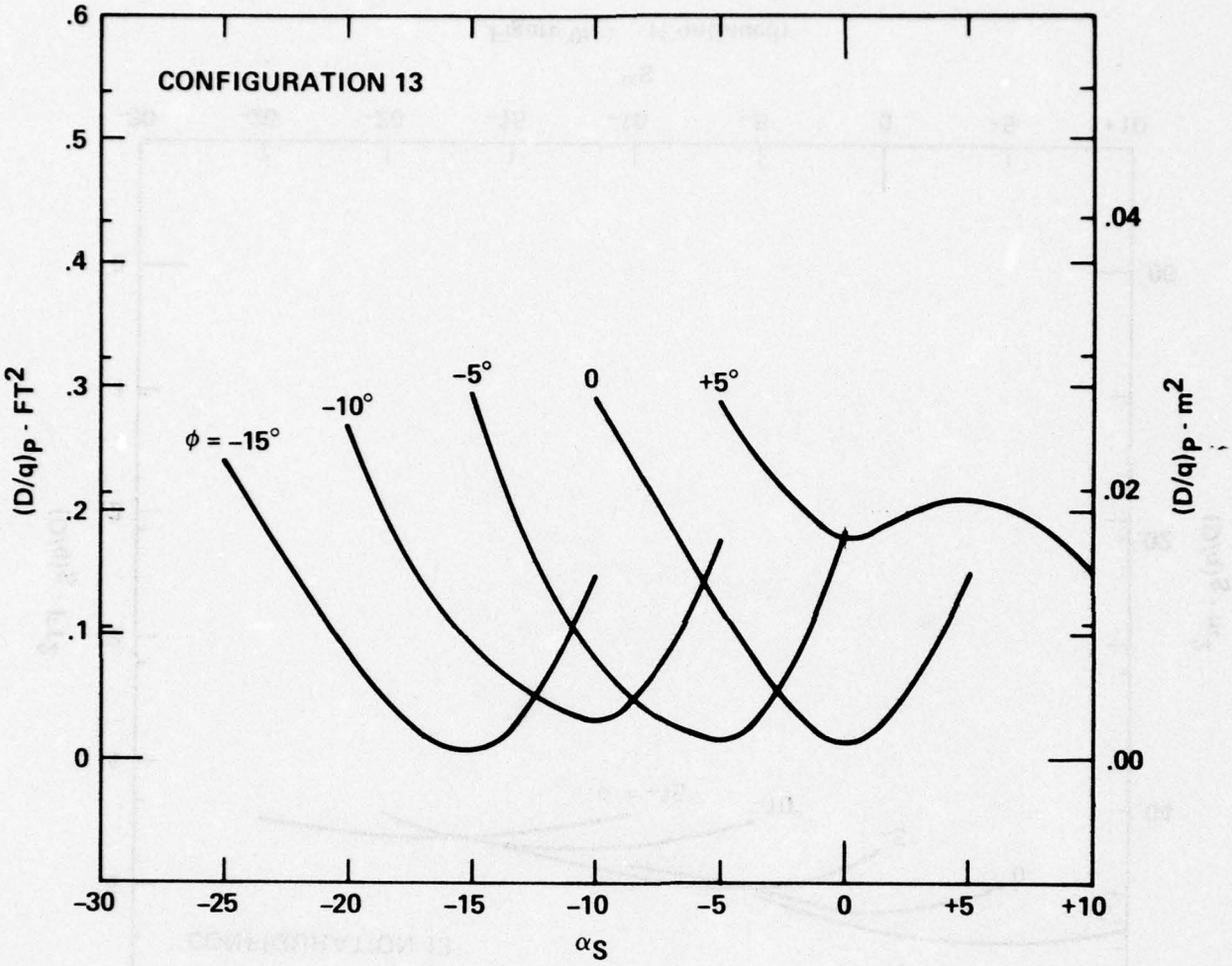

Figure 9(c) – (Concluded)

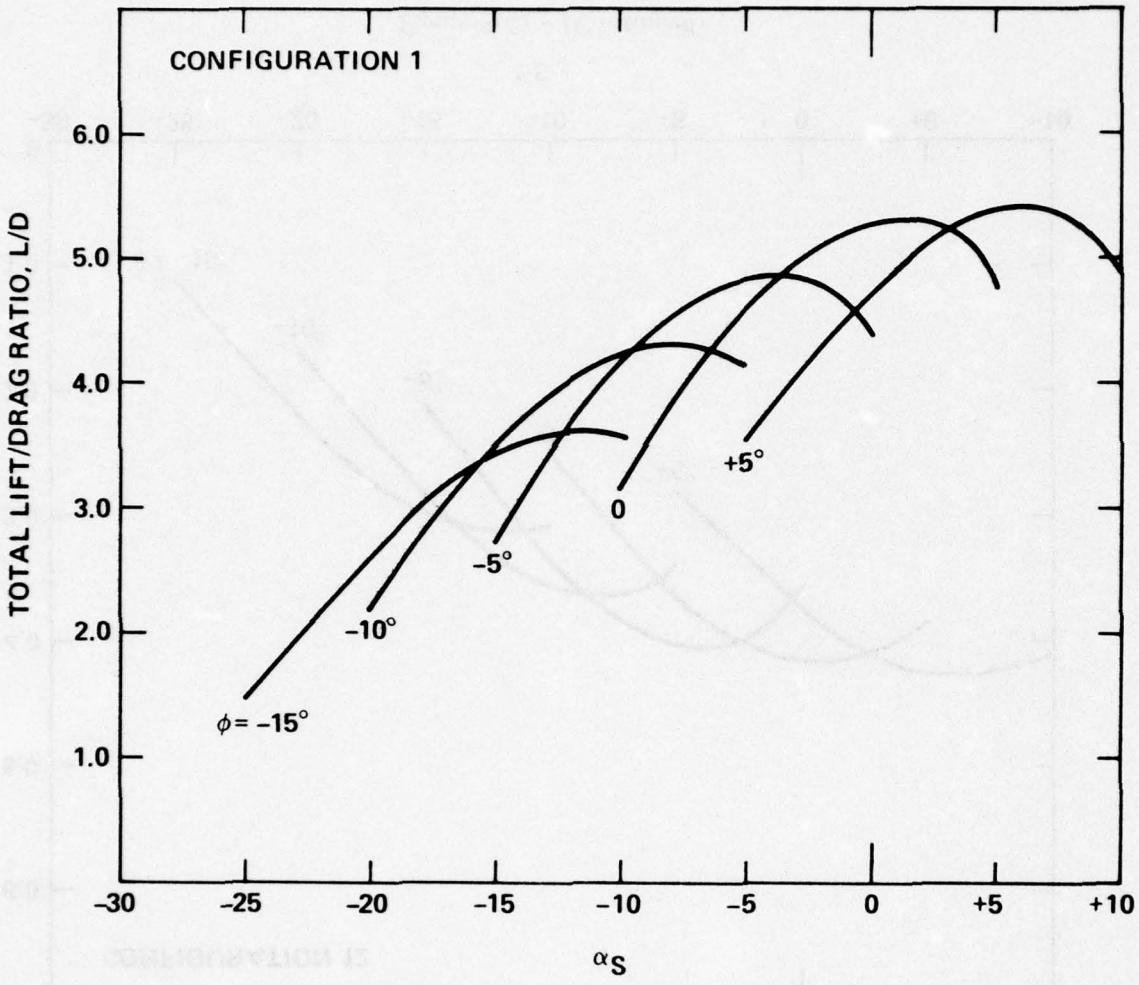

Figure 9 – (Continued)
(d) Lift/Drag Ratio at a Dynamic Pressure of 50 psf (2393 Pa)

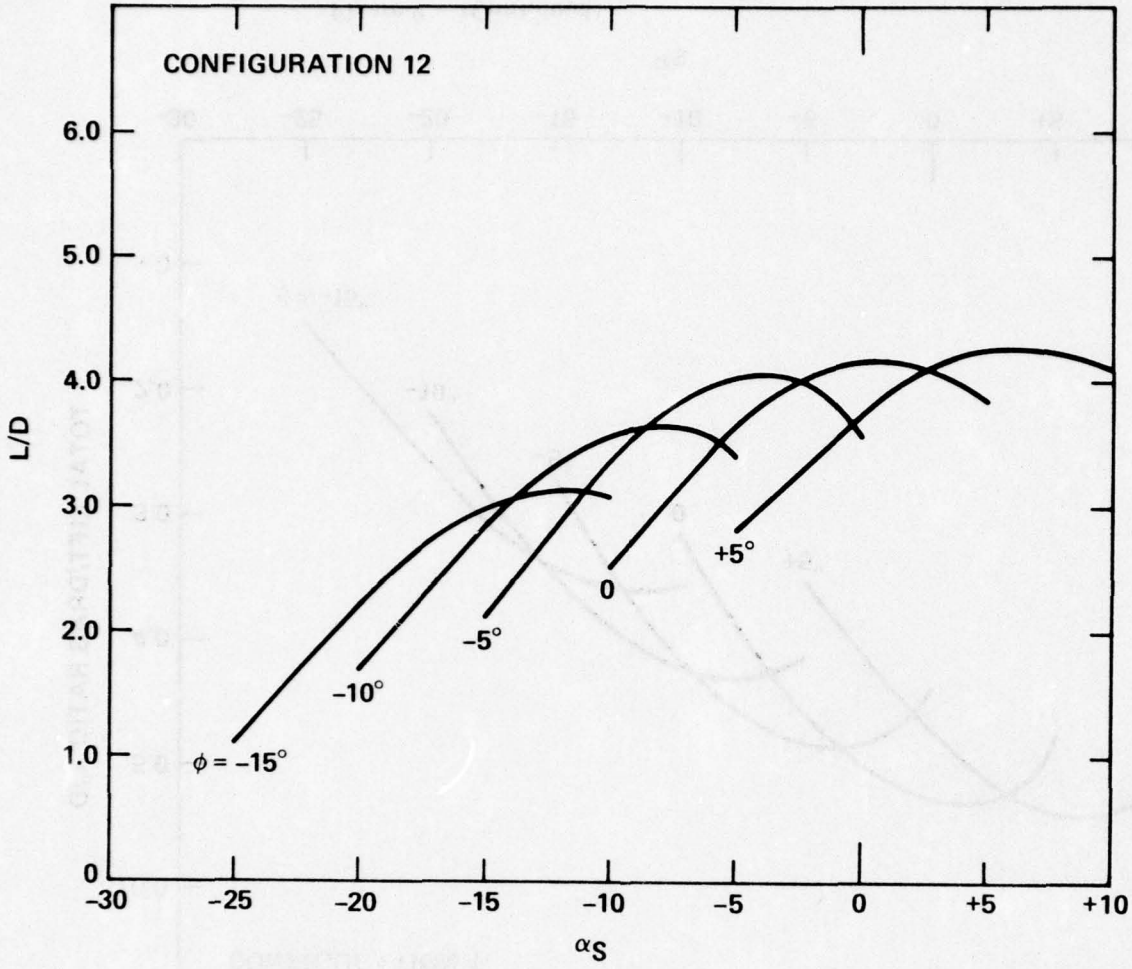

Figure 9(d) – (Continued)

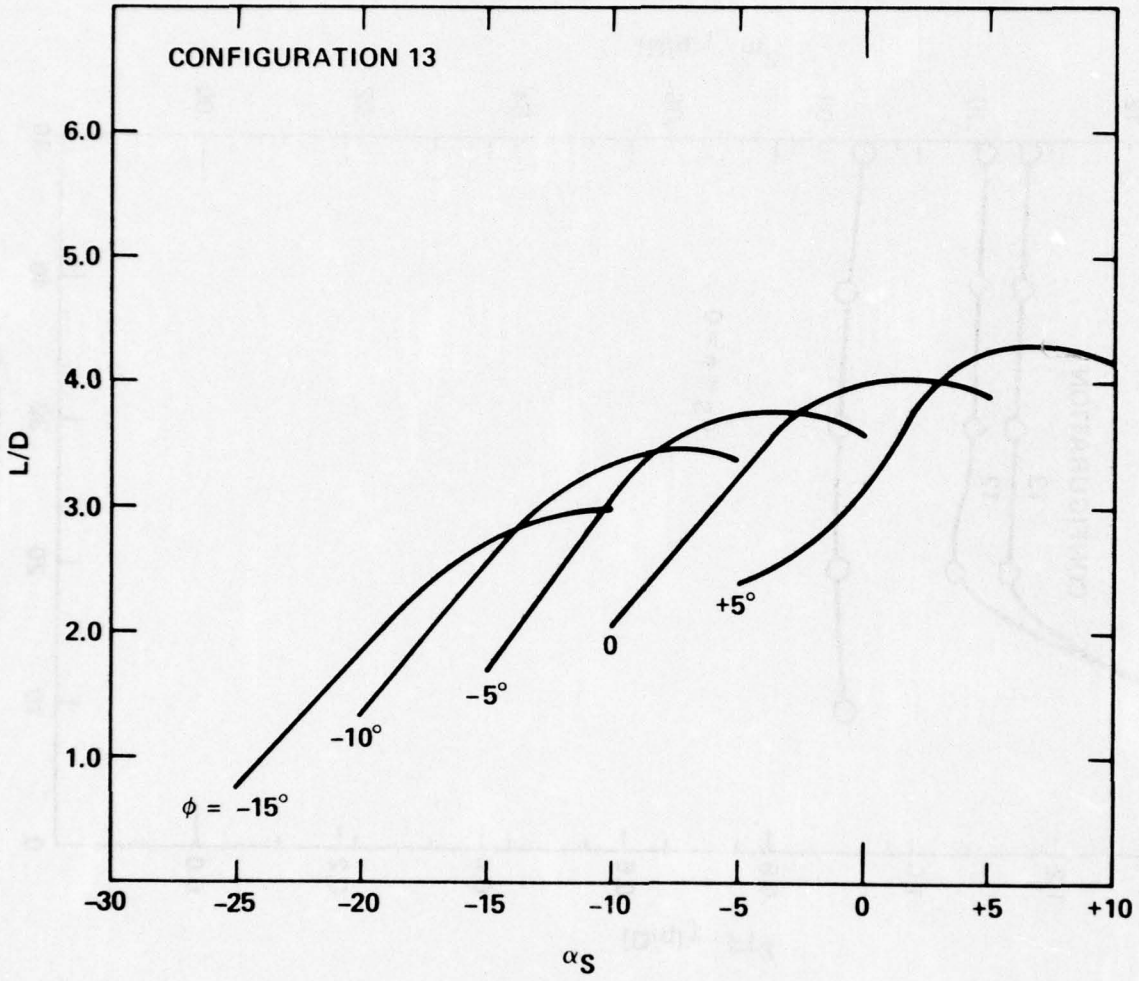

Figure 9(d) – (Concluded)

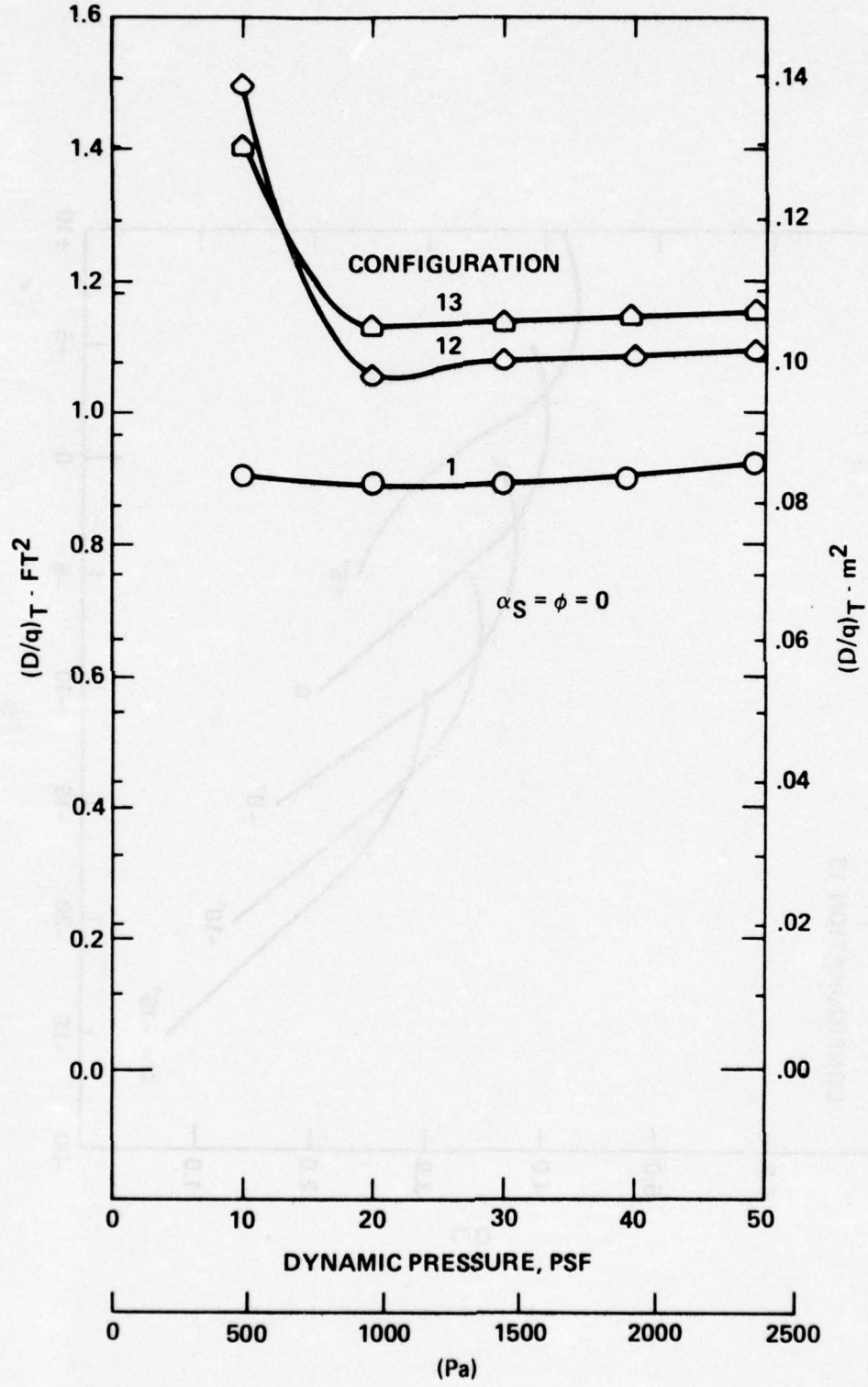

Figure 9 – (Concluded)
(e) Total Parasite Area Versus Dynamic Pressure

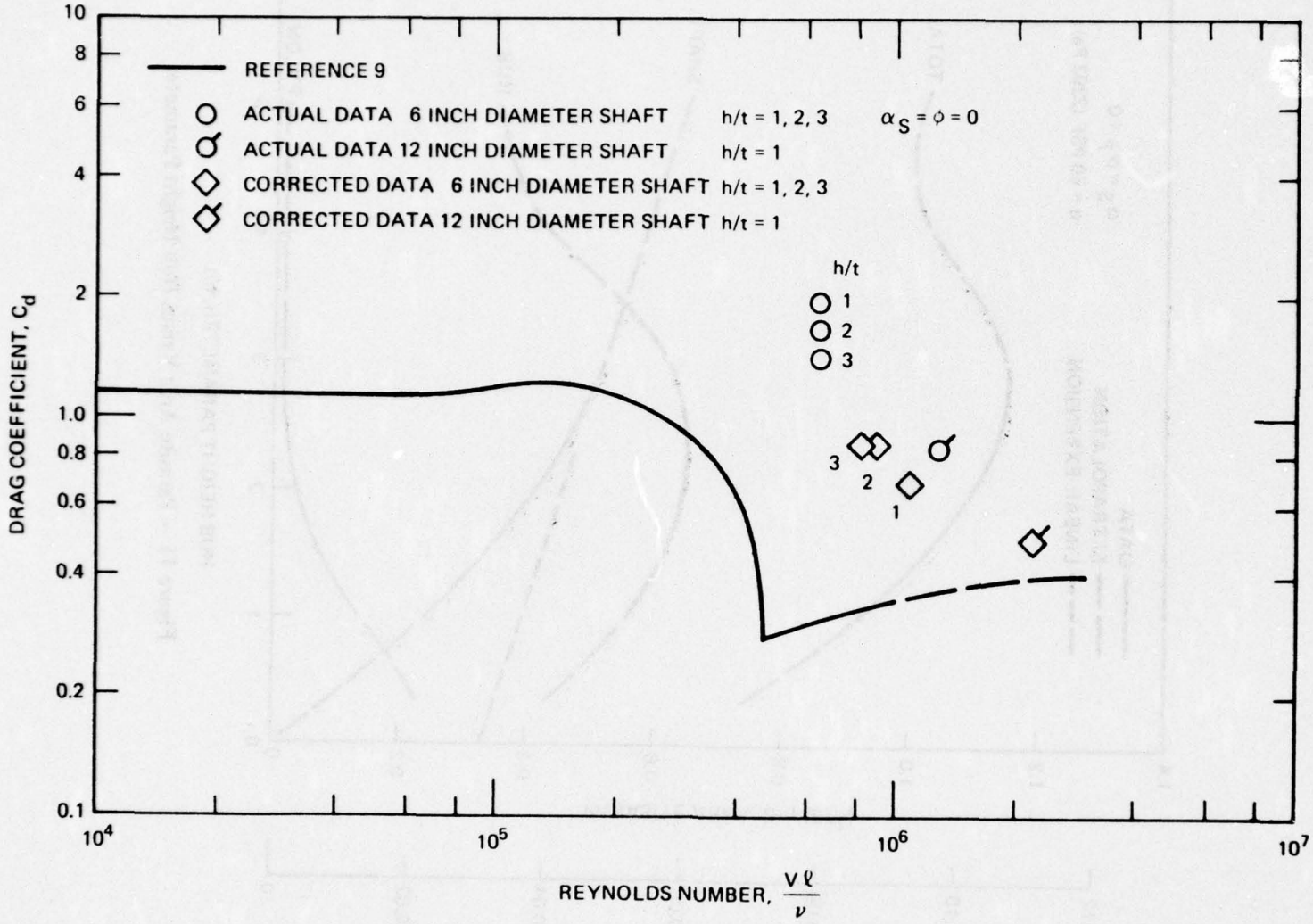

Figure 10 – Cylindrical Shaft Drag Coefficients Versus Reynolds Number

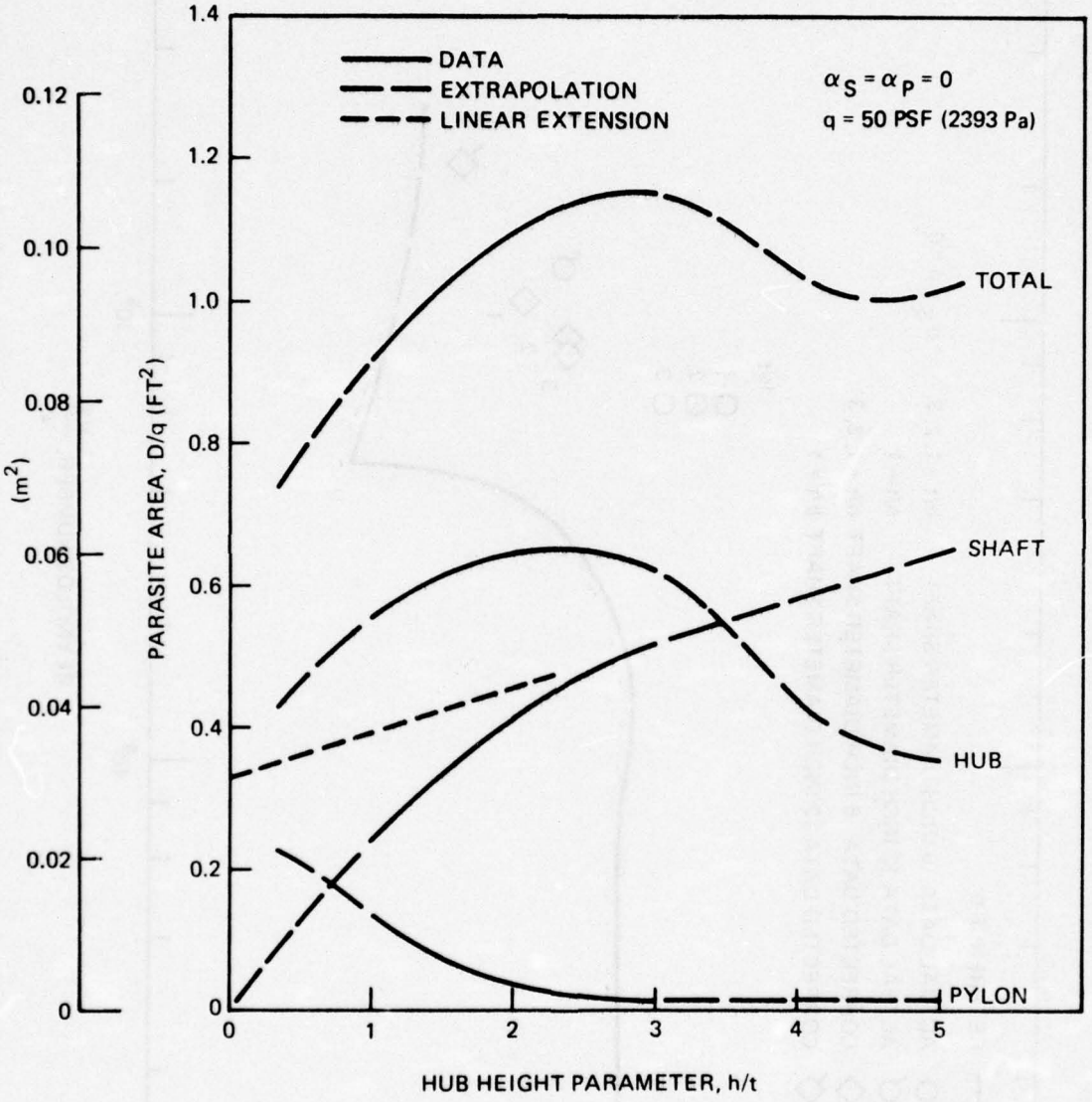

Figure 11 – Parasite Area Versus Hub Height Parameter

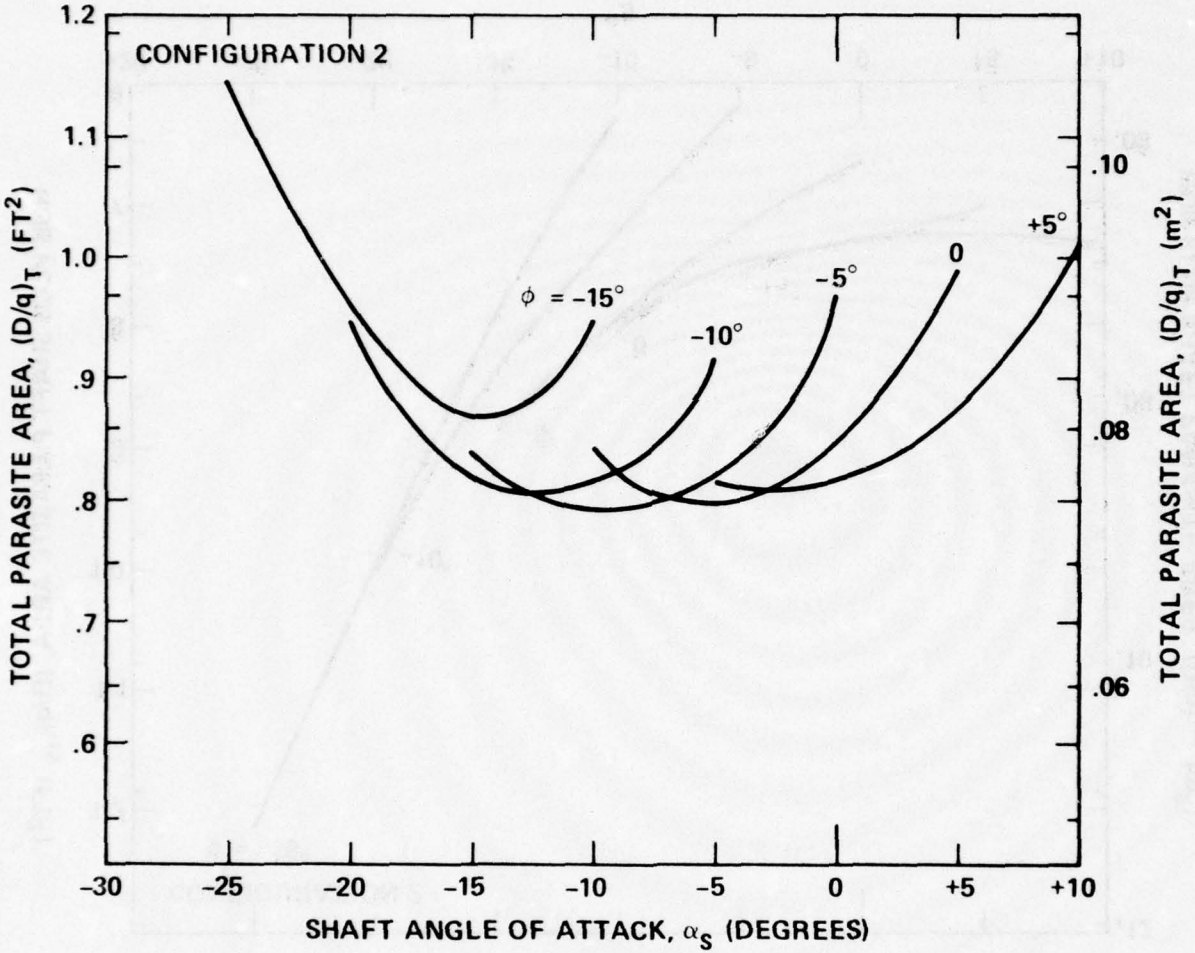

Figure 12 – Area Rule Fairing Configuration Data

(a) Configuration 2 Parasite Area at a Dynamic Pressure of 50 psf (2393 Pa)

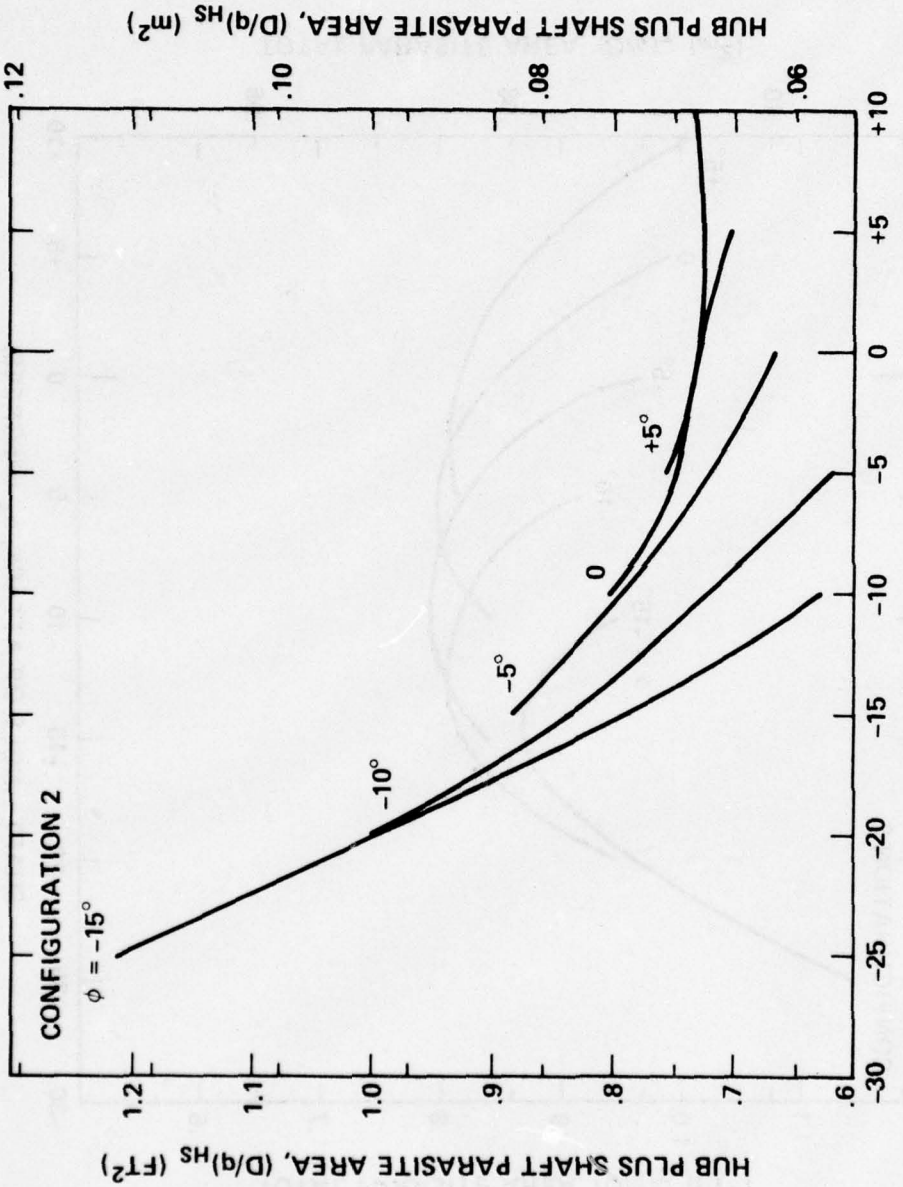

Figure 12(a) – (Continued)

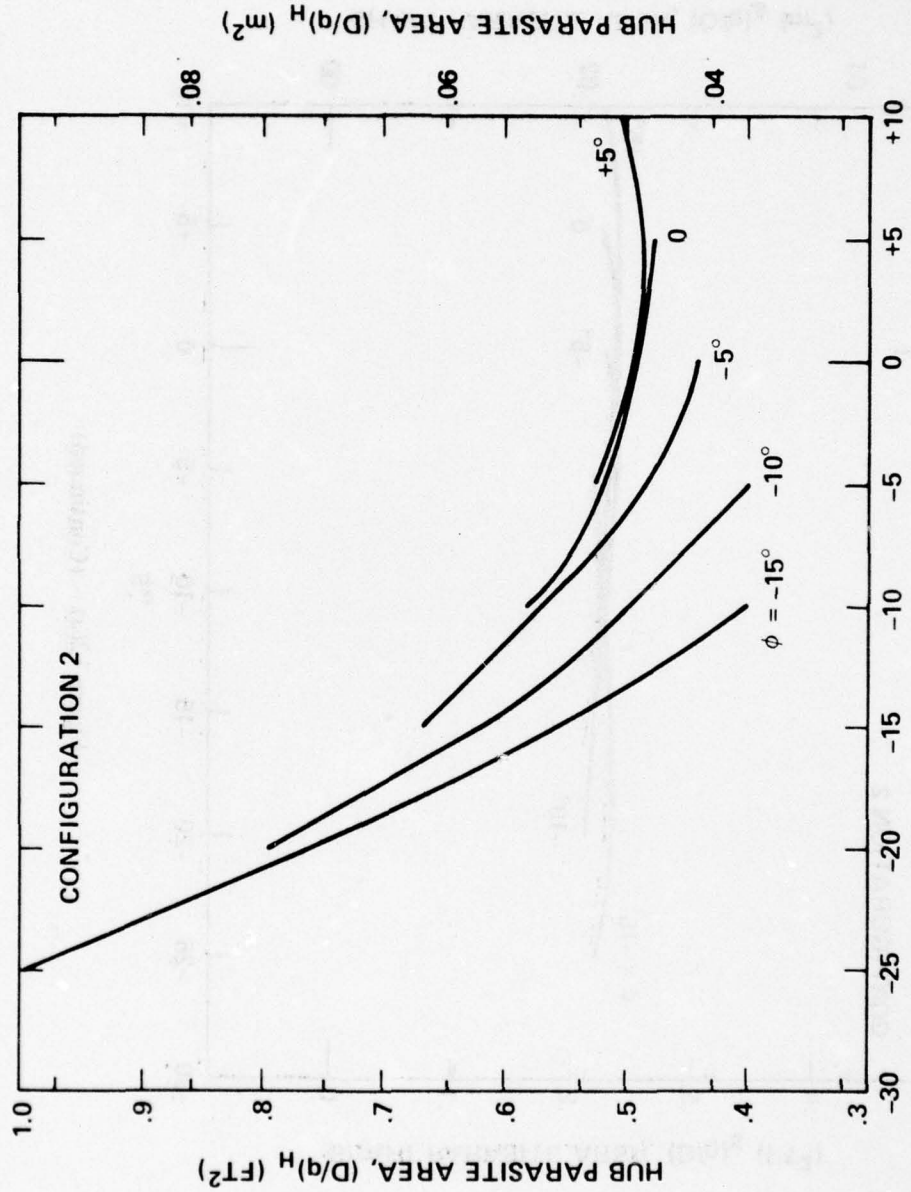

Figure 12(a) – (Continued)

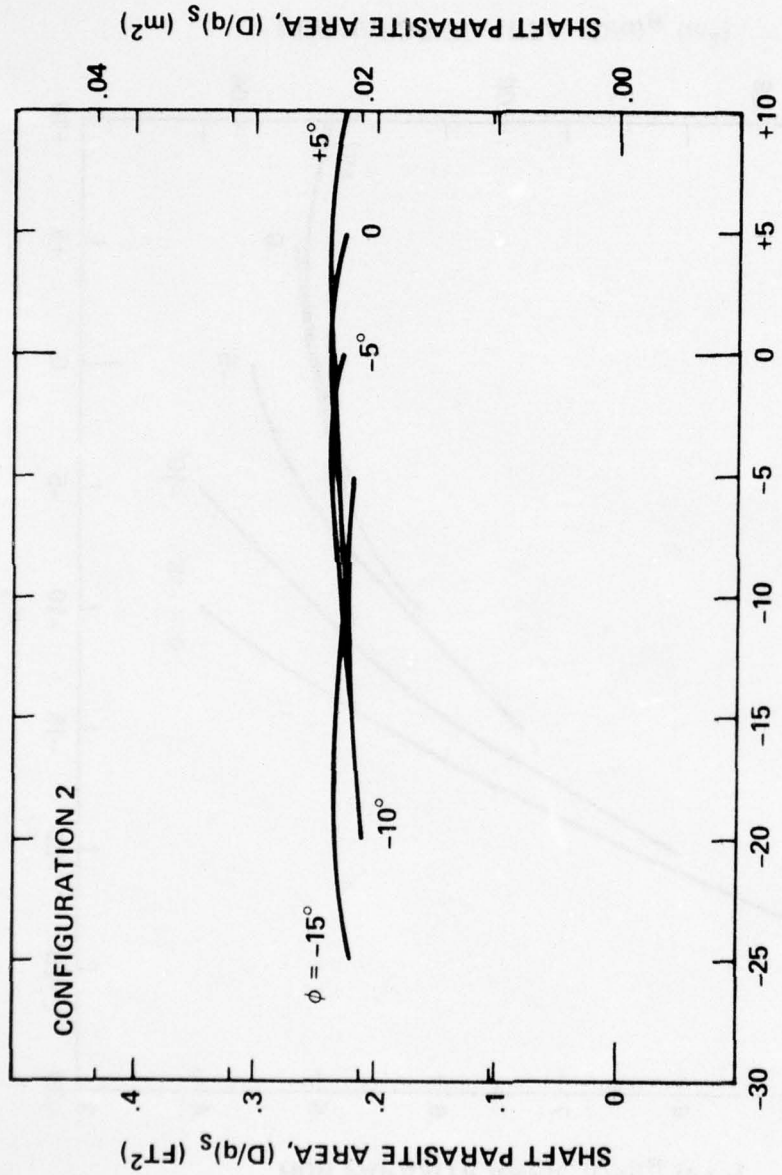

Figure 12(a) – (Continued)

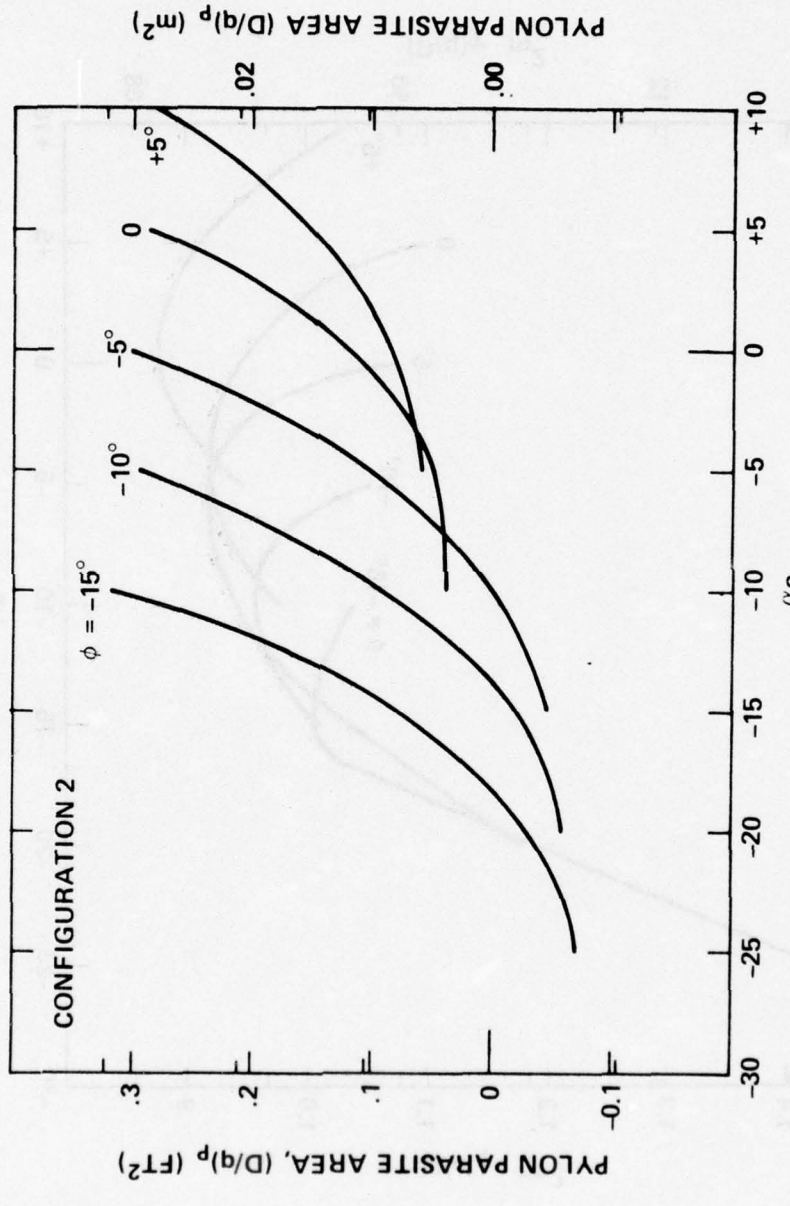

Figure 12(a) – (Concluded)

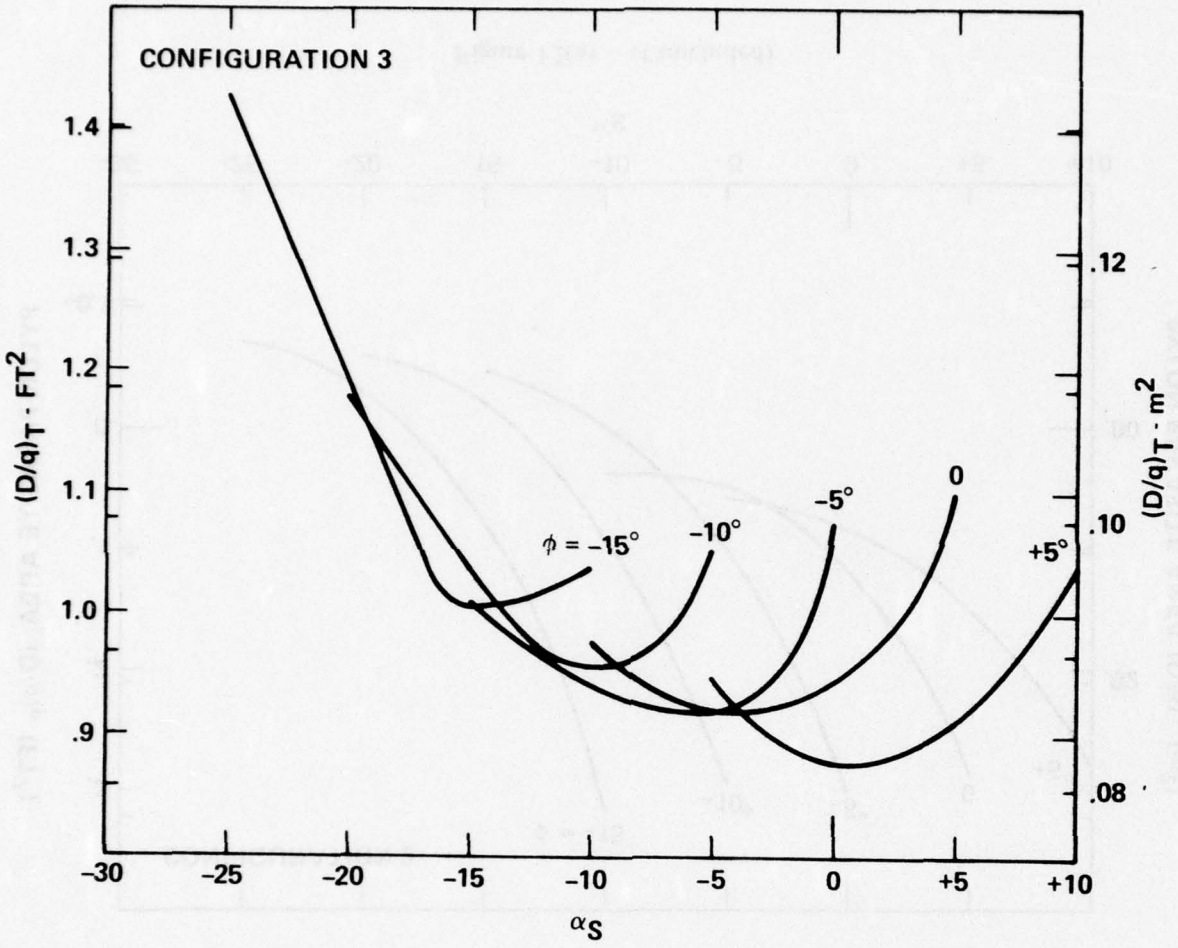

Figure 12 – (Continued)
(b) Configuration 3 Parasite Area at a Dynamic Pressure of 50 psf (2393 Pa)

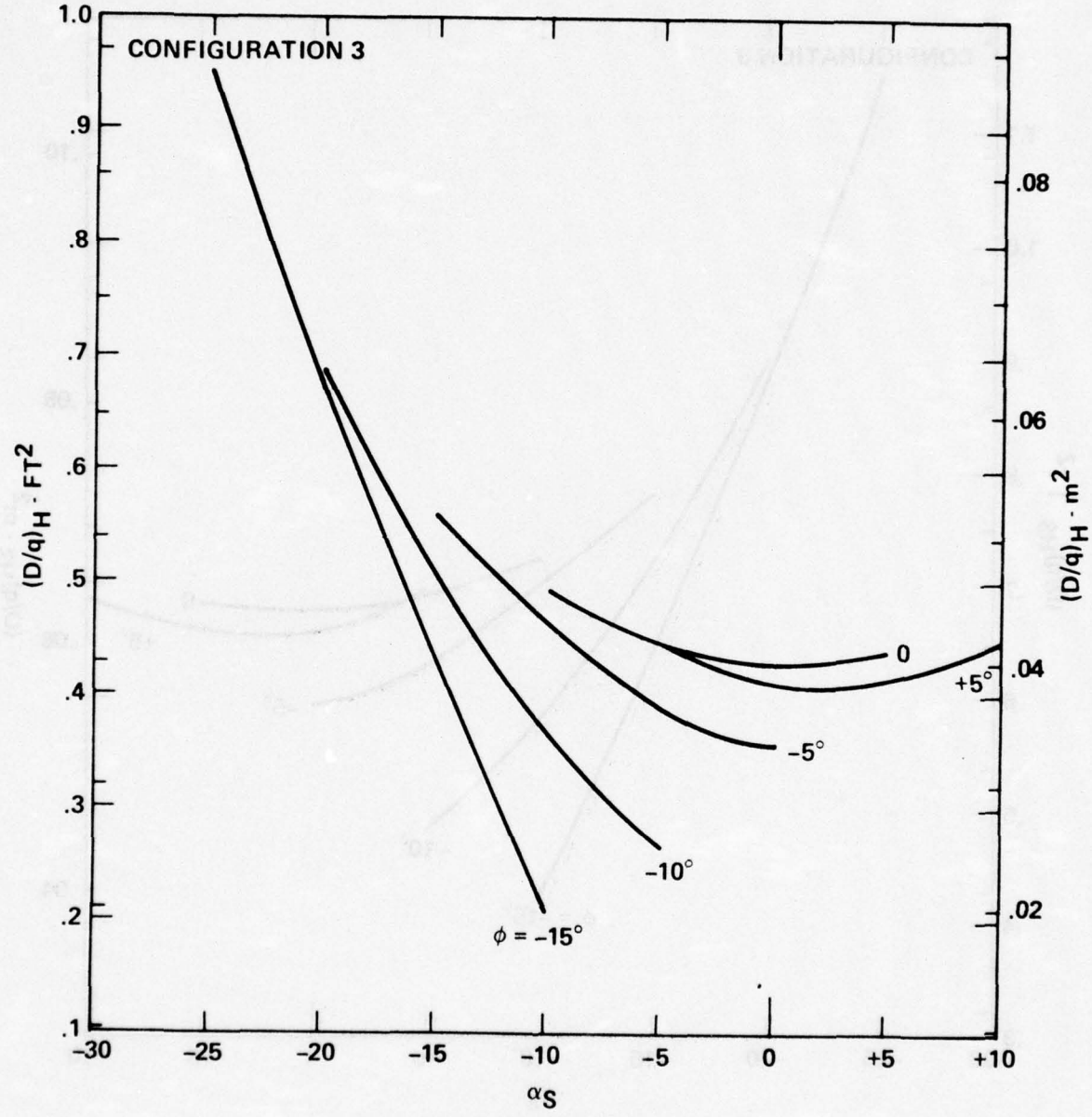

Figure 12(b) – (Continued)

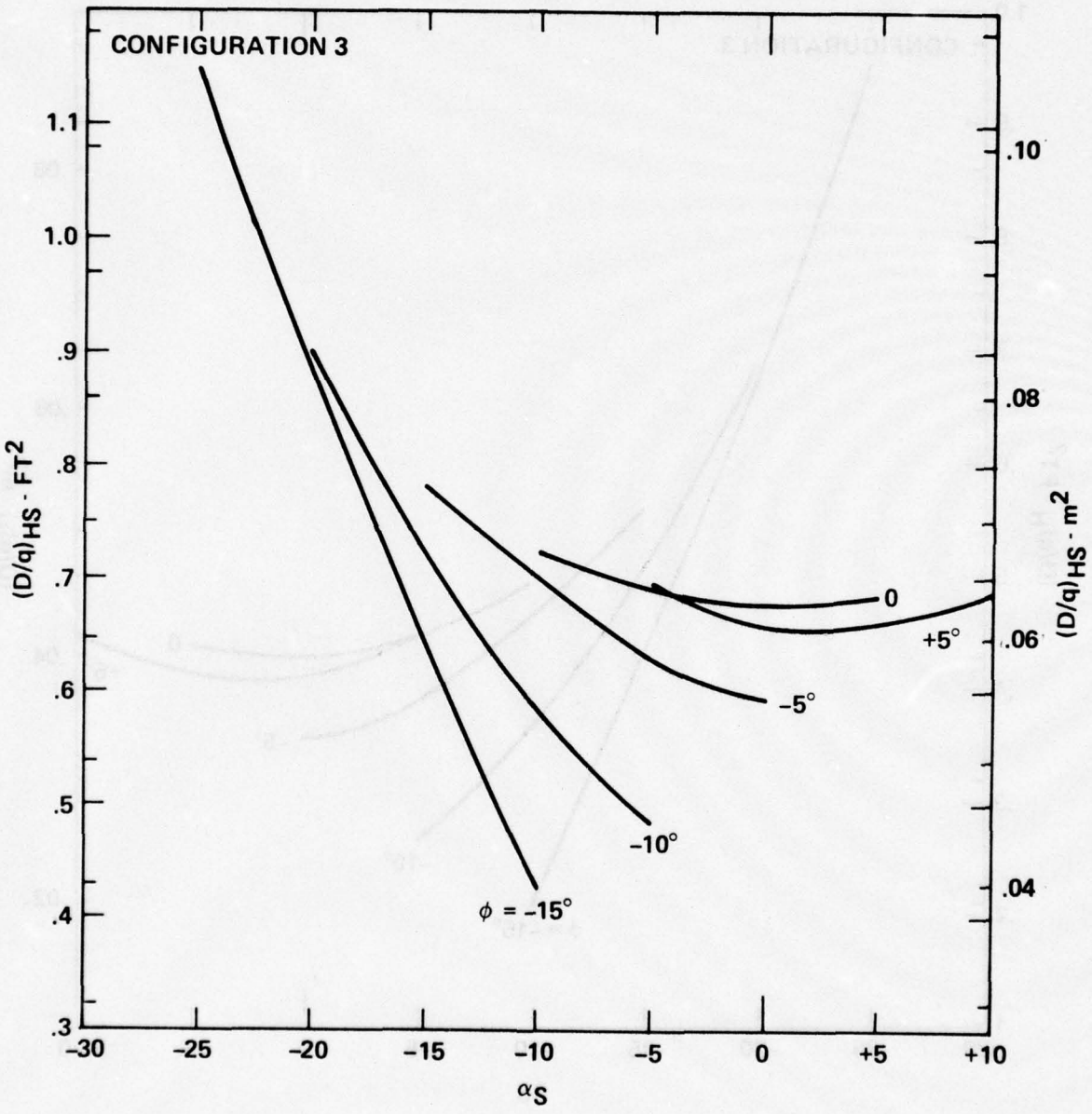

Figure 12(b) – (Continued)

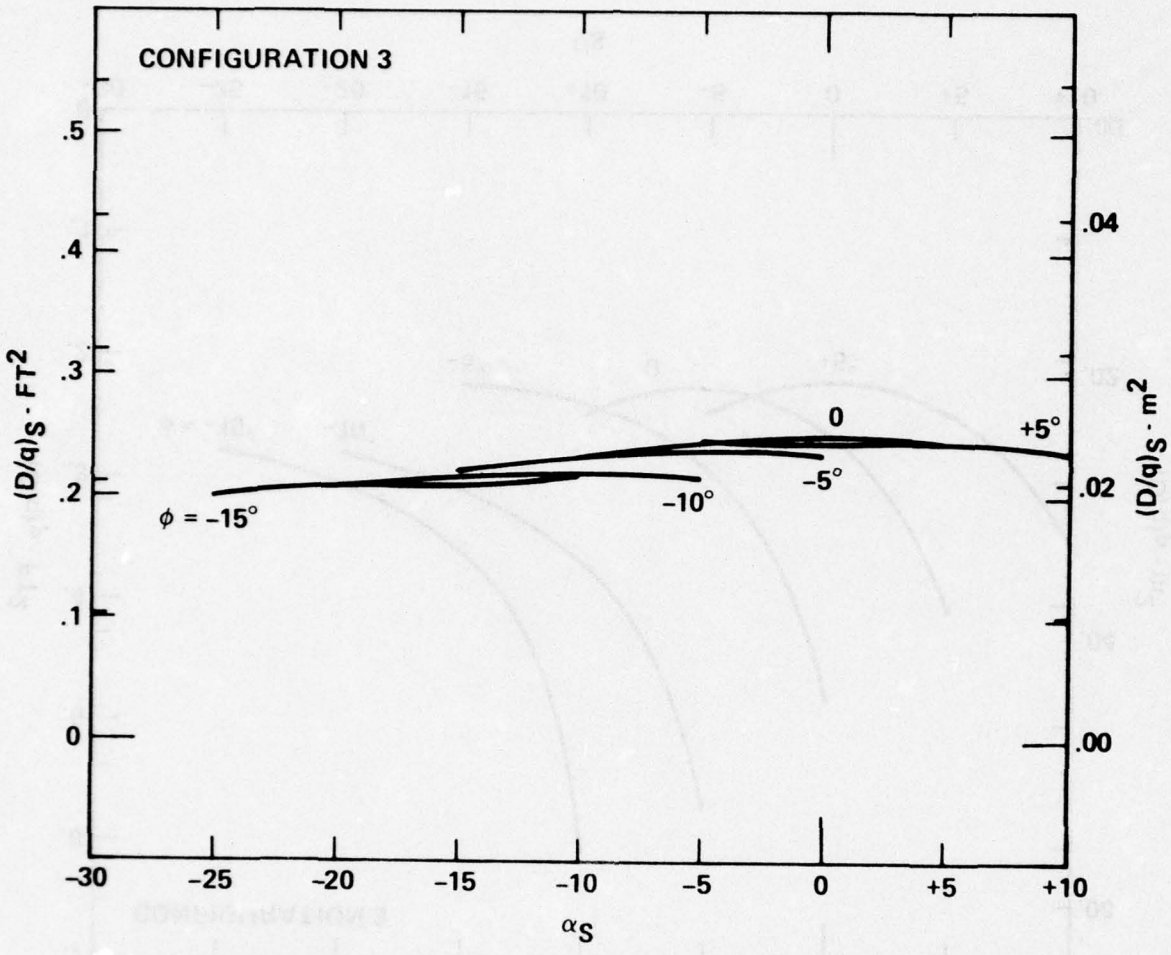

Figure 12(b) – (Continued)

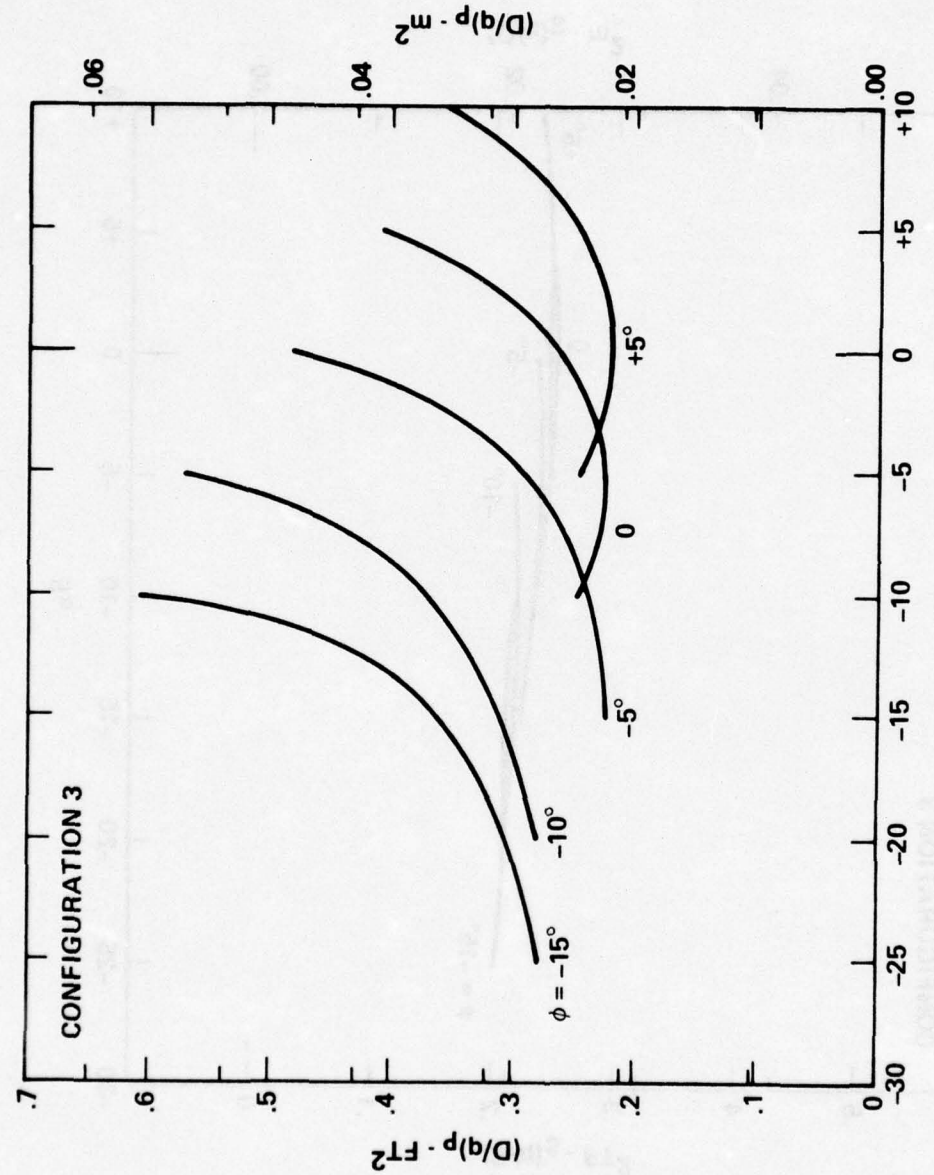

Figure 12(b) – (Concluded)

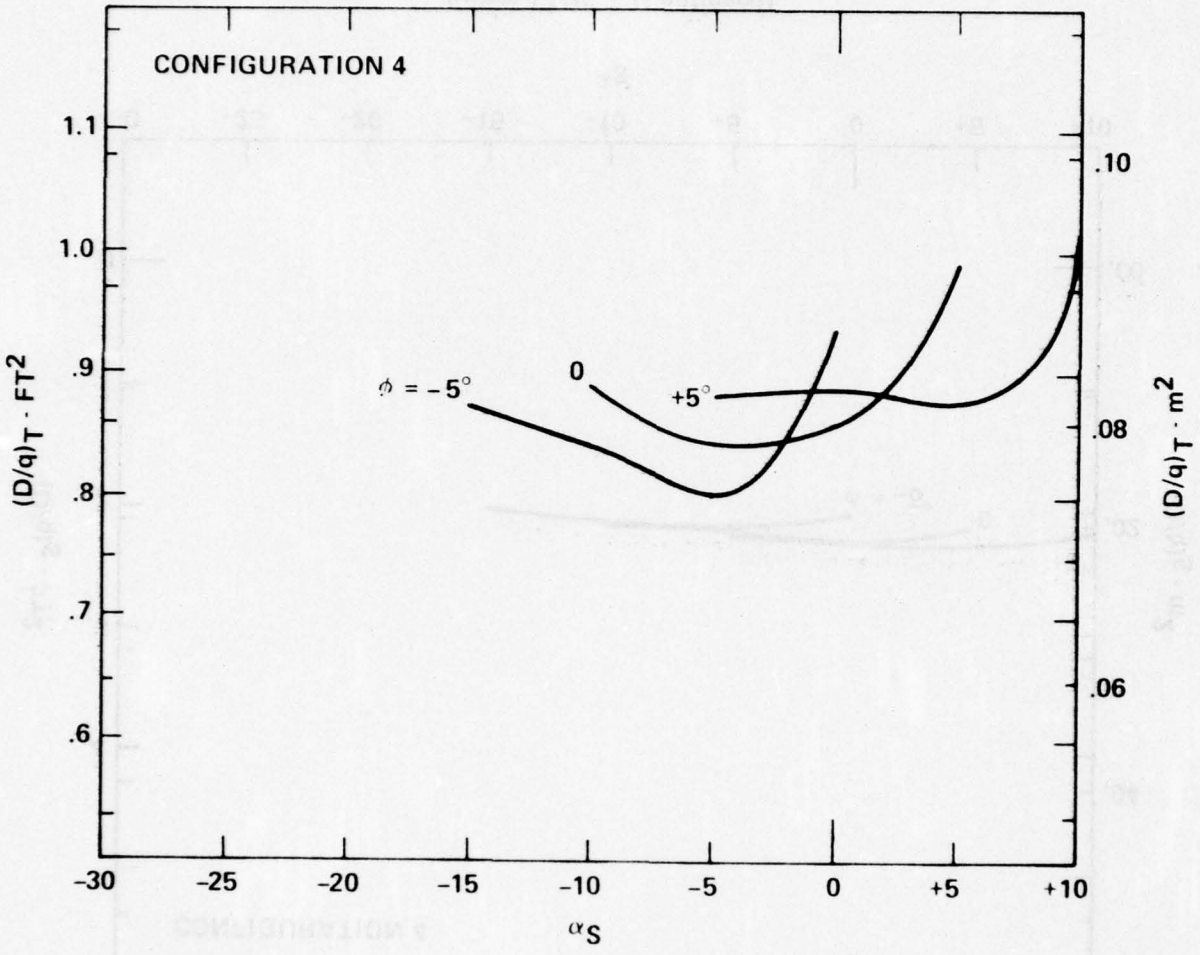

Figure 12 – (Continued)

(c) Configuration 4 Parasite Area at a Dynamic Pressure of 50 psf (2393 Pa)

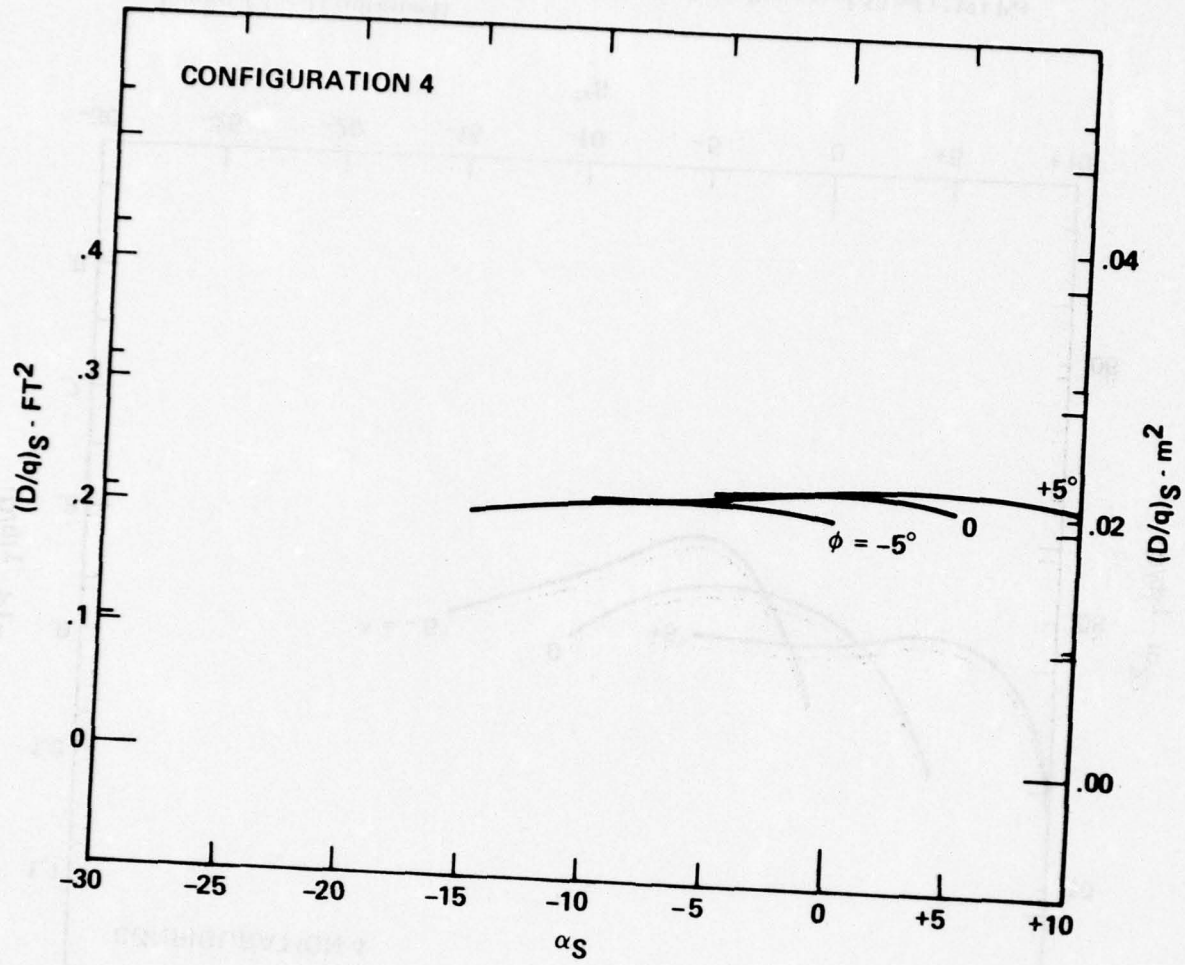

Figure 12 (c) – (Continued)

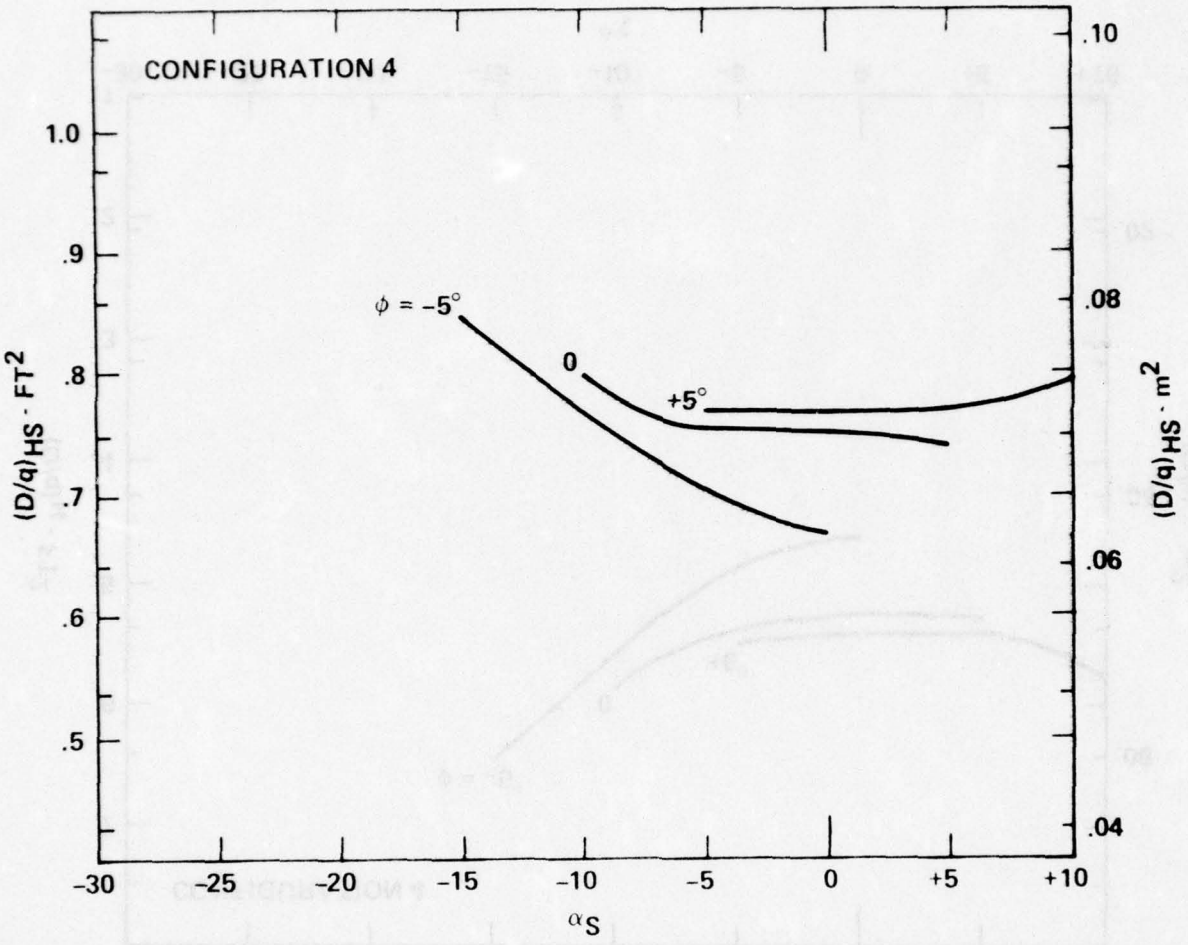

Figure 12(c) (Continued)

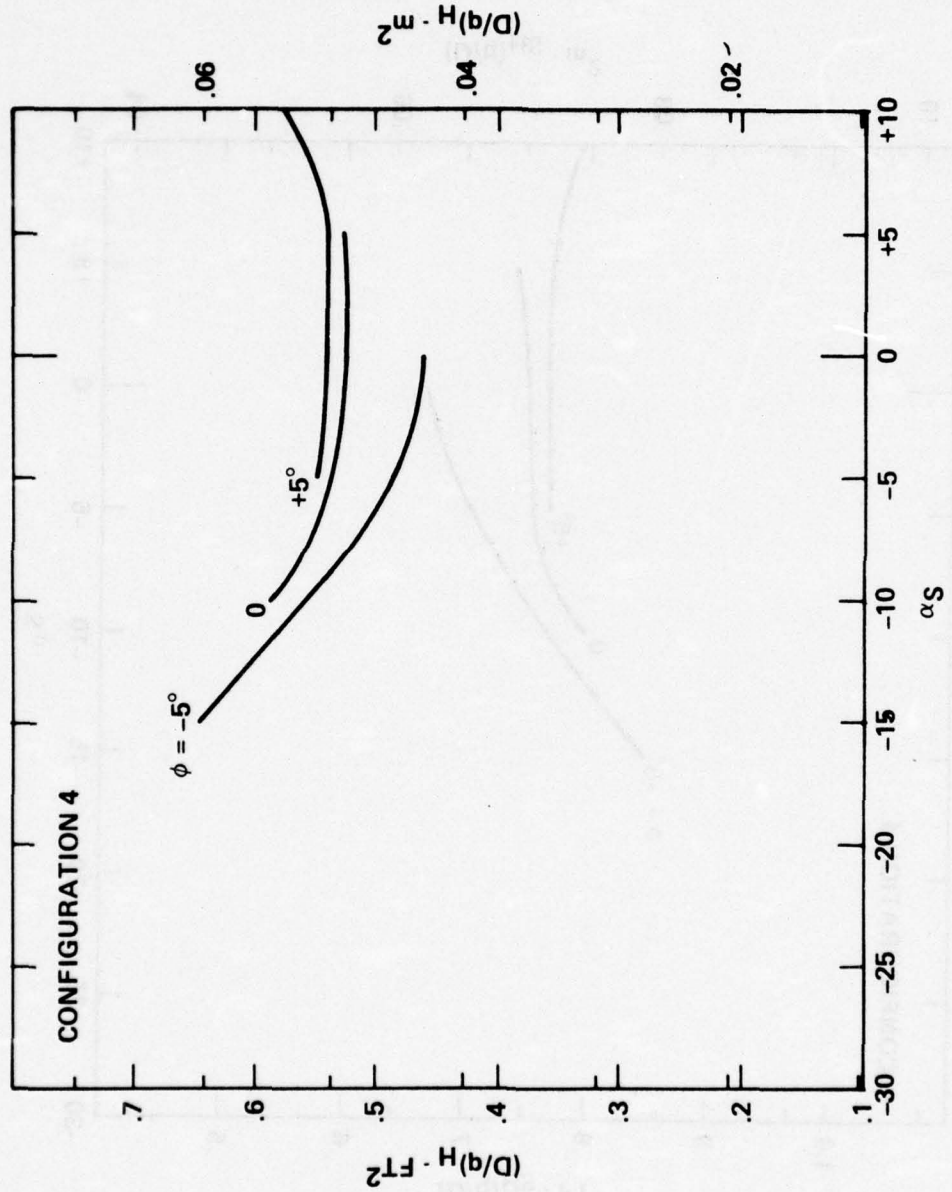

Figure 12(c) – (Continued)

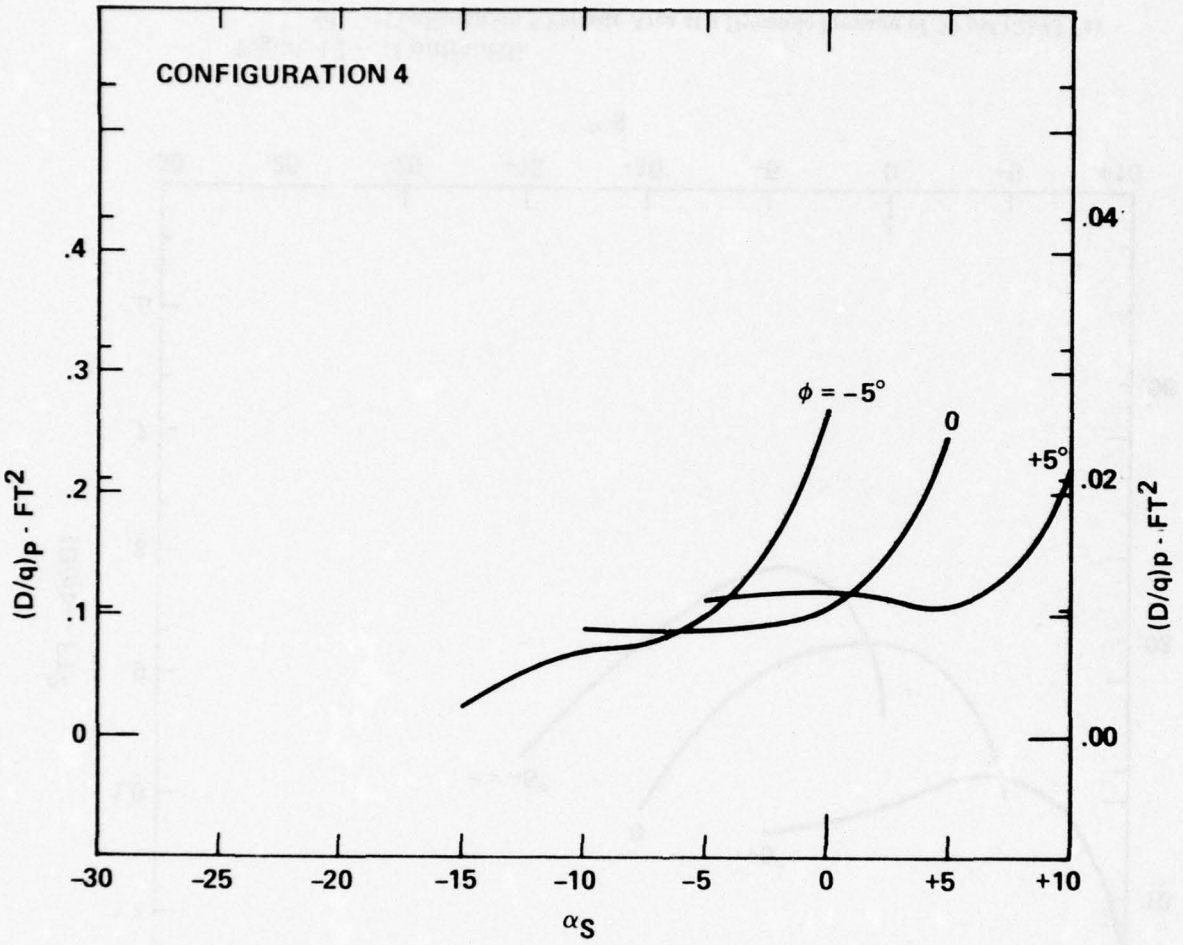

Figure 12(c) – (Concluded)

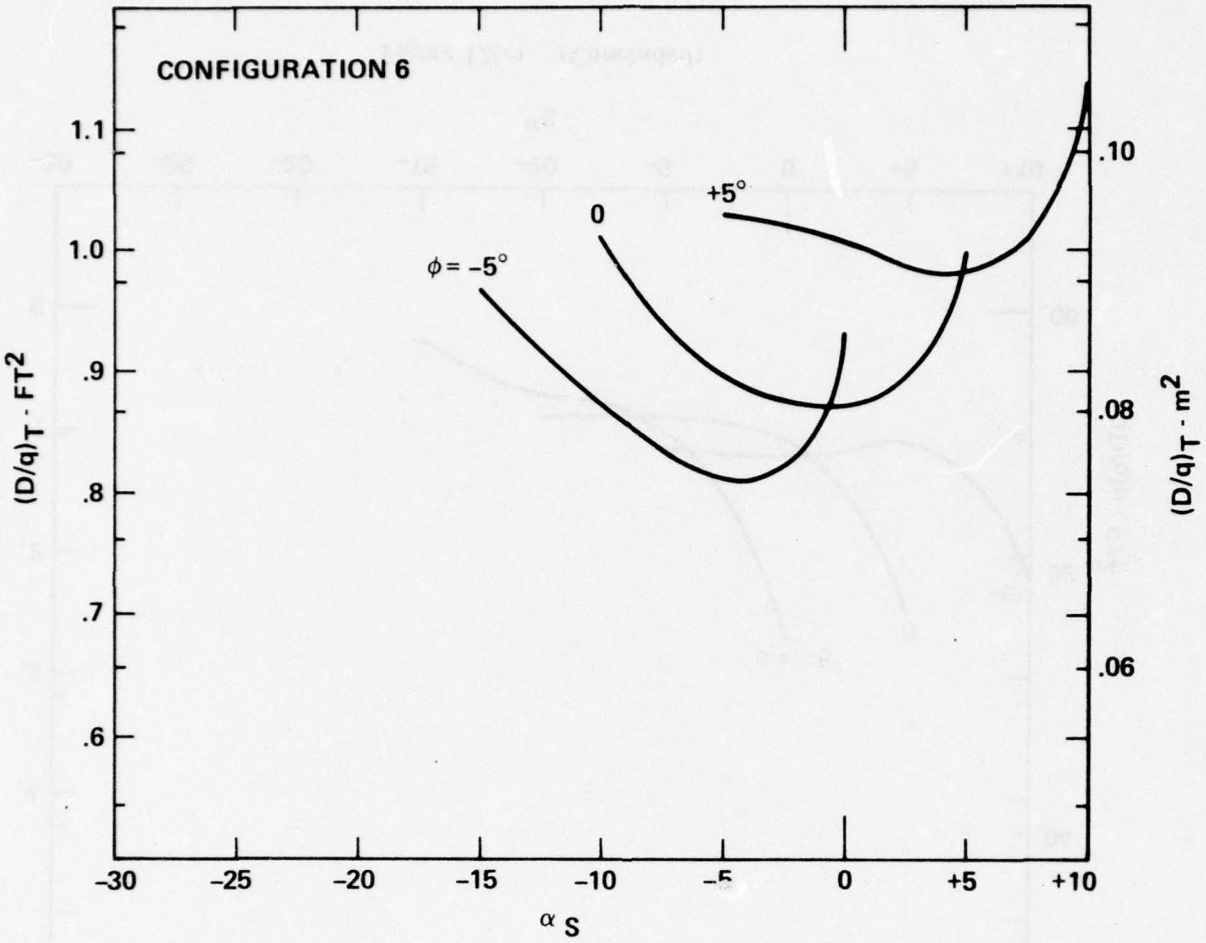

Figure 12 – (Continued)
(d) Configuration 6 Parasite Area at a Dynamic Pressure of 50 psf (2393 Pa)

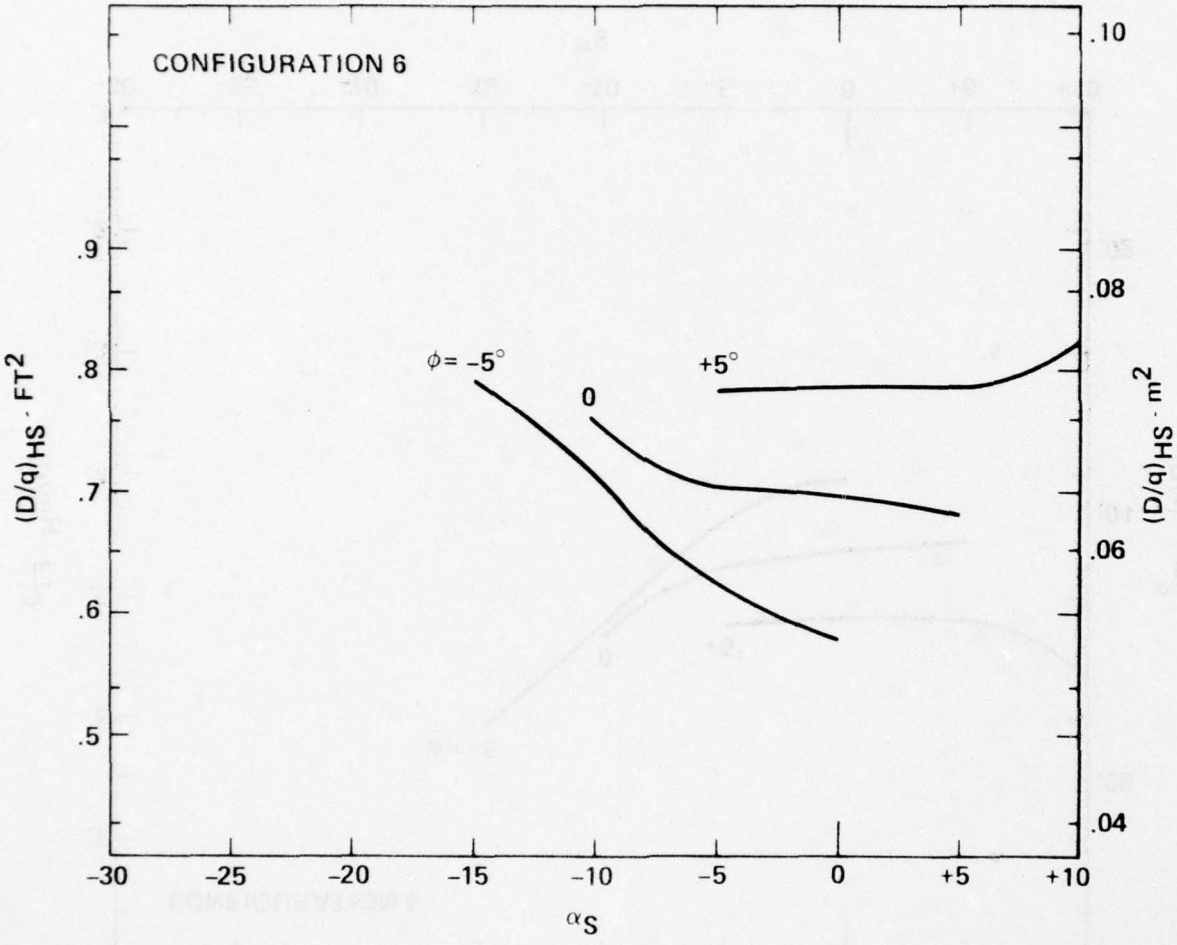

Figure 12(d) (Continued)

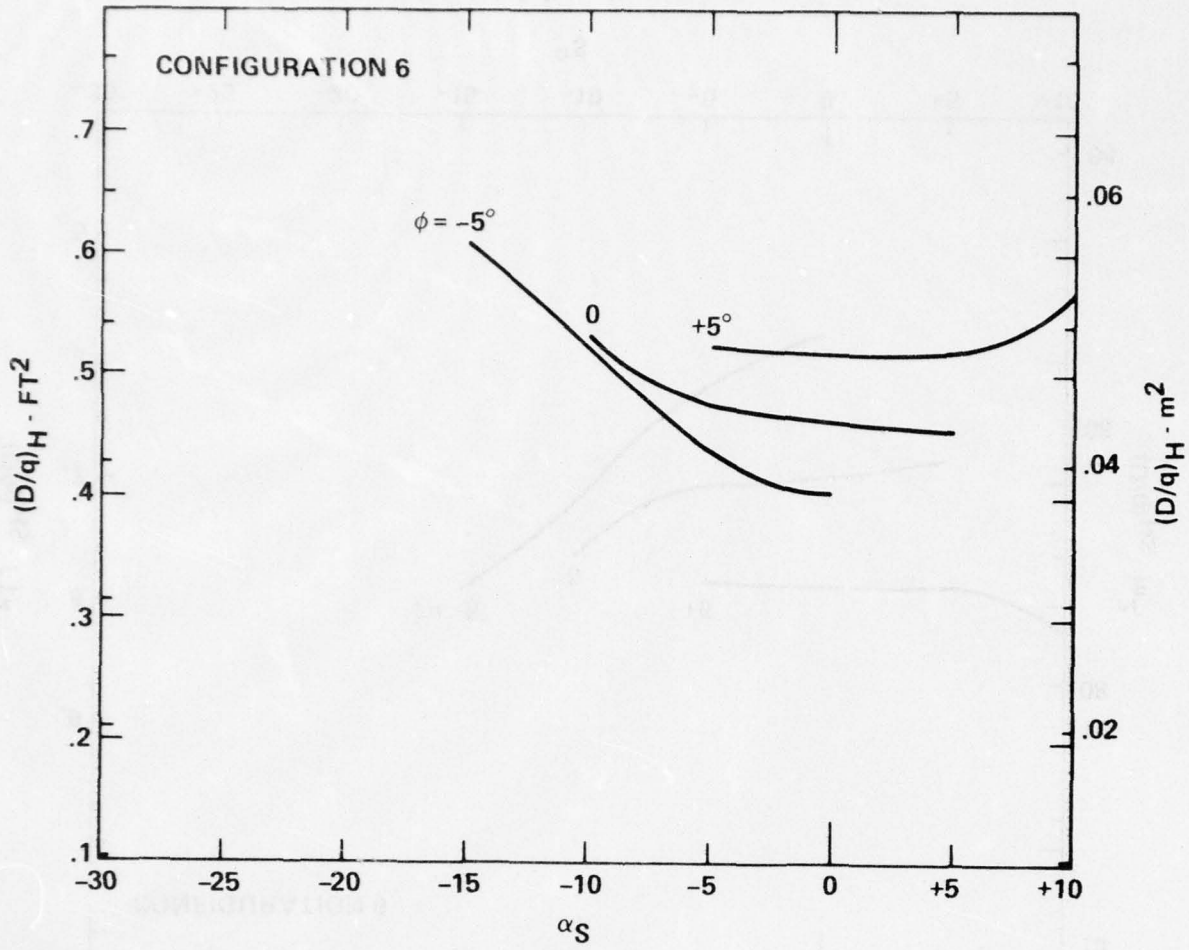

Figure 12(d) – (Continued)

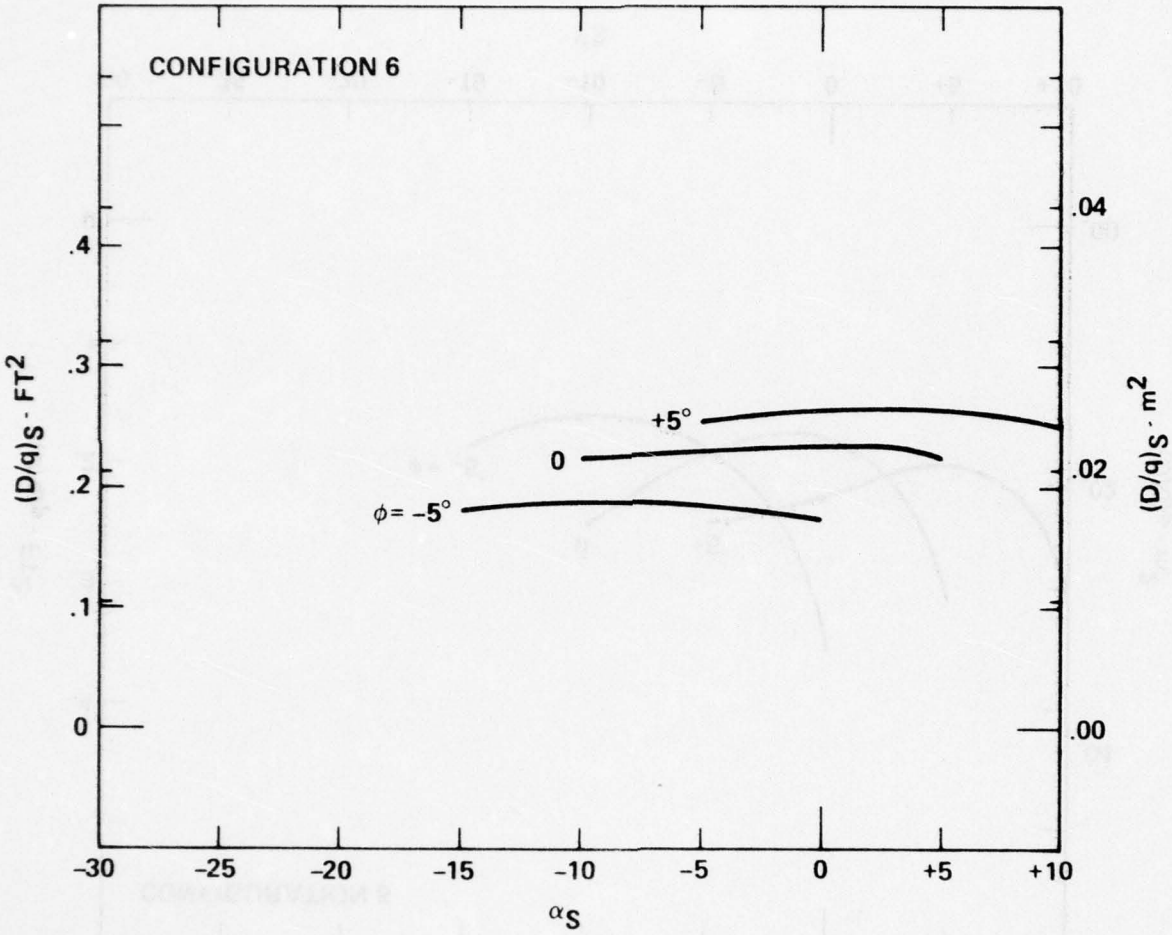

Figure 12(d) – (Continued)

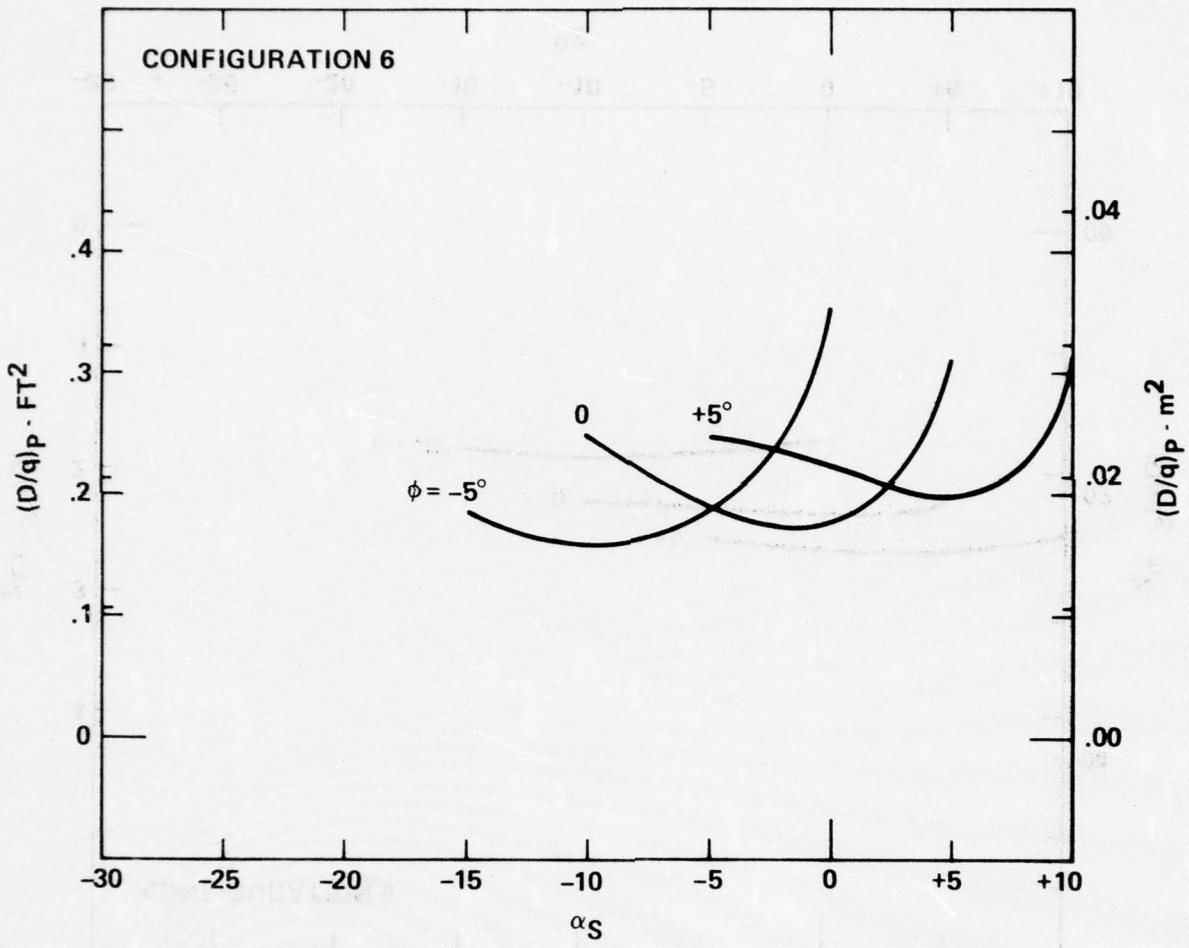

Figure 12(d) – (Concluded)

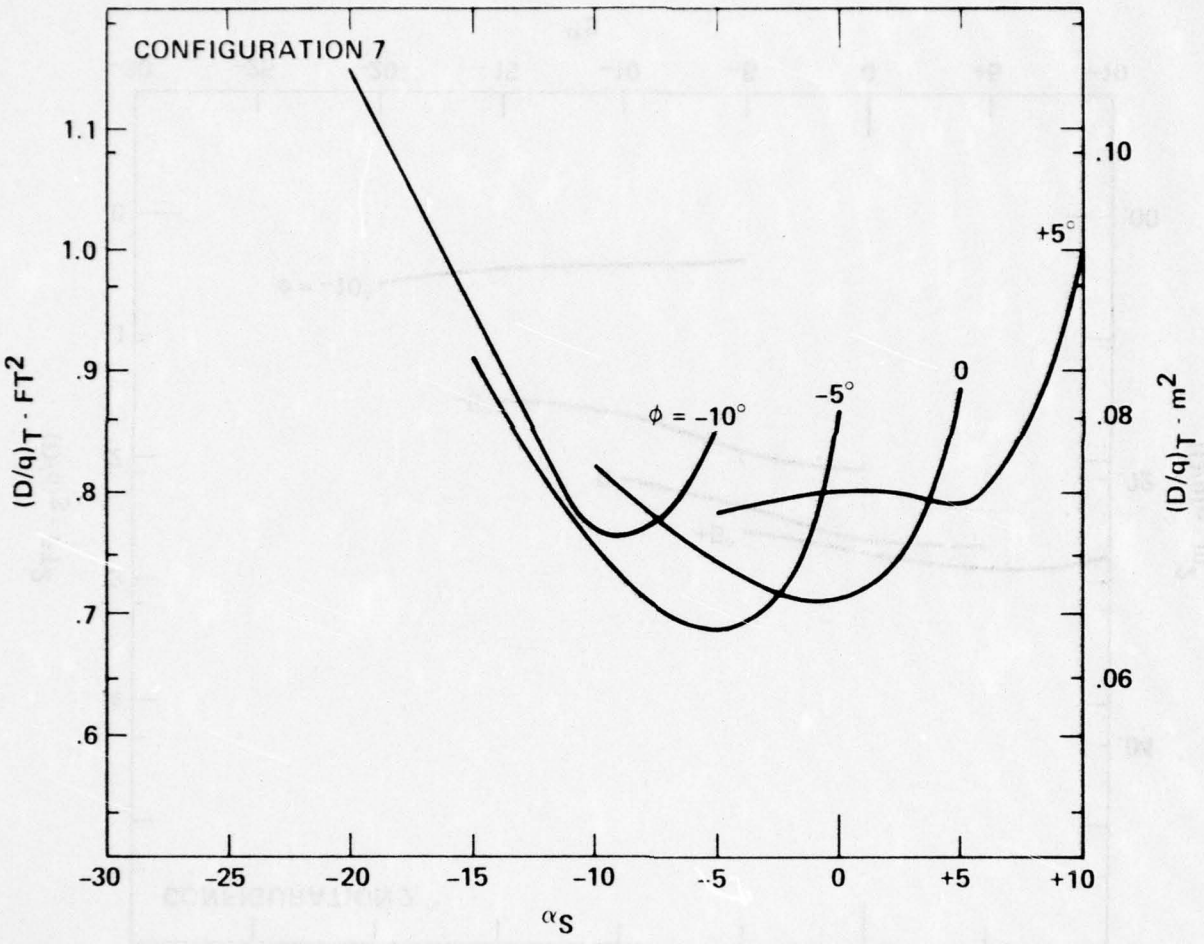

Figure 12 (Continued)
(e) Configuration 7 Parasite Area of a Dynamic Pressure of 50 psf (2393 Pa)

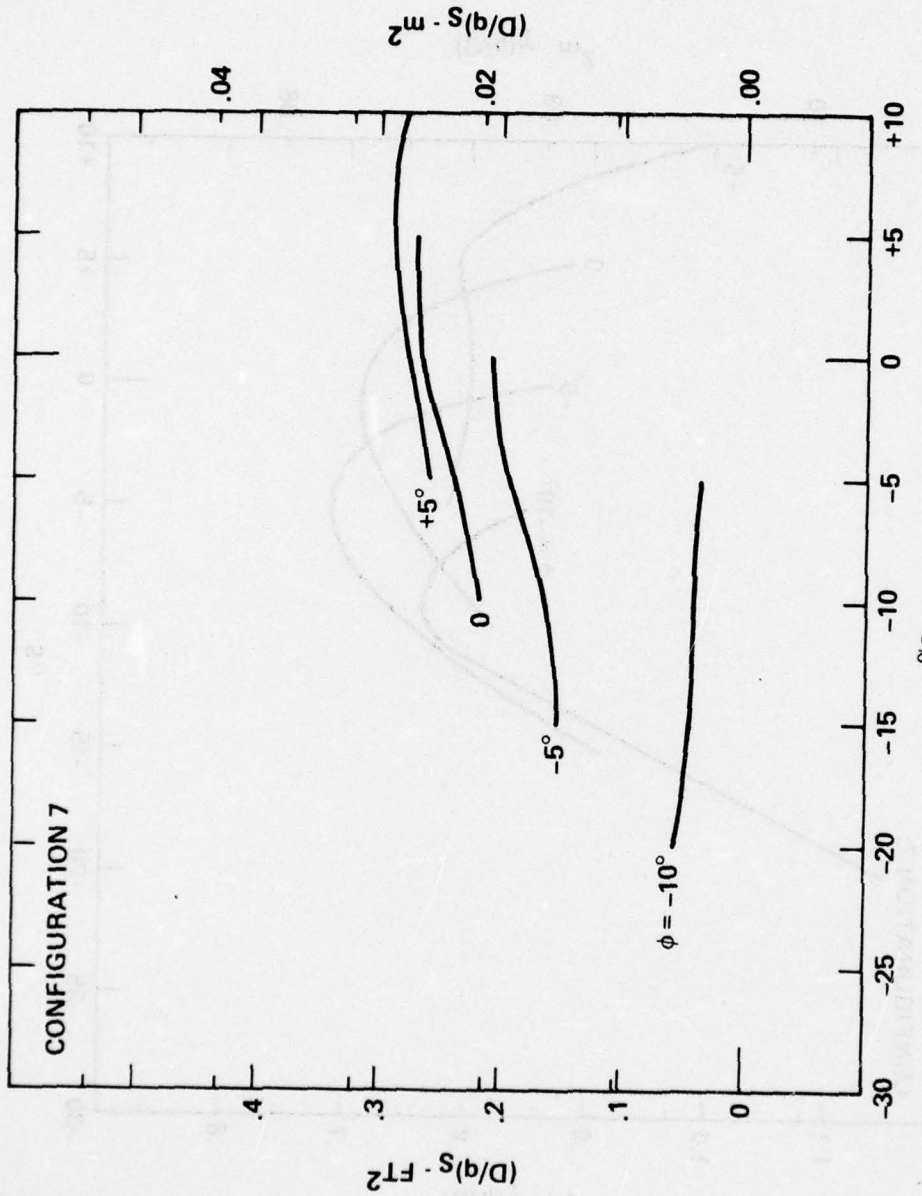

Figure 12(e) – (Continued)

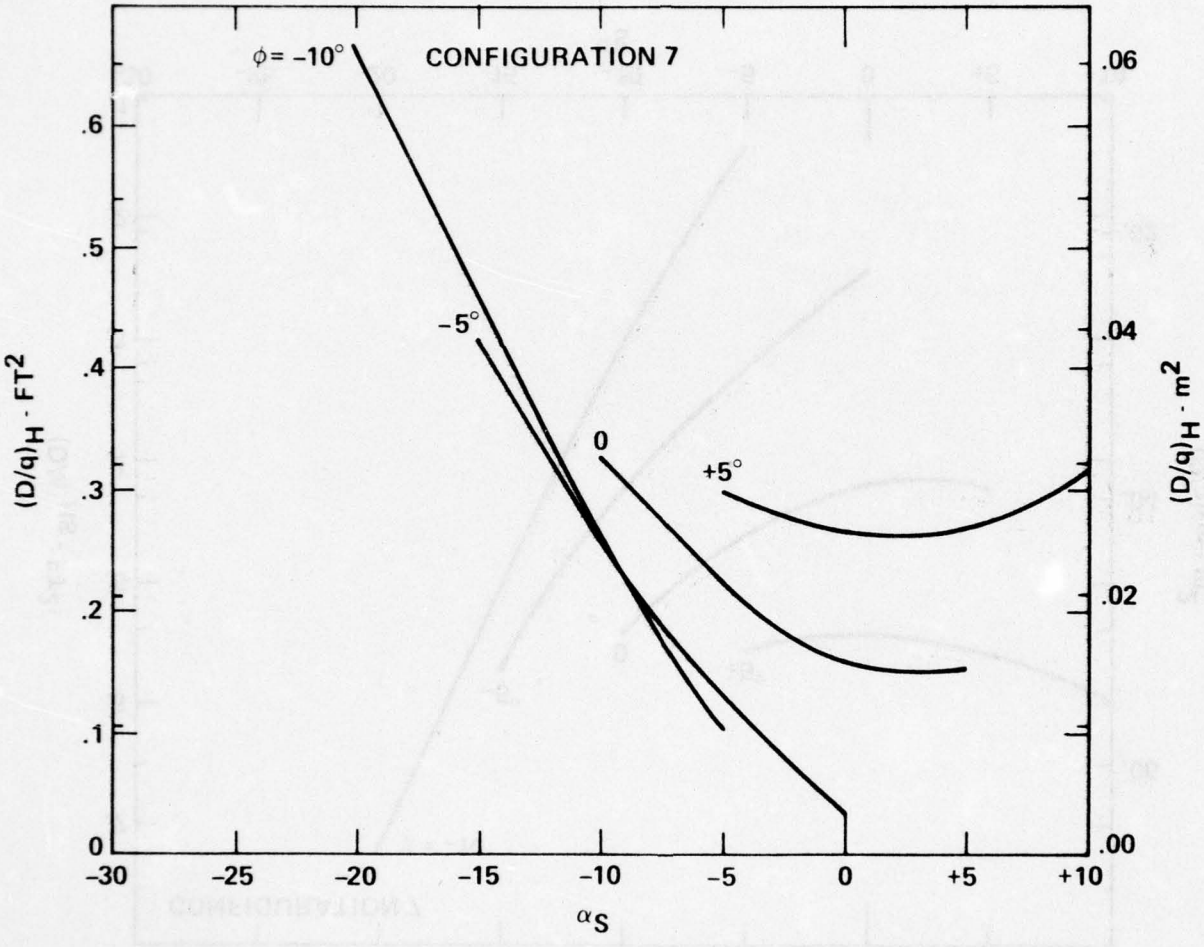

Figure 12(e) (Continued)

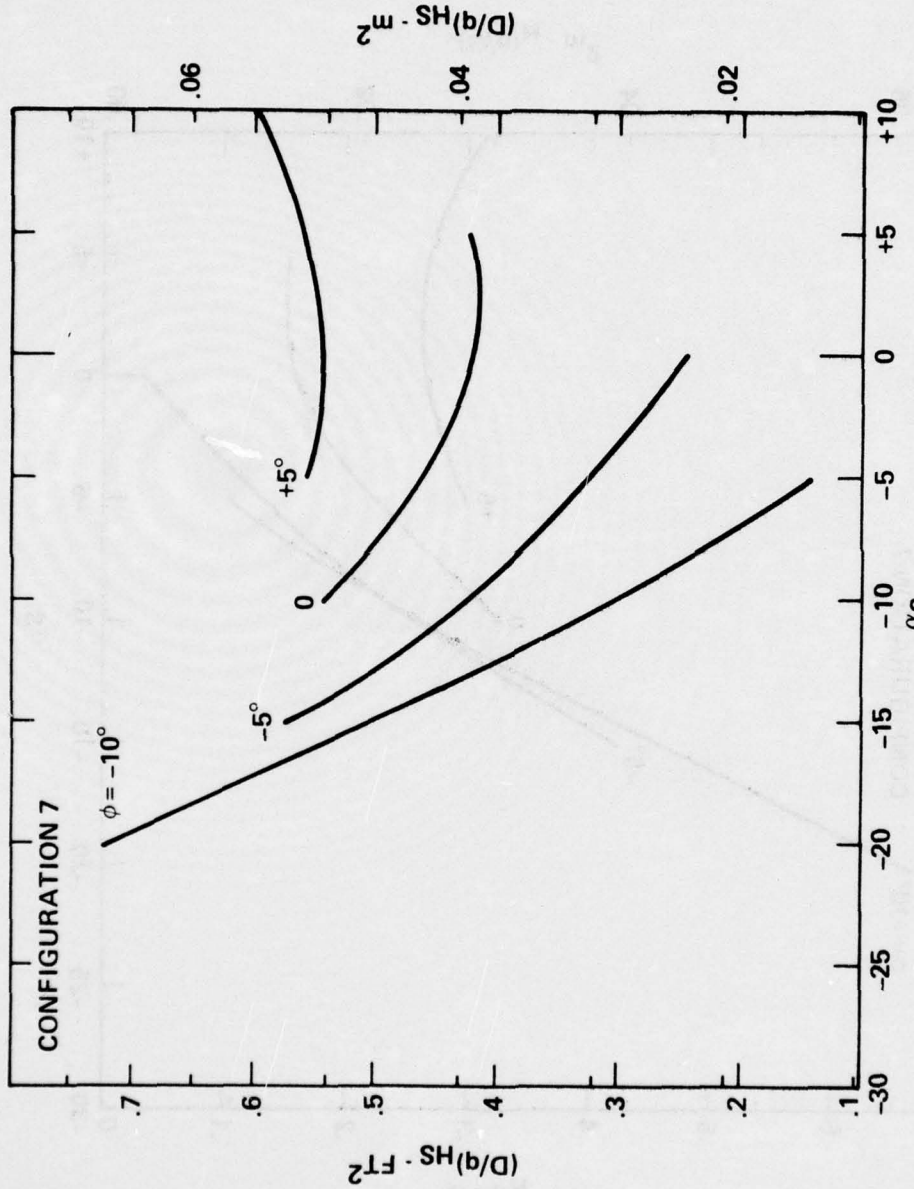

Figure 12(e) – (Continued)

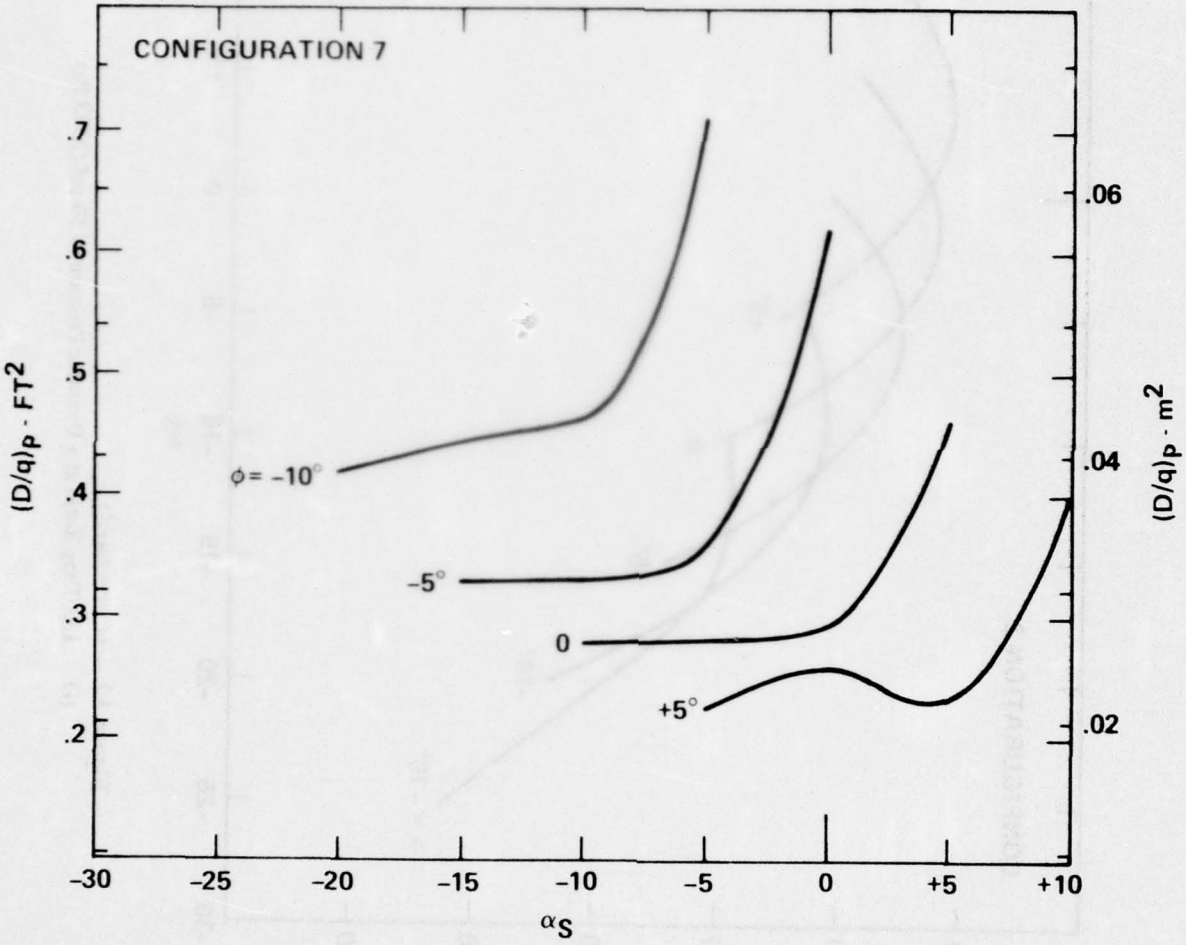

Figure 12(e) (Concluded)

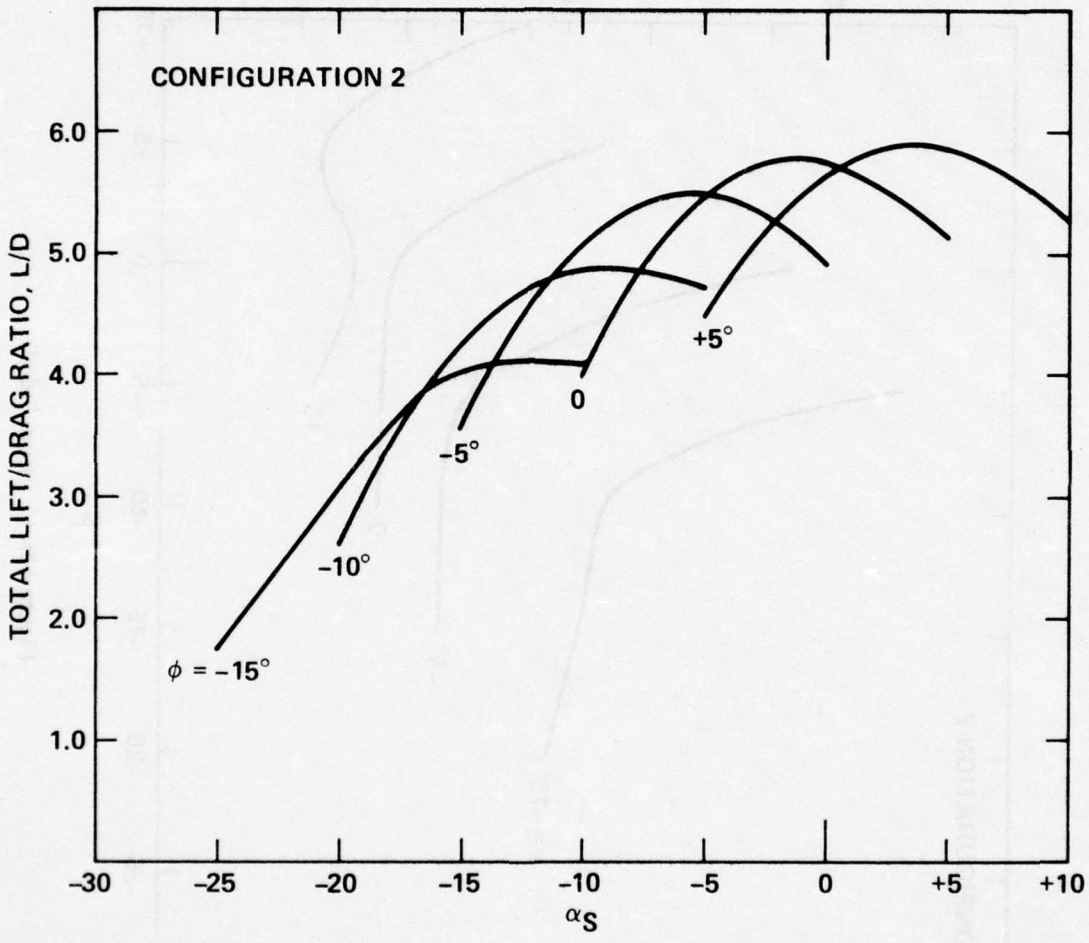

Figure 12 – (Continued)
(f) Lift/Drag Ratio at a Dyanmic Pressure of 50 psf (2393 Pa)

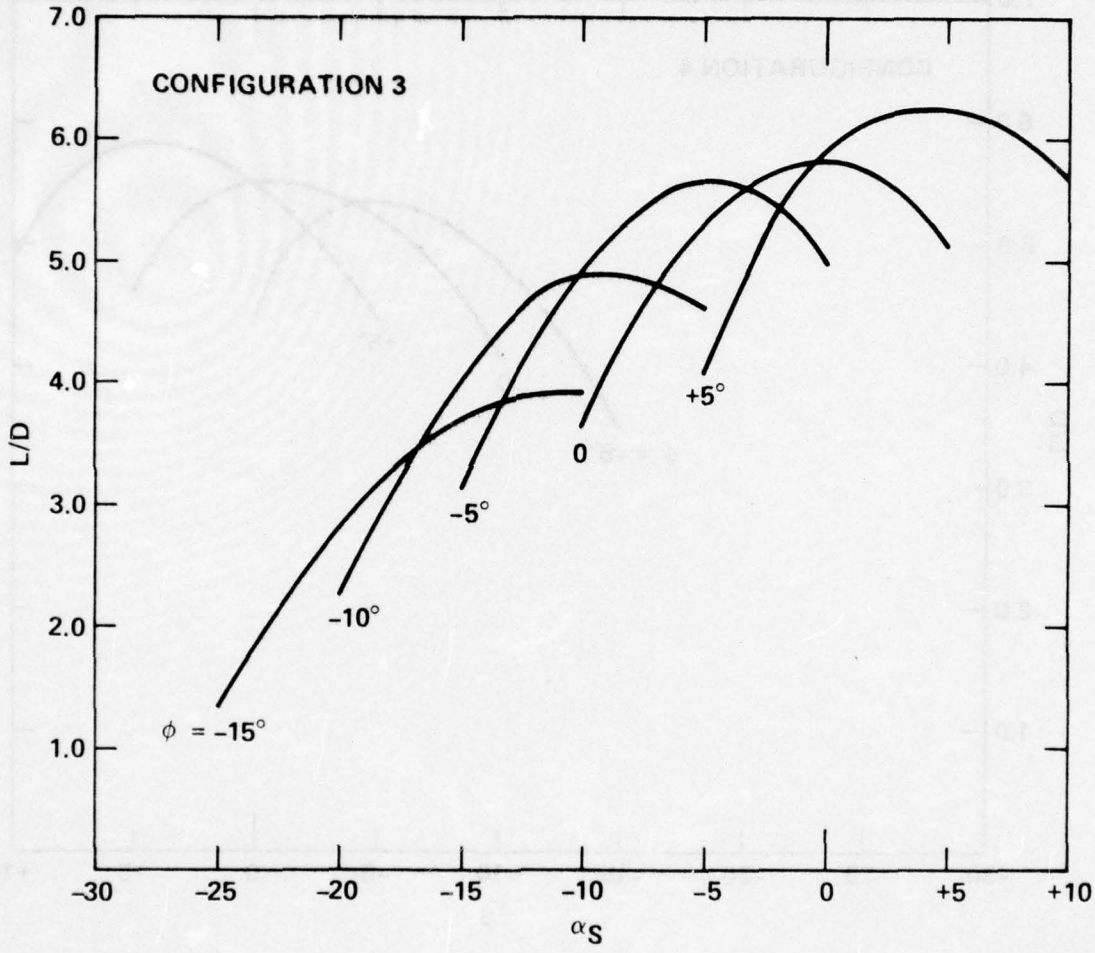

Figure 12(f) – (Continued)

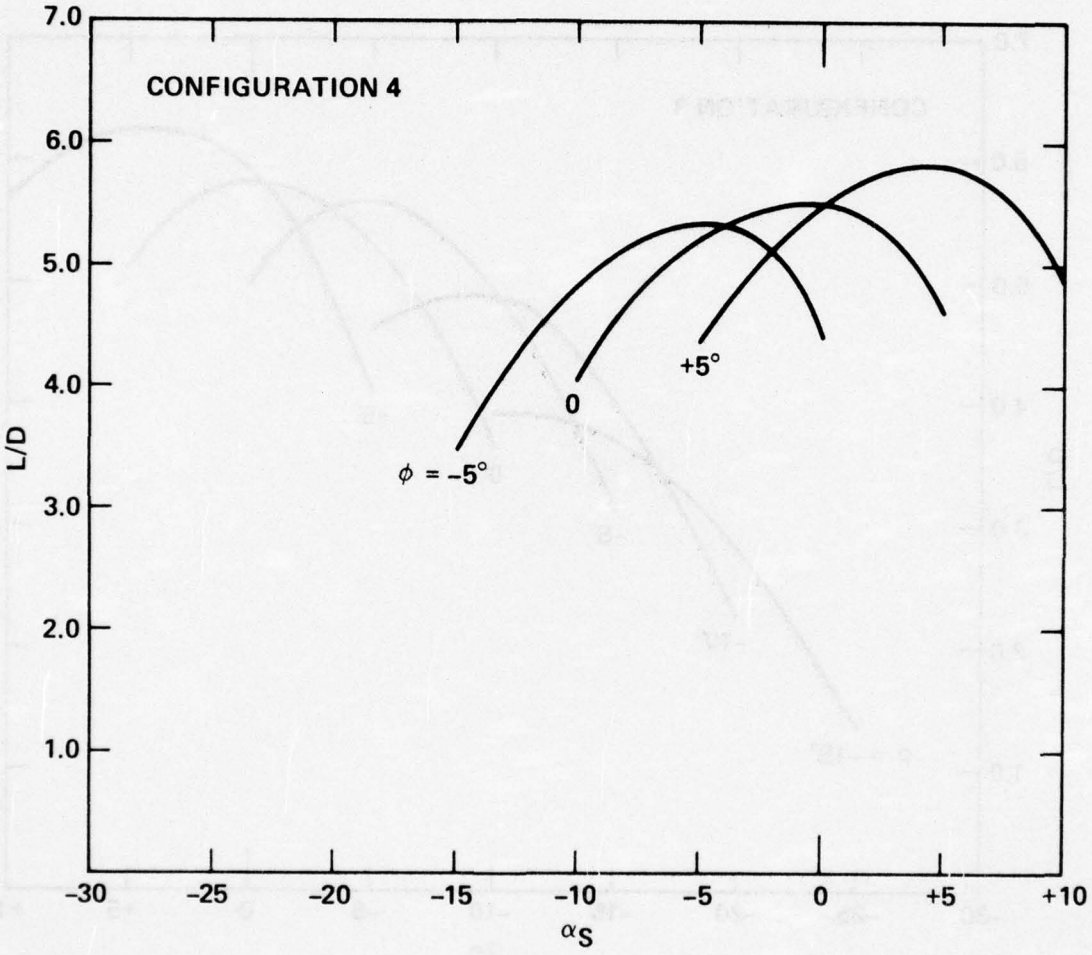

Figure 12(f) – (Continued)

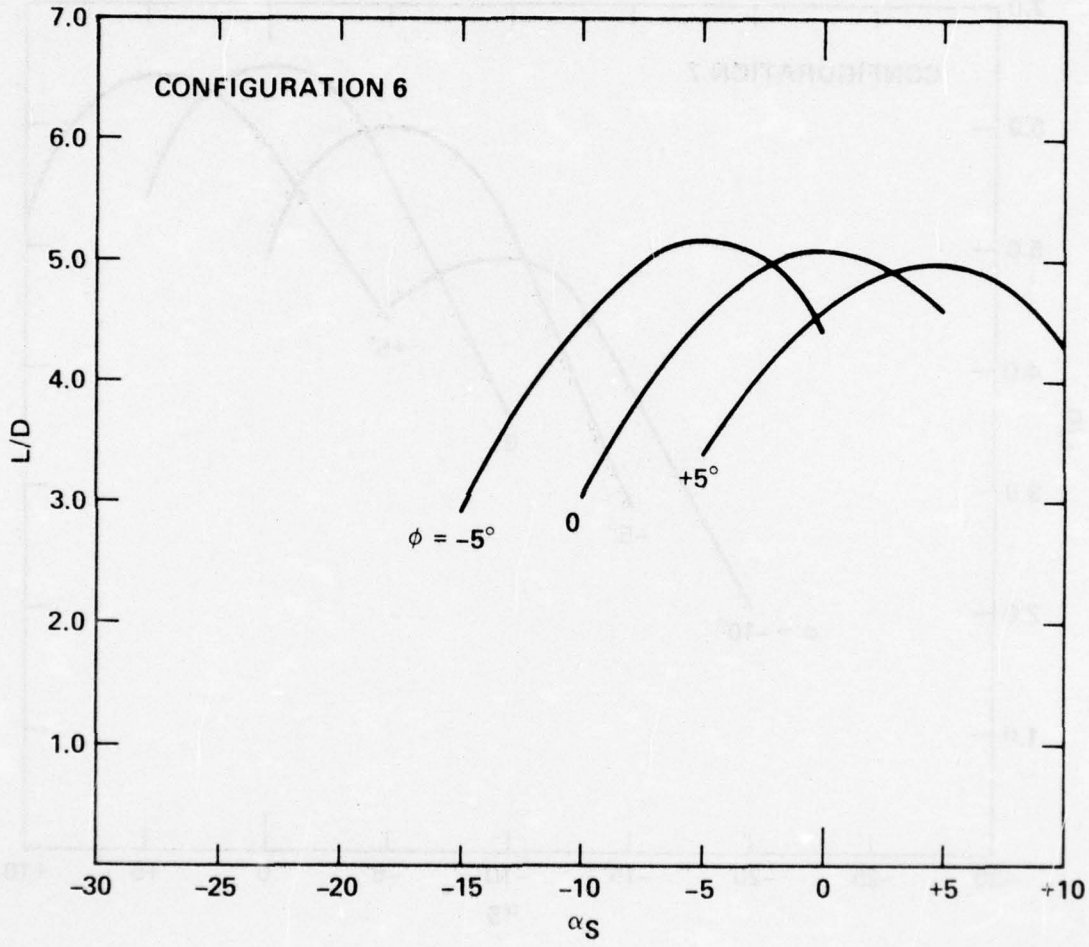

Figure 12(f) – (Continued)

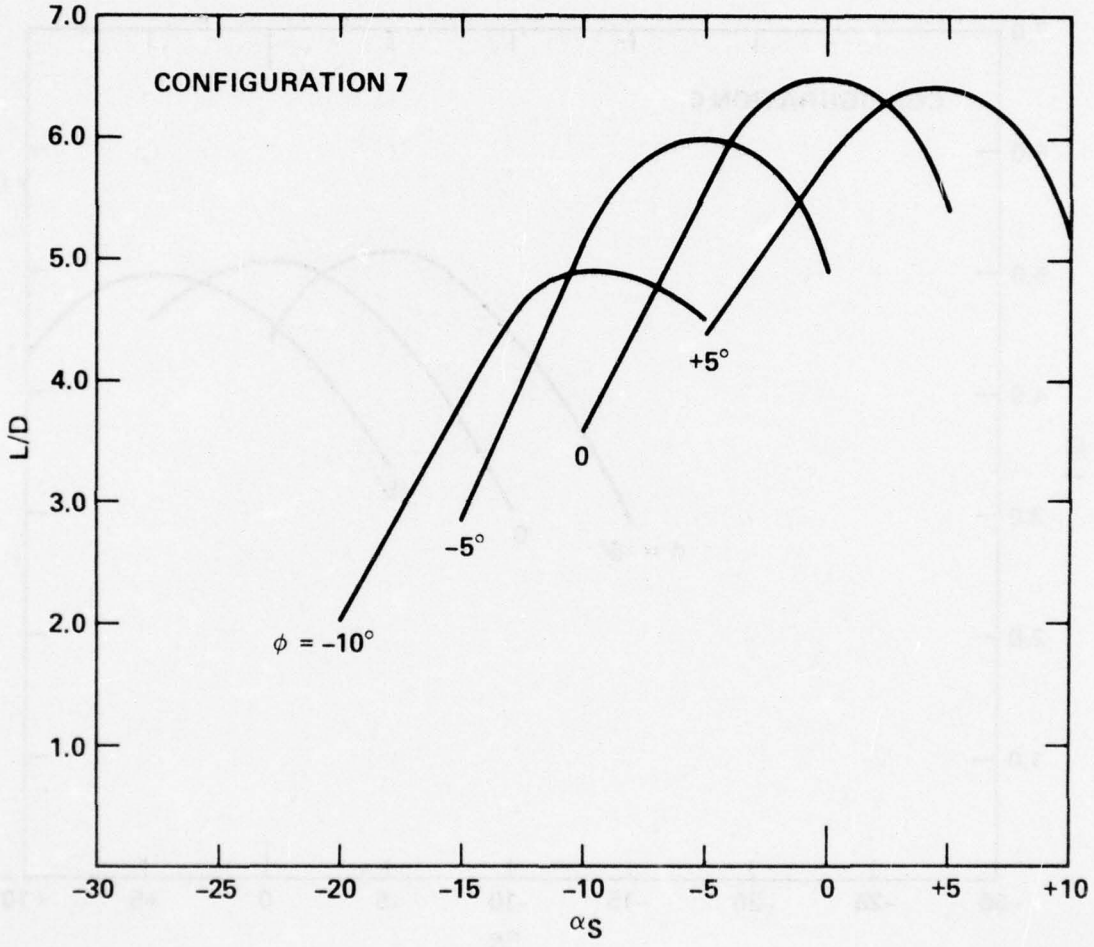

Figure 12(f) – (Concluded)

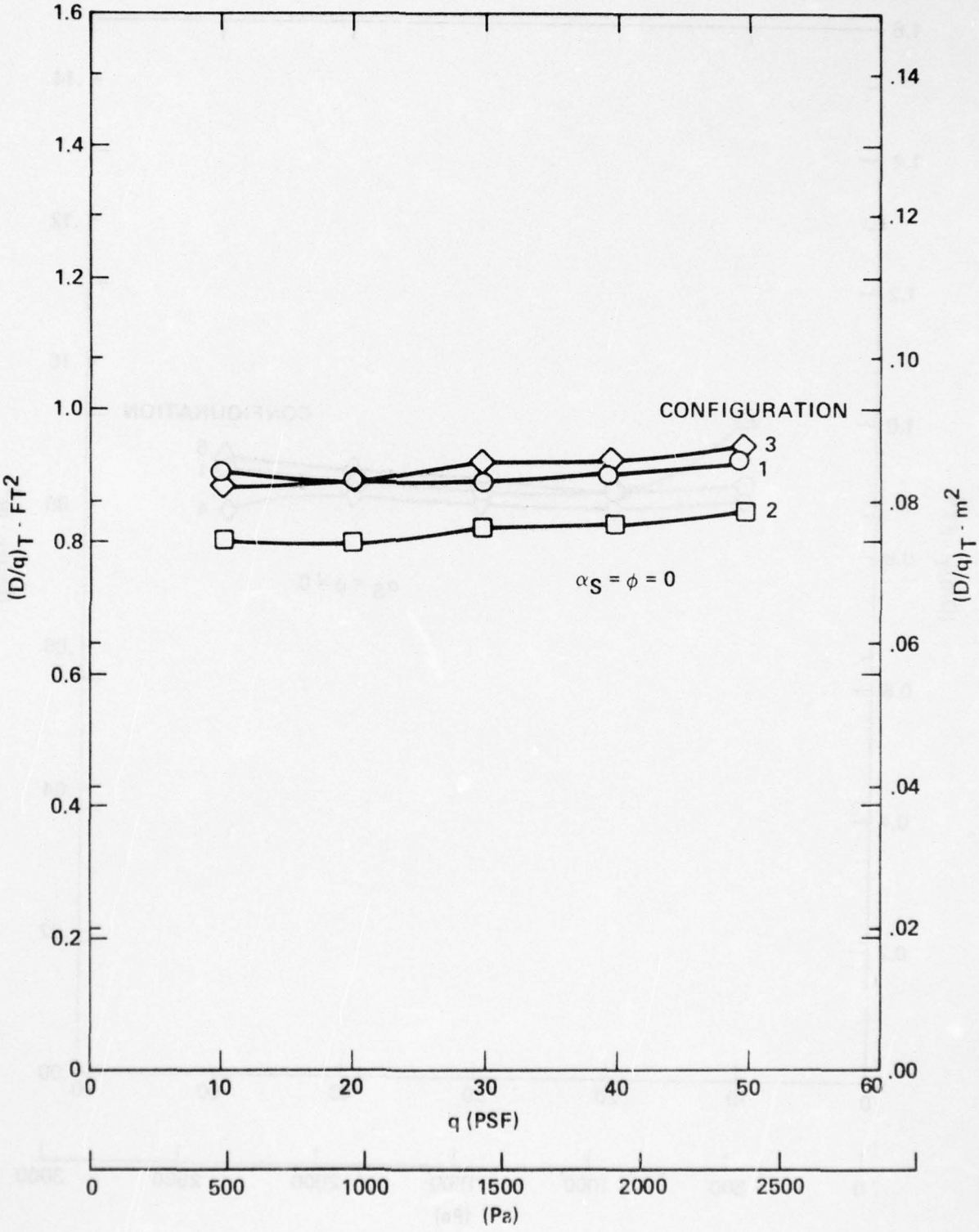

Figure 12 – (Concluded)
(g) Total Parasite Area Versus Dynamic Pressure

AD-A033 554 DAVID W TAYLOR NAVAL SHIP RESEARCH AND DEVELOPMENT CE--ETC F/G 20/4
EXPERIMENTAL EVALUATION OF ANALYTICALLY SHAPED HELICOPTER ROTOR--ETC(U)
JUL 76 P S MONTANA

UNCLASSIFIED DTNSRDC/ASED-355 NL

2 OF 2
AD A033554

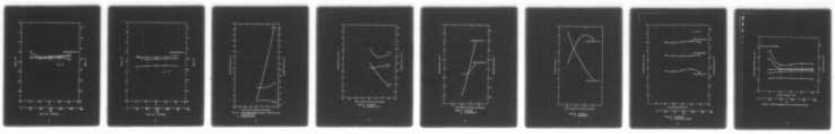

END
DATE FILMED
2-77

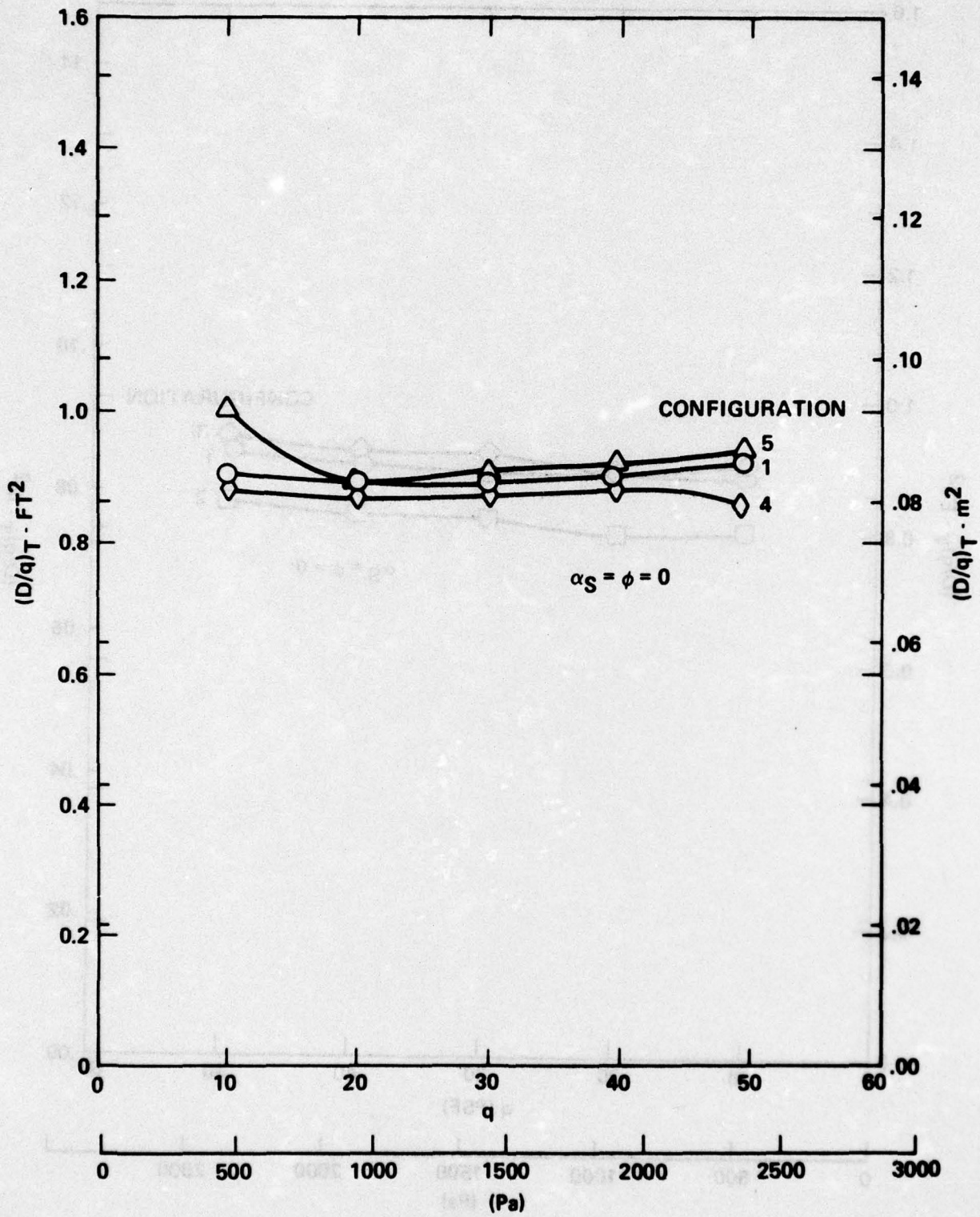

Figure 12(g) – (Continued)

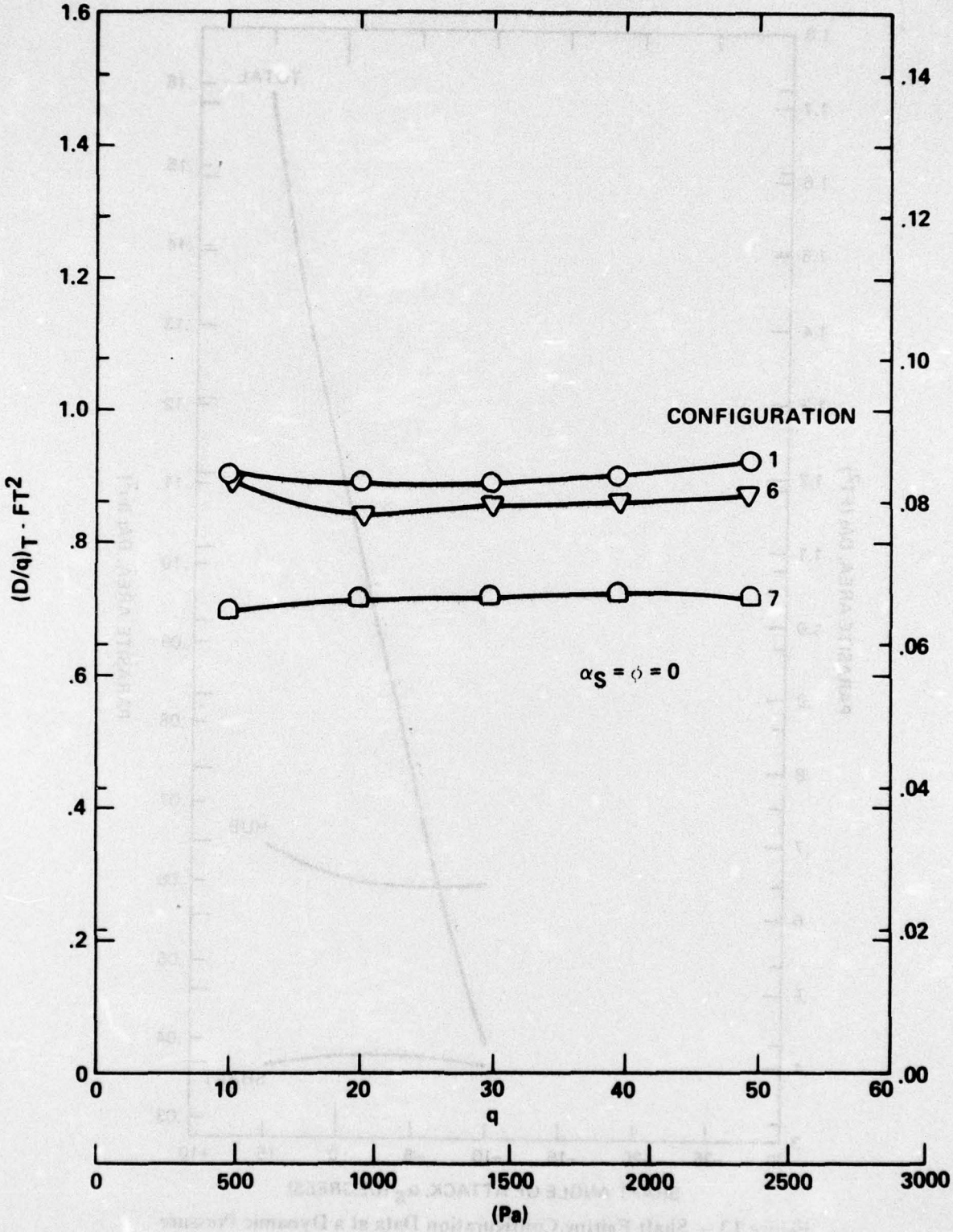

Figure 12(g) – (Concluded)

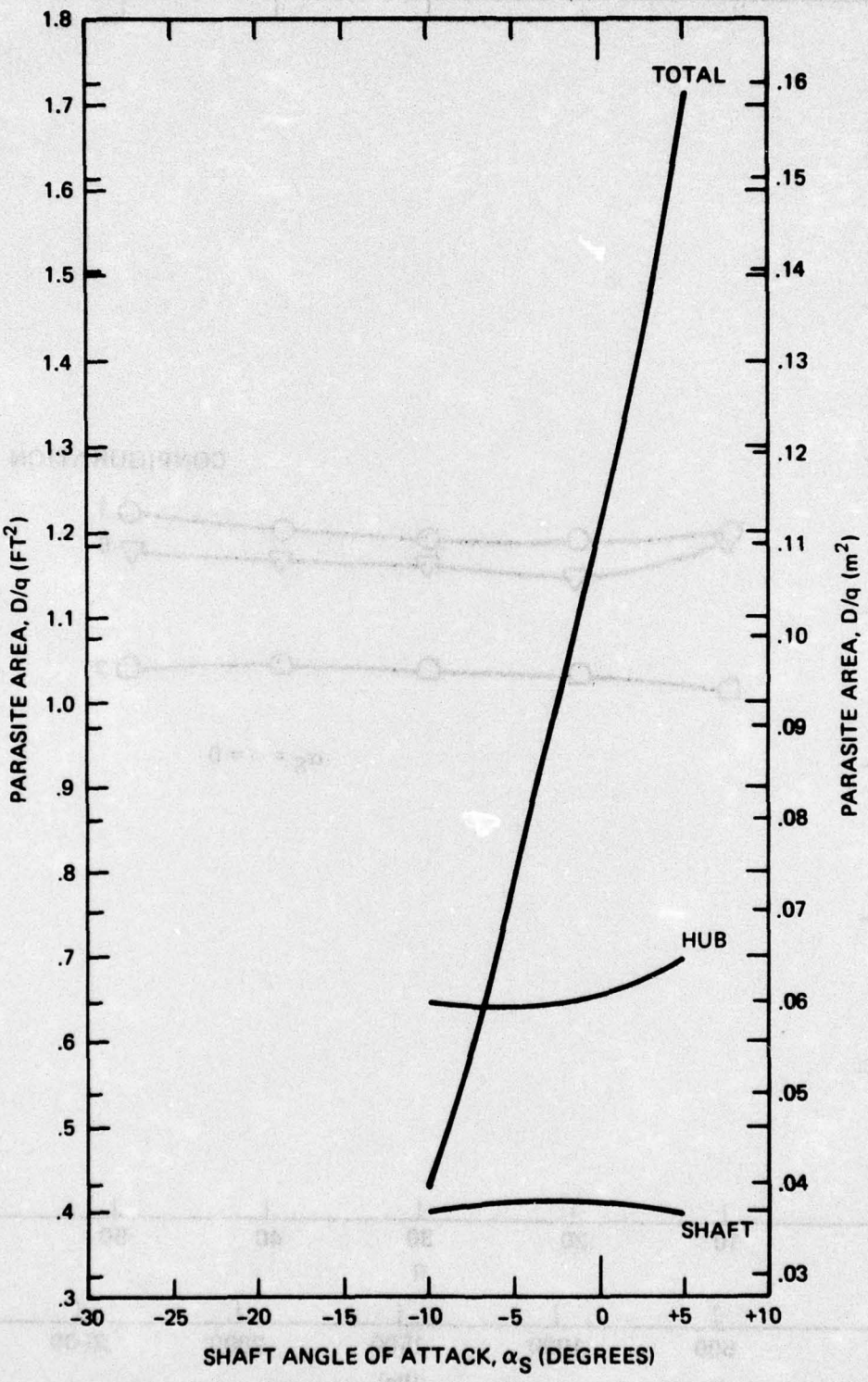

Figure 13 – Shaft Fairing Configuration Data at a Dynamic Pressure of 50 psf (2393 Pa)

(a) Configuration 10, D/q

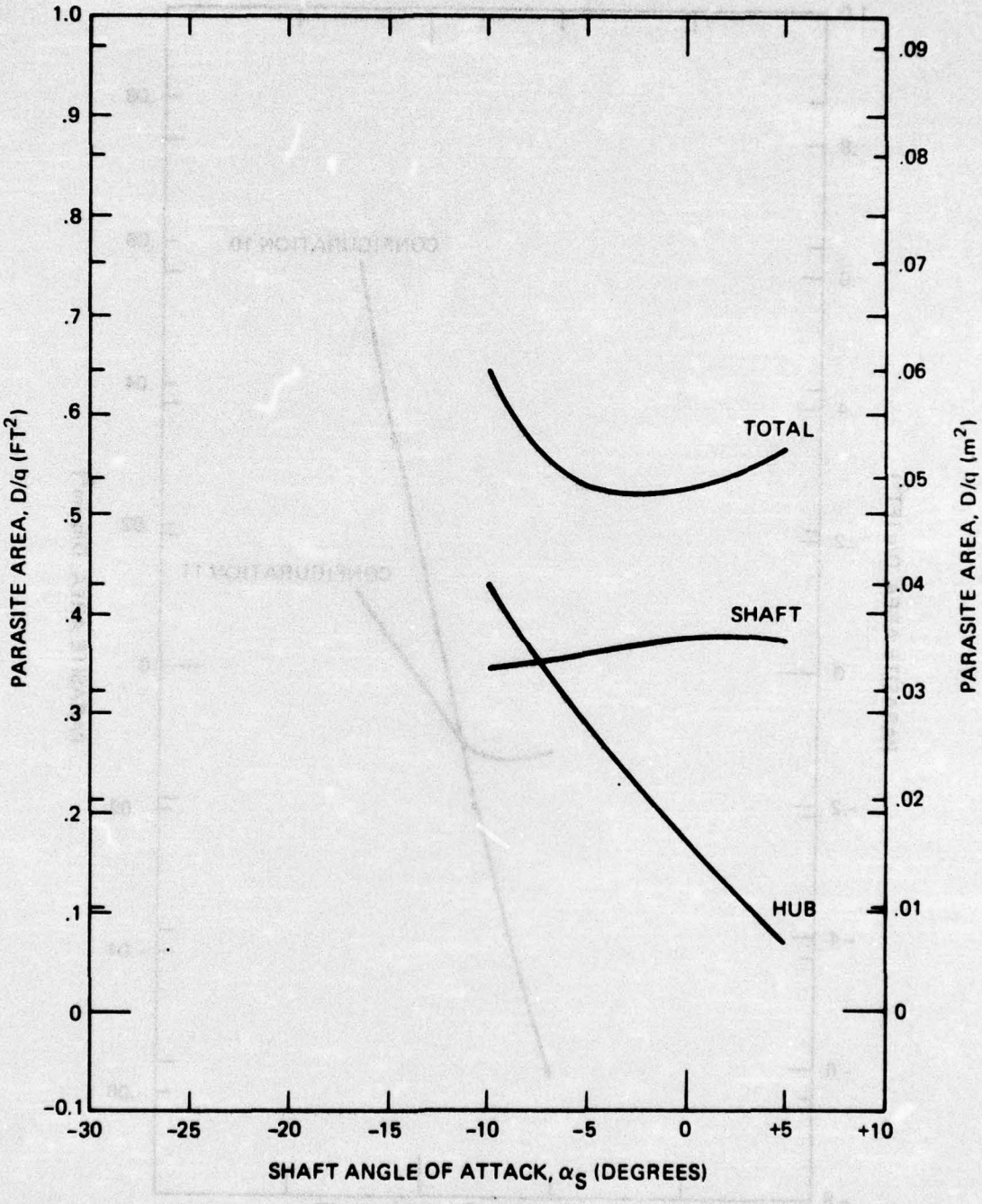

Figure 13 – (Continued)
(b) Configuration 11, D/q

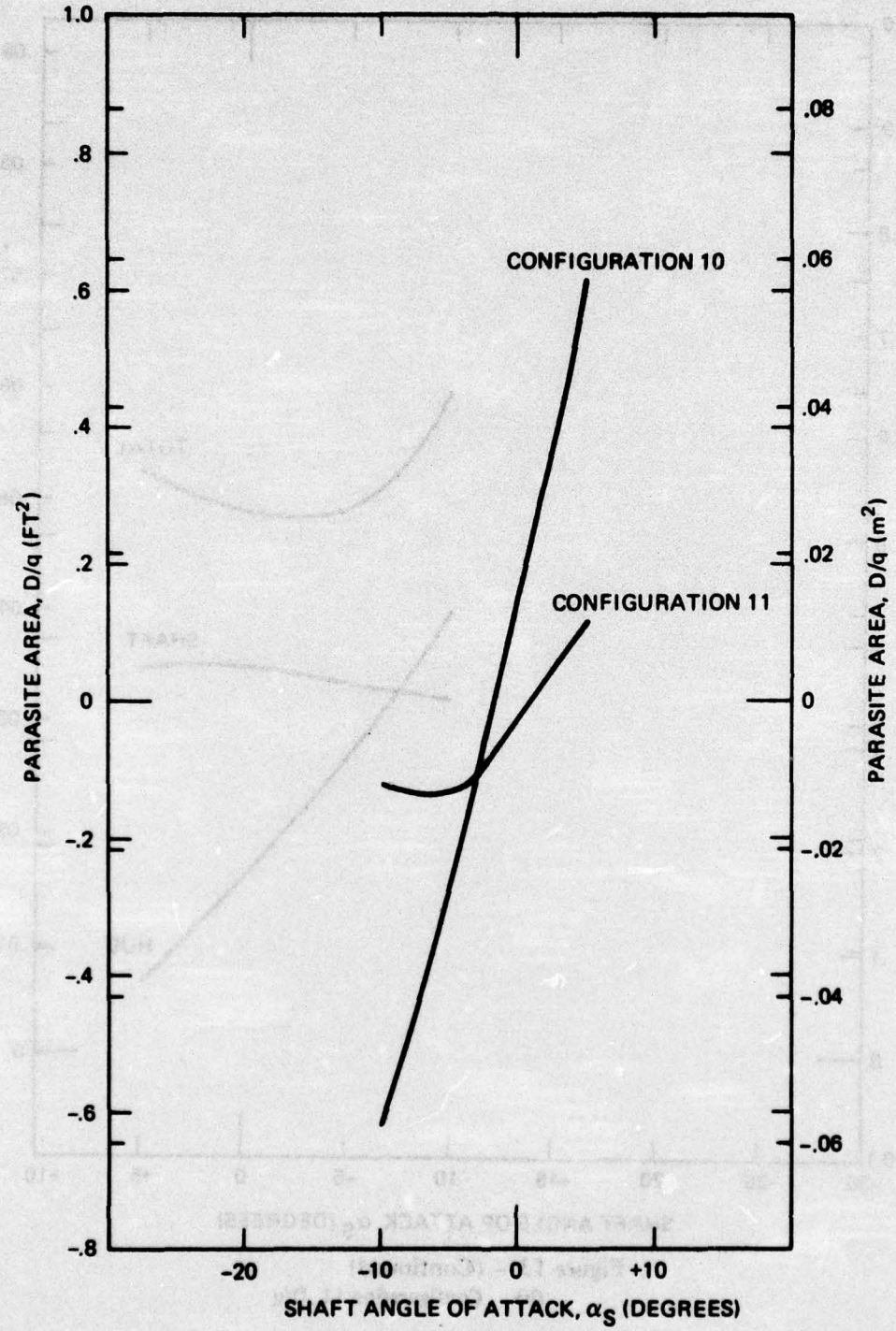

Figure 13 – (Continued)
(c) Pylon Parasite Area

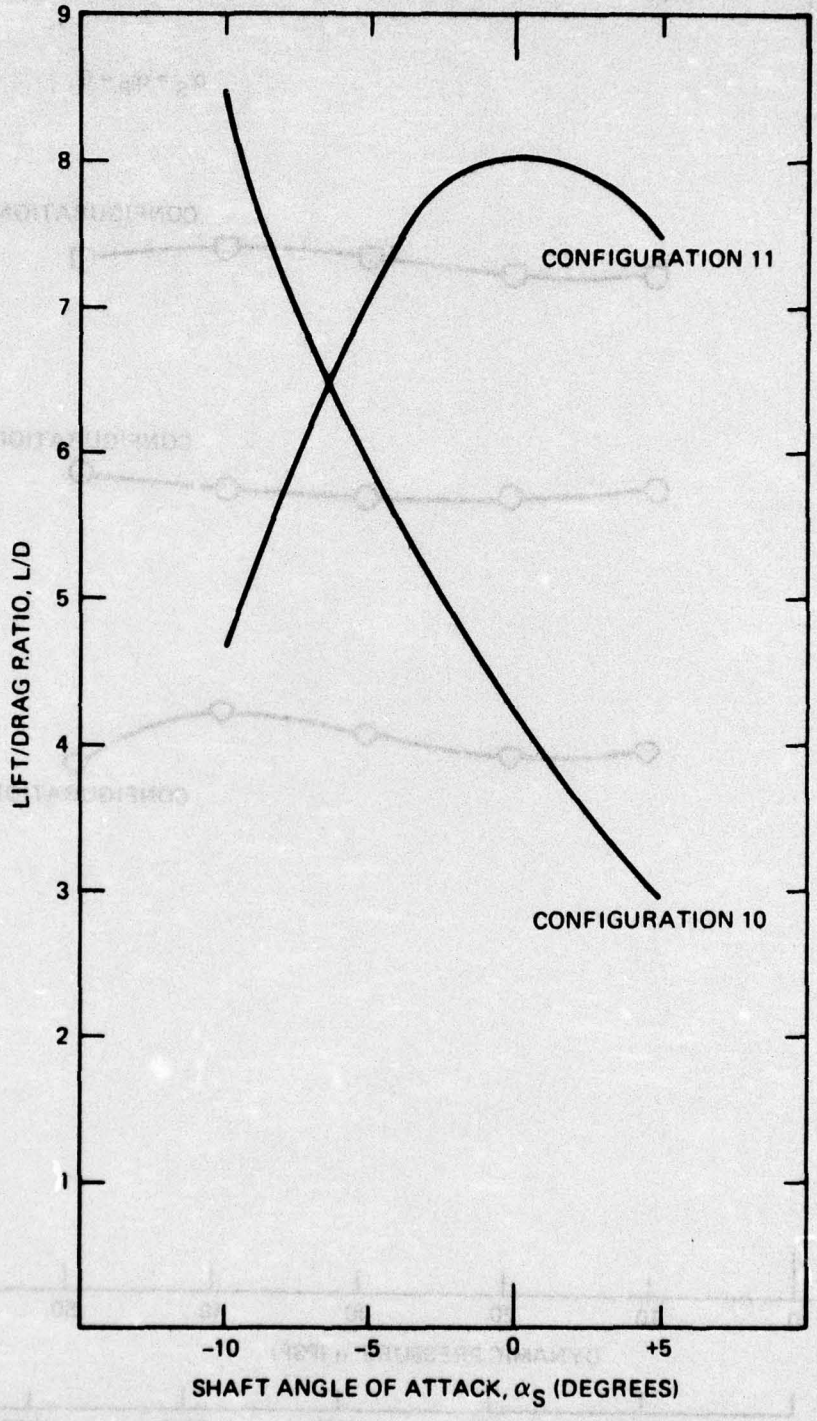

Figure 13 – (Continued)
(d) Lift/Drag Ratio

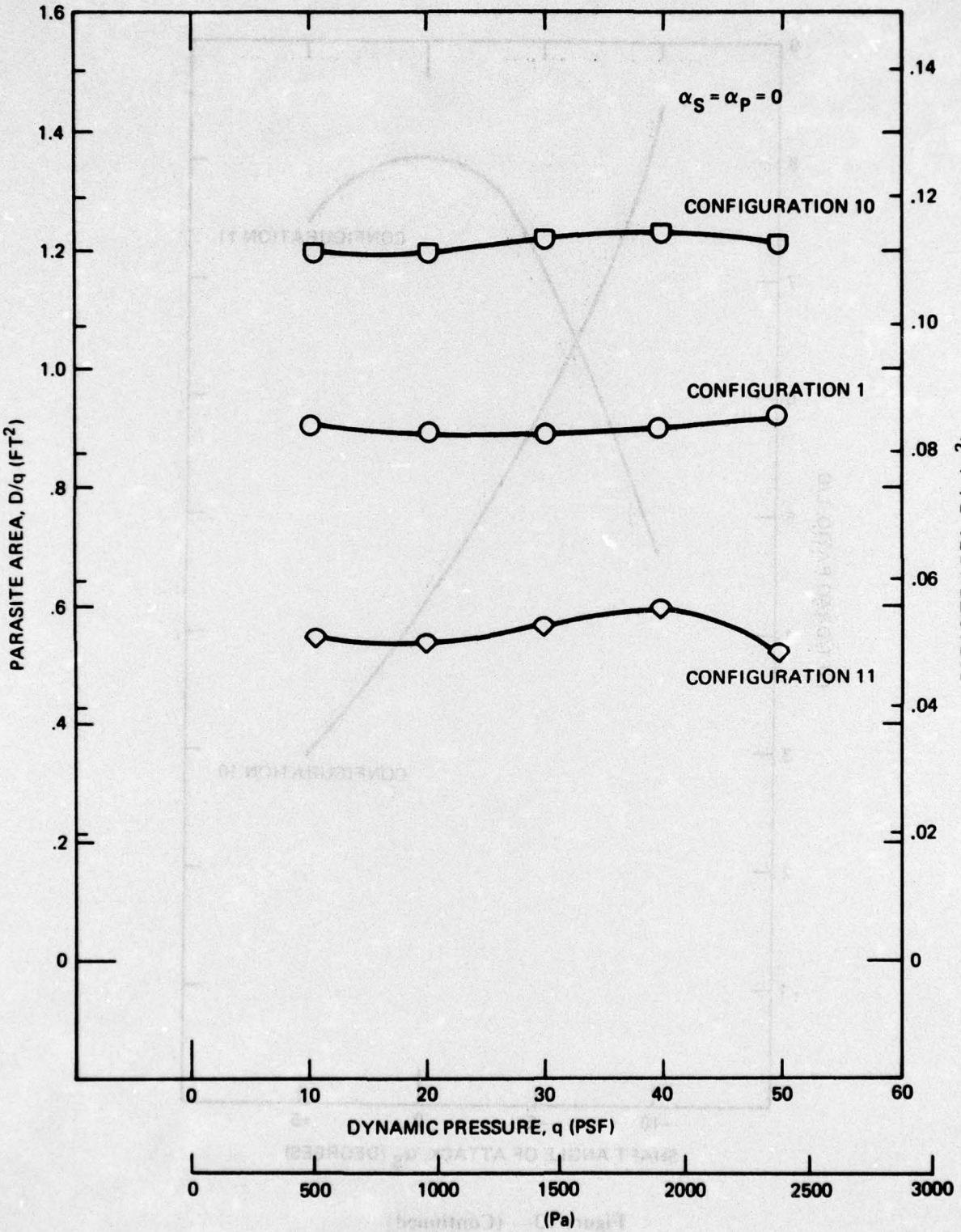

Figure 13 – (Concluded)
(e) Dynamic Pressure Variation

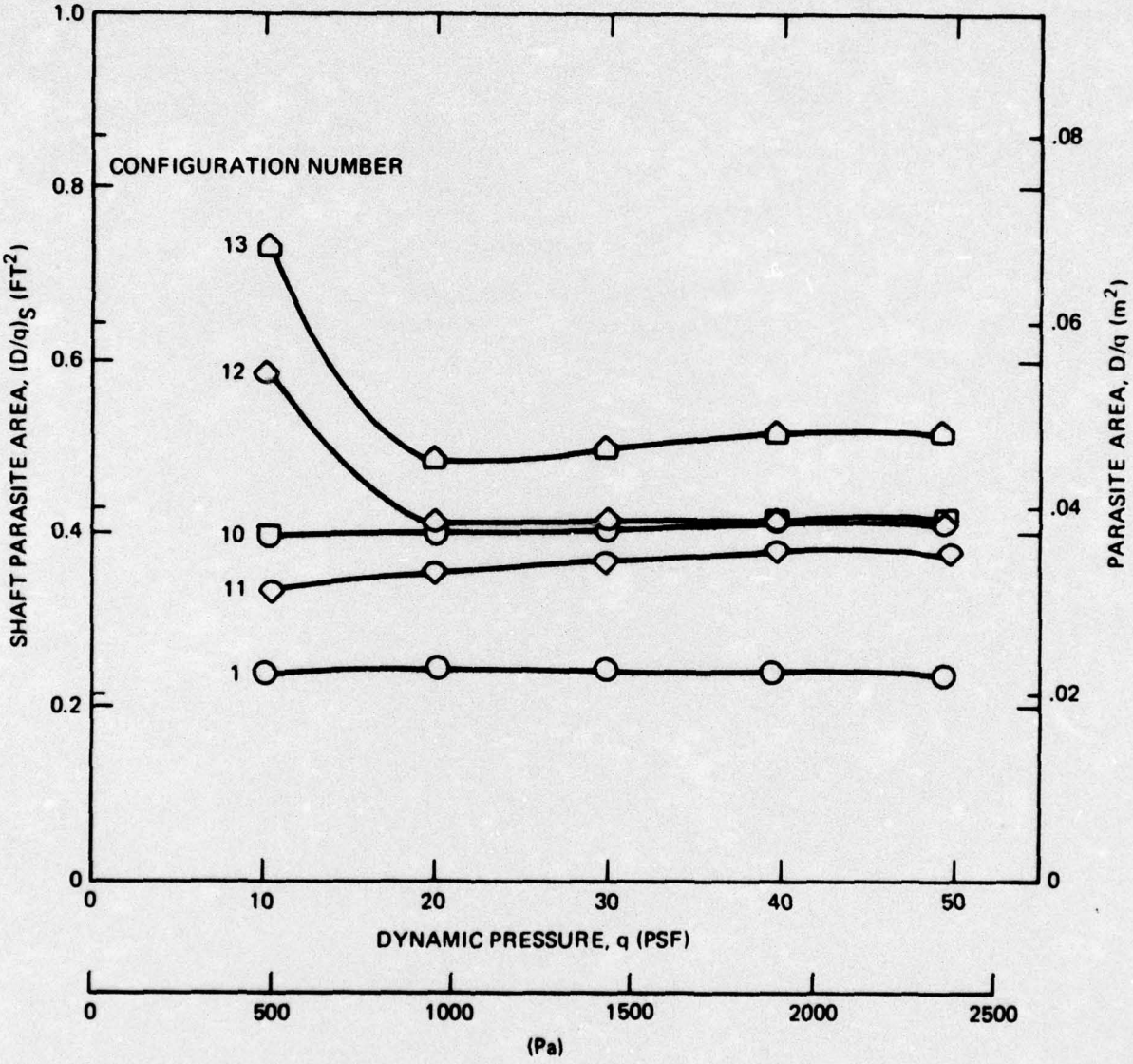

Figure 14 – Shaft Fairing Parasite Area Versus Dynamic Pressure